DEVELOPING VISIBLE-LIGHT SENSITIVE TITANIA/ADSORBENT COMPOSITE AND ITS APPLICATION IN WASTEWATER TREATMENT

Dissertation presented for the

Degree of Doctor of Philosophy in Civil Engineering at the

University of South Australia by

Wei Zhang

Supervisor: Professor Dr. Linda Zou

Associate supervisor: Associate Professor Dr. Lianzhou Wang



SA Water Centre for Water Management and Reuse

School of Natural Built and Environments

University of South Australia

June 2011

CONTENTS

Figure Captions

Table Captions

1. INTRODUCTION

REFERENCES

2. A STATE-OF-ART REVIEW OF PHOTOCATALYTIC TITANIA/ADSORBENT COMPOSITES PREPARED VIA WET CHEMICAL IMPREGNATION FOR WASTEWATER TREATMENT

ABSTRACT

2.1. Introduction

2.2. Influence of porous adsorbents

2.3. Influence of TiO_2 precursors

2.4. Influence of TiO_2 loading and location

2.5. Influence of solvents and pH value

2.6. Influence of post assembly treatments

2.7. Current barriers and research opportunities in using titania/adsorbent composites for wastewater treatment

2.8. Some conclusive remarks

REFERENCES

3. A PARAMETRIC STUDY OF VISIBLE-LIGHT SENSITIVE TITANIA PHOTOCATALYSTS SYNTHESIS VIA A WET CHEMICAL N-DOPING METHOD

ABSTRACT

3.1. Introduction

3.2. Effects of N-doping on TiO_2 visible-light sensitivity

3.3. Experimental

3.3.1. N-TiO_2 preparation

3.3.2. Characterization of the experimental materials

3.3.3. Photocatalytic experiments

3.4. Results and discussion

3.4.1. Effects of calcinations temperature
3.4.2. Effects of N-to-Ti precursor molar ratio
3.5. Conclusions
REFERENCES

4. WET CHEMICAL PREPARATION OF DIFFERENT TITANIA/ADSORBENT COMPOSITES AND THEIR VISIBLE-LIGHT ASSISTED METHYLENE BLUE (MB) REMOVAL

ABSTRACT
4.1. Introduction
4.2. Experimental
4.2.1. Preparation of N-doped titania/adsorbent composites
4.2.2. Characterization of experimental materials
4.3.3. Adsorption and photocatalytic experimental set-up
4.3. Results and discussion
4.3.1. Characterization of as-prepared titania/adsorbent composites
4.3.2. Adsorption and photodegradation of MB by as-prepared titania/adsorbent composites
4.4. Conclusions
REFERENCES

5. A PARAMETRIC STUDY ON THE ADSORPTIVE AND PHOTOCATALYTIC ACTIVITIES OF TITANIA/ZEOLITES COMPOSITES UNDER VISIBLE LIGHT IRRADIATION

ABSTRACT
5.1.Introduction
5.2. Experimental
5.2.1. Materials and chemicals
5.2.2. Preparation of N-doped TiO_2/Beta composite catalysts
5.2.3. Catalysts characterization
5.2.4. Photocatalytic activity test
5.3. Results and discussion
5.3.1. Characterization
5.3.2. Photocatalytic activities

5.3.3. Determining the optimal titania loading on the H-Beta zeolite support
5.3.4. Influences of the solution pH values
5.4. Conclusions
REFERENCES

6. AN COMPARATIVE STUDY OF CONVENTIONAL AND CHARGE-DRIVEN SELF-ASSEMBLY METHOD TO PREPARE VISIBLE-LIGHT SENSITIVE TITANIA/ACTIVATED CARBON (AC) COMPOSITES

ABSTRACT
6.1.Introduction
6.2. Experimental
6.2.1. Visible-light sensitive TiO_2/activated carbon composites preparation
6.2.2. Characterization of experimental materials
6.2.3. Experimental set-up for dissolved organic compound removal
6.3. Results and discussion
6.3.1. Characterisation of as-prepared TiO_2/AC composites
6.3.2. Adsorptive evaluation of as-prepared TiO_2/AC composites
6.3.3. Photocatalytic evaluation of as-prepared TiO_2/AC composites
6.3.4. pH effects on the performance of as-prepared TiO_2/AC composites
6.4. Conclusions
REFERENCES

7. CONCLUSIONS AND SUGGESTIONS FOR THE FUTURE WORKS

APPENDIX 1 PUBLICATIONS RELATED WITH THIS WORK

FIGURE CAPTIONS

Figure 1.1: Schematic diagram of photocatalytic process initiated by photon acting on the semiconductor.

Figure 2.1: A schematic wet chemical assembly of TNC

Figure 2.2: Cross sectional SEM of a TiO_2/AC pellet in which three different regions are pointed out. Ti wt% in Region I (a), II (b) and III is 76, 7 and 2 respectively.

Figure 2.3: Structural features of hydrogen-titanate (top left), anatase (top right), and rutile (bottom right), as well as the phase transitions from the hydrogen-titanate to anatase and rutile, in dilute and concentrate acid solutions, respectively.

Figure 2.4: Reaction mode of photoinduced mineralization of propyzamide substrate over naked TiO_2 (a) and TiO_2-loaded adsorbent (b).

Figure 2.5: Schematic models for (a) substitutional N-doping, (b) interstitial N-doping, (c) substitutional NO-doping, (d) substitutional NO_2-doping, and (e) interstitial NO-doping. Each atom of the supercell (16 TiO_2 units) is fully relaxed to stabilize the system.

Figure 2.6: A conceptual N-doped TNC preparation via wet chemical impregnation

Figure 3.1: Sketch of the proposed mechanism for the processes induced by vis-light irradiation of the N-doped sample in O_2 atmosphere

Figure 3.2: A schematic set-up of the experimental photocatalysis reactor

Figure 3.3: Visible-light photocatalytic activities of N-TiO_2 photocatalysts under calcinations temperature

Figure 3.4: XRD patterns (a), surface area (b), nitrogen adsorption-desorption isotherm (c), pore size distribution (d), UV-Vis DRS spectra (e), and fluorescence spectra (f) of N-doped TiO_2 under different calcinations temperatures

Figure 3.5: Visible-light photocatalytic activities of N-TiO_2 photocatalysts prepared under different N-to-Ti precursor molar ratio

Figure 3.6: XRD patterns (a), surface area (b), nitrogen adsorption-desorption isotherm (c), pore size distribution (d), UV-Vis DRS spectra (e) and fluorescence spectra (f) of N-TiO_2 photocatalysts prepared under different N-to-Ti precursor molar ratio

Figure 3.7: Zeta-potentials of N-TiO_2 sol as a function of pH

Figure 4.1: FTIR spectra of different as-prepared TNCs

Figure 4.2: Typical SEM images of different as-prepared TNCs

Figure 4.3: MB removal rate (C/C_0) as a function of time using different adsorbent-based TNCs, where ♦ represents the result using bare adsorbent, ▲ is that using its TNC without light and ■ is that using its TNC with light.

Figure 4.4: Adsorption capacity of different adsorbents and their supported TNCs

Figure 4.5: The part of MB removal rate by photocatalytic degradation for different TNCs

Figure 5.1: XRD patterns of the naked $TiO_{2-x}N_x$ and $TiO_{2-x}N_x$/Beta-x% composites samples coated with 10%, 40% and 90% titania loading.

Figure 5.2: TEM images of the bare N-doped TiO_2 (A, B), $TiO_{2-x}N_x$/Beta-10% (C, D) and $TiO_{2-x}N_x$/Beta-90% (E, F) samples.

Figure 5.3: (a) XPS spectra of the bare N-doped TiO_2 sample in the whole banding energy region and the banding energy region for N1s; The Ti 2p region (b) and O 1s region (c) of XPS spectra from different samples: the bare N-doped TiO_2 and $TiO_{2-x}N_x$/Beta-x% composites samples with different titania loadings.

Figure 5.4: UV-vis diffuse reflectance spectra of the naked $TiO_{2-x}N_x$ and the $TiO_{2-x}N_x$/Beta-x% composite samples with different titania loading.

Figure 5.5: FTIR spectra of the materials: $TiO_{2-x}N_x$/Beta-90%, $TiO_{2-x}N_x$/Beta-40%, $TiO_{2-x}N_x$/Beta-10%, H-Beta samples.

Figure 5.6: Removal efficiency of MB on $TiO_{2-x}N_x$/Beta-x% composite materials under visible light irradiation.

Figure 5.7: Comparison of removal efficiency of MB on the $TiO_{2-x}N_x$/Beta-90%, the $TiO_{2-x}N_x$ and the mixed catalyst of bare $TiO_{2-x}N_x$ (90%) with H-Beta (10%) under visible light irradiation.

Figure 5.8: Removal efficiency of MB on $TiO_{2-x}N_x$/Beta-x% catalysts under visible light irradiation.

Figure 5.9: Removal rate of MB on bare N-doped TiO_2 (a), H-Beta (b), $TiO_{2-x}N_x$/Beta-90% (c) and $TiO_{2-x}N_x$/Beta-10% (d) during adsorption process.

Figure 5.10: Comparison of photocatalytic removal Rate of MB on $TiO_{2-x}N_x$/Beta-90% (a) and $TiO_{2-x}N_x$/Beta-10% (b) samples under visible light irradiation.

Figure 6.1: A schematic charge-driven self-assembly process of TiO_2/AC composites

Figure 6.2: FTIR spectra of AC before and after the PSS surface modification

Figure 6.3: Overlay of the measured TGA plots for C_{SG} and C_{SA}, where the insets are corresponding first order derivative weight loss profiles.

Figure 6.4: XRD pattern (a) of AC, C_{SA} and N-TiO_2 nanoparticles; XPS spectra (b) of C_{SA}

Figure 6.5: Typical SEM images and corresponding EDX results (insets), where (a) is for C_{SG} and (b) is for C_{SA}; Typical TEM image of C_{SA} (c) and that in higher magnification (d)

Figure 6.6: Nitrogen adsorption-desorption isotherms at 77k and BJH desorption pore volume (dV/dlogd) plots (inset) for C_{SG} (a) and C_{SA} (b) composites

Figure 6.7: HA removal rate with and without visible light irradiation for C_{SG} (a) and C_{SA} (b), where A_0 is the initial light absorption at 254nm and A is that at given time, t;

(c) and (d) are pseudo first order representation of the HA removal rate by sole TiO_2 photocatalysis for C_{SG} and C_{SA}, respectively, where A_p is the light absorption at given time, t.

Figure 6.8: Plot of Q_t vs. $t^{0.5}$ for both as-prepared TiO_2/AC composites, where Q_t is the amount of HA adsorbed on TiO_2/AC composites per unit weight (mg/g) at a given time, t.

Figure 6.9: Possible mechanism of HA species migration to the TiO_2 photoactive sites

Figure 6.10: Total removal rate of HA species (defined as $1-A/A_0$) associated with 5 removal-regeneration cycles. Experimental conditions were [HA] =11.2ppm and [C_{SA}] =30mg.

Figure 6.11: Adsorption (a) of AC and C_{SA} and photocatalytic ability (b) of C_{SA} at different pH, where A_0 is the initial light absorption at 254nm and A is that at given time, t. Experimental conditions were [HA] =11.2ppm and [AC or C_{SA}] =30mg.

TABLE CAPTIONS

Table 2.1: Reported experimental conditions and properties of the as-synthesized TNC via wet chemical impregnation

Table 3.1: experimental conditions and properties as-synthesized N-doped TiO_2 via wet chemical methods

Table 4.1: Physical properties of experimental materials

Table 5.1: The physicochemical properties of the bare $TiO_{2-x}N_x$ and the composite samples

Table 6.1: Decomposition temperatures and corresponding weight loss percentages together at different stage with remaining residue amounts after heating to 800°C

Table 6.2: Some physical properties of AC, C_{SG} and C_{SA} composites

PREFACE

This Ph.D. thesis is prepared based on different papers published and/or submitted for publication in international journals, during the work carried out mainly at SA Water Centre for Water Management and Reuse (CWMR), University of South Australia throughout the period between March 2009 and June 2011.

The main goal of this dissertation is first trying to investigate and understand the preparation and application of visible-light sensitive titania/adsorbents composites. Then it determines the main experimental factors that control the visible-light decomposition/adsorption of the dissolved organic content present in different wastewater sources and their synergistic effects. Different types of adsorbents (i.e. activated carbon, zeolites, mesoporous silica) are selected as the study target objects.

To obtain this knowledge can be a great contribution in its successful application to industry wastewater treatment, but require a more detailed understanding of the main advantages and drawbacks of this technology.

The dissertation is organized in 7 chapters. **Chapter 1** considers a general introduction and **chapter 2** provides a state-of-the-art review which is focused on the textile and winery wastewaters, and also in the treatment technologies that will be tested in this thesis – photocatalysis combined with adsorption.

In **chapter 3,** a parametric study related to the titania visible-light sensitization via wet chemical N-doping is conducted. Optimal sensitization parameters, i.e. calcinations temperature and N-to-Ti precursor ratio, will be established as general guidance for the subsequent coupling between visible-light sensitive titania and adsorbents.

In **chapter 4**, a conventional wet chemical assembly of visible-light sensitive titania and adsorbents is carried out. The performance of several titania/adsorbent composites are evaluated, with adsorbents such as zeolites (F-9, HSZ-690 and HSZ-930), mesoporous silica (MPS-2.7 and 4) and activated carbon (PS-1300), in the removal of one of the most representative dye compounds methylene blue (MB) used in textile industry.

Chapter 5 presents the parametric study of experimental factors during titania/adsorbent coupling. H-Beta zeolites are chosen in this chapter as the adsorbent substrate. This work makes possible to understand the existence of optimal titania loading into the adsorbents. Methylene blue (MB) is also used as model pollutant to assess the adsorption and photocatalytic ability of resulting titania/beta composites.

Chapter 6 compares the conventional wet chemical and charge-driven self-assembly method to prepare the stitania/activated carbon composites. The study investigates the effects of poly (sodium styrene sulfonate) surfactant on the enhanced coupling between titania and activated carbon substrate. Humic acid (HA), a common contaminant in most fresh surface water sources is used in this chapter to assess the adsorption photocatalytic ability of resulting titania/activated carbon composites.

Finally, in **chapter 7**, the main conclusions are summarized and future research developments are proposed.

I declare that:

- *this thesis presents work carried out by myself and does not incorporate without acknowledgment any material previously submitted for a degree or diploma in any university;*

- *to the best of my knowledge it does not contain any materials previously published or written by another person except where due reference is made in the text; and all substantive contributions by others to the work presented, including jointly authored publications, is clearly acknowledged.*

ACKNOWLEDGEMENTS

I wish to express my gratitude here to all the people who offered their invaluable supports and thus made this thesis possible.

To my supervisor Prof. Linda Zou, whose encouragement and professionalism has always guided me in the most difficult time throughout the whole project.

Technical and professional supports during my PhD candidature from person below are gratefully acknowledged for the completion of this thesis: XRD analysis performed by Dr. Nobuyuki Kawashima (Mawson Institute), XPS analysis conducted by Dr. Andrew Michelmore (Mawson Institute), EDX support from Angus Netting (Adelaide Microscopy Instrumentation), and zeta potential measurement with pH titration from Andrew Robinson (Ian Wark Research Institute).

I would also like to thank the technicians of Desalination and Membrane Laboratory at CWMR where I have worked, especially for the assistance of some laboratory set-up and advice from Mr. Victor Vorel.

To my parents, who have always stood beside me and supported me patiently through all the tough years. I thank them for their affection and love.

Finally, I would like to thank the Australian Research Council (ARC) linkage fund (LP0989240) to support this work financially. In particular, the project industry partner City West Water, including Mr Nigel Corby and Ms Audra Liubinas, are gratefully acknowledged for their interest and support in this research work. I am also very grateful to University of South Australia for offering me the Australian Postgraduate Awards (APA) and Industry scholarship, which help made this thesis possible.

My deepest gratitude to them all!!!

CHAPTER 1

INTRODUCTION

Long-term water shortages driven by population growth and climate change are forcing people to learn to live with less water. Manufacturing industries consume a large quantity of clean water, but until now very limited reuse has taken place. In many cases, such as meat or food processing factories, industrial wastewater streams are only slightly contaminated and contain low levels of dissolved organic compounds , e.g. polysaccharides, proteins, amino sugars, nucleic acids, humic and organic acids and cells. These dissolved organics pose a problem to the direct reuse of the lightly contaminated water without treatment, due to issues of bacterial growth, odour generation and biofouling on the utility surface. Of the current applicable treatments, adsorption process, through functionalizing the adsorbents to trap dissolved organic compounds, has shown promise due to the reasonable efficacy and comparatively low costs. Highlighting its commercial viability is the fact that activated carbon (AC) adsorption has been cited by the US Environmental Protection Agency as one of the best available environmental control technologies[1]. However, the main disadvantage of such methodology is its non-destructive nature i.e. dissolved organic compounds will be adsorbed but not decomposed; as a result, the spent or saturated adsorbents must be regenerated before reuse, or otherwise must simply be disposed of as hazardous waste. Therefore, decomposition of the adsorbed dissolved organic compounds and regeneration of the adsorbents is a very critical step to the cost-effective use of porous adsorbents and continuous large-scale operation in wastewater treatment. Several methods, based on either desorption or decomposition, have been used to regenerate the spent adsorbents, such as activated carbon[2]. For example, the most commonly used thermal or microwave treatments promote the drying and loss of highly volatile compounds below 200 °C, vaporization and decomposition of unstable compounds at temperatures between 200 and 500 °C, and the pyrolysis of non-volatile adsorbates at temperatures over 500 – 700 °C. In these methods, special high temperature facilities such as multiple hearth furnaces or rotary kilns are needed to desorb effectively, and usually at the expense of decreased adsorption capacity of adsorbents due to carbon loss and surface alteration after repeated regeneration cycles.

An alternative for the degradation of dissolved organic compounds and regeneration of spent porous adsorbents, heterogeneous photocatalysis can effectively oxidize a wide range of organic compounds, more to its advantage, at room or moderate ambient conditions. Scientific research in heterogeneous photocatalysis began as early as the 1970s. In recent years, applications to environmental cleanup, especially water treatment, have been one of the most active areas in the heterogeneous photocatalysis[3,4]. Some other advantages of heterogeneous photocatalysis over other adsorbent regeneration methods include: (1) No dedicated post-treatment is needed since the organic pollutants can be mineralized into nontoxic by-products such as H_2O, CO_2, and mineral acids; (2) The possibility of being activated by solar radiation could result in low energy cost; (3) Possible on-site regeneration of spent adsorbents and destruction of adsorbed organic materials; (4) Reduced loss of adsorbents due to attrition and burn-off which occurs in thermal regeneration. In the literature, materials with photocatatlytic abilities could be found abundantly. These mainly belong to the metal oxide semiconductors. As the nature of wastewater purification for human consumption and more stringent water quality standards demand the minimal level of toxicity, many metal oxides with photocatalyitc ability are excluded. Among those available, TiO_2 nanoparticles has proven to be the most promising[5], with reported advantages of low cost, non-toxicity, greatly enhanced surface area, tunable properties which can be modified by size reduction, doping, or sensitizer, no substantial loss of photocatalytic activity after repeated process cycles, enhanced photo-induced charge transport[6] and no depletion layer formation on the surface[7]. Besides, due to the intensive research on the photocatalytic activity of TiO_2, the mechanism of its purification on dissolved organic compounds is well understood. It usually involves the following and also illustrated in Fig. 1.1[8]:

1. Absorption of efficient photons ($h\nu \geq EG=3.2e$) by TiO_2

$$(TiO_2)+h\nu \rightarrow e^-_{CB}+h^+_{VB} \quad (1)$$

2. Oxygen ionsorption (first step of oxygen reduction; oxygen's oxidation degree passes from 0 to -1/2)

$$(O_2)_{ads} + e^-_{CB} \rightarrow O_2^{\bullet -} \quad (2)$$

3. Neutralization of OH^- groups by photoholes which produces $OH^\bullet$ radicals

$$(H_2O <=> H^+ + OH^-)_{ads} + h^+_{VB} \rightarrow H^+ + OH^\bullet \quad (3)$$

4. Oxidation of the organic reactant via successive attacks by OH radicals

$$R + OH^\bullet \rightarrow R^{`\bullet} + H_2O \quad (4)$$

5. Direct oxidation by reaction with holes

$$R + h^+ \rightarrow R^{\bullet +} \rightarrow \text{degradation products} \quad (5)$$

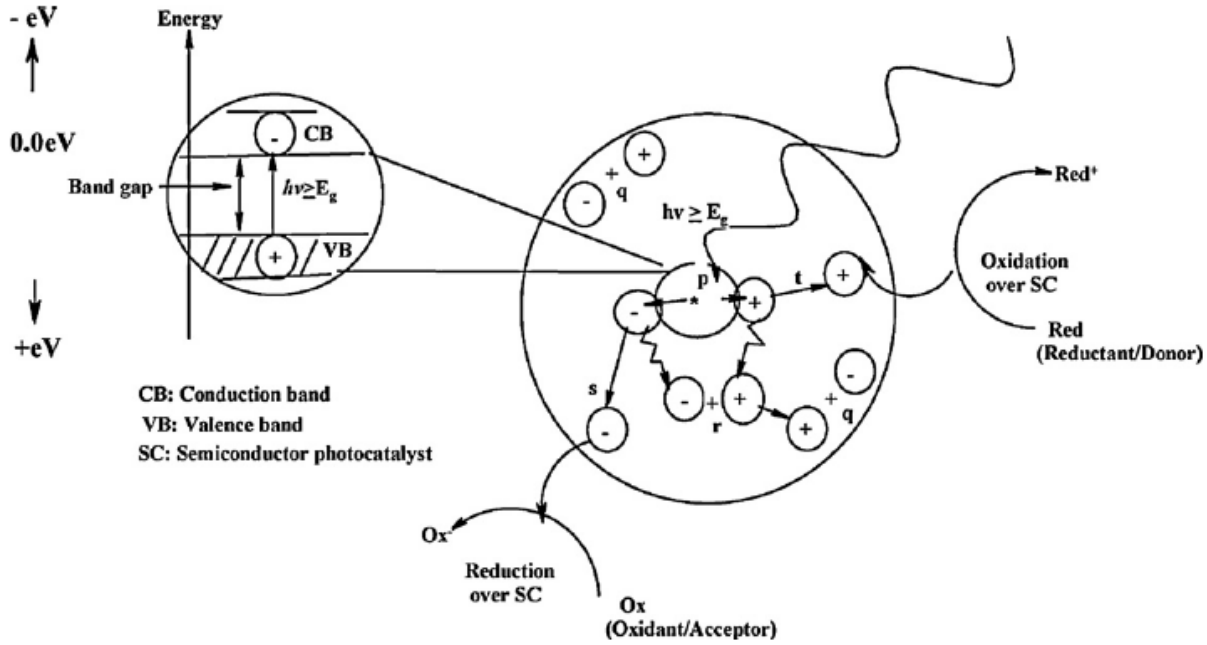

Figure 1.1: Schematic diagram of photocatalytic process initiated by photon acting on the semiconductor.

Although the research in this direction began with the interest to utilize photocatalysis as a separate procedure for post-adsorption regeneration of the spent adsorbent, it soon become evident that incorporating the photocatalytic regeneration during the adsorption process by coating TiO_2 photocatalyst on the surface of adsorbents would combine the advantages of both techniques: i.e. on one hand, large surface-area adsorbents work as the support of nano-sized TiO_2 photocatalysts and concentrate the pollutants and intermediates around the TiO_2, of which the photodecomposition rate is intrinsically low due to the limited surface area; on the other hand, nano-sized TiO_2

photocatalysts can decompose the pollutants thus regenerating the adsorbents in situ. A variety of coating methods for the synthesis of TiO_2/adsorbent nano-structured composites (TNC) have been reported. Some are chemical methods, such as carbonization of coal and TiO_2 mixture[9], ionized cluster beam deposition[10], chemical vapor deposition[11]and wet chemical methods[12,13]. Others are physical methods, such as impregnation–desiccation[14], boiling and dip-coating deposition[15]. At the current stage, wet chemical impregnations are of great interest, i.e. hydrolysis and impregnation of TiO_2 precursors to adsorbents, due to their facile nature, continuous process ability, low temperature and energy costs, uniform coating with good reproducibility and adhesion, and the simplicity in controlling crystal structure/morphology and particle size by simple variations in experimental conditions, such as hydrolysis rate, solution pH and solvents.

In summary, progress on developing TNC has been made in lab-scale synthesis particularly via wet chemical methods. However, it is also noteworthy that to this end, most attempts on these TNC applications are severely confined to UV-light range. This means a special energy intensive UV light source is required for the efficient photocatalytic decomposition. At the meantime, the recent research is very active to incorporate certain changes within the nano-sized TiO_2 system so as to make it suitable for receiving and utilizing visible light source (45% of total solar energy) with good efficiency. It is envisaged that developing a visible-light sensitive TNC could result in considerable large-scale energy saving, which is especially significant in the current climate of global energy crisis and concerns on sustainability.

The aims of this project are to combine the visible light sensitive TiO_2 nanoparticles with the porous adsorbent such as activated carbon and zeolite, to design a new hybrid adsorbent (TNC) that is able to not only trap the dissolved organic compounds but also decompose them efficiently in-situ. Three important features of this research are: 1) the developed material can achieve trapping and decomposing of dissolved organics within one process, without generating any waste for disposal; 2) the cutting edge TiO_2 nanoparticles will be sensitized under visible light condition, no UV irradiation is required; and 3) the increased adsorption of dissolved organics on the surface of catalysts will accelerate the degradation reaction. As a result, the new composites are expected to have a higher photocatalytic activity under visible

irradiation. The proposed research will be a significant innovation in water treatment field that reduces the energy consumption, uses low cost materials and targets real applications. This research will achieve the following objectives:

- Preparation of visible-light sensitive TiO_2 nanoparticles by doping with non-metallic species, such as nitrogen;
- Characterizations of as-prepared titania/adsorbent composites to understand the relationship between their properties (i.e. pore structure, surface area and surface hydrophobicity) and the performances;
- Test of the removal and decomposing efficiencies of the various loaded adsorbents and use the outcome to optimize the loading process;
- Chemical modification of adsorbents/porous materials (i.e. using surfactant) and self-assembly of porous material and visible light sensitive TiO_2 to prepare nanocomposite adsorbents;
- Establishment of the composite photocatalysis and adsorption kinetics in the aqueous phase.

The scope of the research will be limited on the visible light sensitive TiO_2/adsorbent composites by wet chemically doping with nitrogen, and the investigation of their degradation efficiencies of dissolved organic compounds. The adsorbents to be used include commercial zeolites, activated carbons and mesoporous silica.

References

[1] F. Derbyshire, M. Jagtoyen, R. Andrew, A. Rao, I. Martin-Gullon, E. Grulke, Carbon materials in environmental applications. In: L. R. Radovic, editor. Chemistry and physics of carbon, Vol. 27. Marcel Dekker, New York, 2001, pp. 1-66.

[2] M. Sheintuch, YI. Matatov-Meytal, Comparison of catalytic processes with other regeneration methods of activated carbon, Catal. Today 53 (1999) 73-80

[3] O. Legrini, E. Oliveros, A. M. Braun, Photochemical processes for water treatment, Chem. Rev. 93 (1993) 671-698.

[4] M. A. Fox, M. T. Dulay, Heterogeneous photocatalysis, Chem. Rev. 93 (1993) 341-357.

[5] M. Graetzel, Photoelectrochemical cells, Nature 414 (2001) 338-344.

[6] A. Hagfeldtt, U. Bjorksten, S. E. Lindquist, Photoelectrochemical studies of colloidal TiO_2-films: the change separation process studied by means of action spectra in the UV region, Sol. Energy Mat. Sol. Cell 27 (1992) 293-304.

[7]M. K. Nazeruddin, A. Kay, I. Rodicio, R. Humphry-Baker, E. Muller, P. Liska, N. Vlachopoulos, M. Graetzel, Conversion of light to electricity by cis-X2bis (2,2'-bipyridyl-4,4'-dicarboxylate)ruthenium(II) charge-transfer sensitizers (X = Cl-, Br-, I-, CN-, and SCN-) on nanocrystalline titanium dioxide electrodes, J. Am. Chem. Soc. 115 (1993) 6382-6390.

[8] L. Zou, B. Zhu, Enhancing reuse of treated effluent by photocatalytic process, J. Adv. Oxid. Technol. 10 (2007) 273-281.

[9] J. Przepiorski, N, Yoshizawa, Y, Yamada, Activated carbons containing TiO_2: characterization and influence of a preparation method on the state of supported TiO_2, J. Mater. Sci. 36 (2001) 4249-4257.

[10] H, Yamashita, M. Haraha, A. Tanii, M. Honda, M. Takeuchi, Y. Ichihashi, M. Anpo, N. Iwamoto, N. Itoh, T. Hirao, Preparation of efficient titanium oxide photocatalysts by an ionized cluster beam (ICB) method and their photocatalytic reactivities for the purification of water, Catal. Today 63 (2000) 63-69.

[11] Z. Ding, X. Hu, Q. L. Gao, P. L. Yue, P. F. Greenfield, Novel silica gel supported TiO_2 photocatalyst synthesized by CVD method,Langmuir 16 (2000) 6216-6222.

[12] Y. Luo, L. Zou, E. Hu, Enhanced degradation efficiency of toluence using titania/silica photoctalysis as a regeneration process, Environ. Technol. 27 (2006) 359-366.

[13] L. Zou, Y. Luo, M. Hooper, E. Hu, Removal of VOCs by photocatalysis process using adsorption enhanced TiO_2-SiO_2 catalyst, Chem. Eng. Proc. 45 (2006) 959-964.

[14] S. X. Liu, C. L. Sun, S. R. Zhang, Photocatalytic regeneration of exhausted

activated carbon saturated with phenol, Bull. Environ. Contam. Toxicol., 73 (2004) 1017-1024

[15] M. Lu, J. Chen, K. Chang, Effect of adsorbents coated with titanium dioxide on the photocatalytic degradation of propoxur, Chemosphere 38 (1999) 617-627.

CHAPTER 2

A STATE-OF-ART REVIEW OF PHOTOCATALYTIC TITANIA/ADSORBENT COMPOSITES PREPARED VIA WET CHEMICAL IMPREGNATION FOR WASTEWATER TREATMENT*

Abstract

In present chapter, the recent progress on preparation of TiO_2/adsorbent composites (TNC) via wet chemical impregnation has been reviewed. The potential applications of TNC are growing continuously and the material is very likely to find its place in future applications of wastewater treatment. In a TNC preparation via wet chemical impregnation, electronic properties (i.e. amount of charger carrier and its lifetime) and morphological properties (i.e. particle size, surface area and crystal phase) of TiO_2 in as-prepared resultants are sensitively dependent on the experimental conditions during the synthesis. Currently, one major limitation in this promising area is that visible-light capacity has yet to be introduced into TNC systems. It is envisaged that this could be realized via a single wet chemical procedure without significant increase of the process complexity.

* This chapter has been adapted from: Apply Catalysis A: General 71 (2009)1-9.

2.1. Introduction

As discussed in last chapter, progress on developing TNC has been made in lab-scale synthesis particularly via wet chemical impregnation. A systematic study of different experimental conditions during these published TNC preparation is yet to be conducted. This gap has seriously hindered its optimization and commercial viability at present. In such context, the recent progress on various TNCs synthesized via wet chemical route, along with a special focus on its potential and current limitations are reviewed in this chapter. Relevant experimental conditions and properties of as-synthesized products in each study are highlighted where possible and compared in order to identify and optimize the key preparation parameters.

In the literature, wet chemical assembly of TNC could be simplified as a three-module procedure, which is illustrated in Fig. 2.1: (1) contacting the adsorbents with the TiO_2 impregnating solution for a certain period of time, (2) drying the support to remove the absorbed liquid, and (3) activating the catalyst by calcinations.[1].

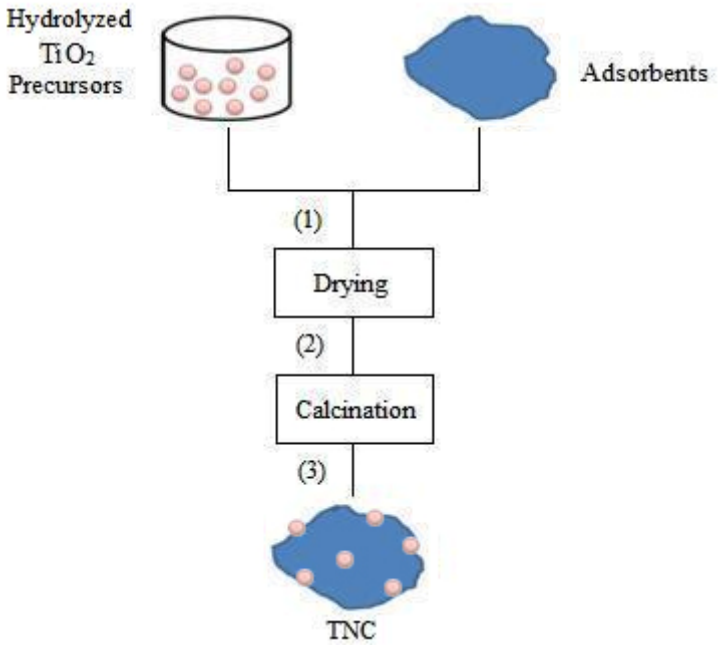

Figure 2.1: A schematic wet chemical assembly of TNC

Relevant studies of TNC synthesis via wet chemical impregnation in literature are summarized in Table 2.1, where key variables of the preparing conditions and corresponding as-synthesized TNC properties are listed for comparison. Each variable

and its influences on the TNC prepared via wet chemical hydrolysis are further discussed in the following sections.

2.2 Influence of porous adsorbents

The overall performance of TNC on the dissolved organic compounds removal basically consists of two parts: adsorption by porous substrate and photocatalytic-decomposition by nano-sized TiO_2. Even with the latest progress in this field, the adsorption by porous substrates still works as the major mechanism in dissolved organic compounds removal, because the adsorption rate is far better than that of photodecomposition. As a result, choosing a proper adsorbent is critical to the efficient TNC synthesis for practical wastewater purification. However, to facilitate the effective photocatalysis by loaded TiO_2, a balance between adsorption capacity and affinity of the TNC needs to be taken into consideration, that is, the adsorbing capacity should be high for the dissolved organic compounds of target and yet the affinity should be moderate to allow the efficient diffusion of adsorbed substrates to the photocatalytic active sites. In general, the adsorption capacity and affinity of a TNC is dependent on some inherent properties of its adsorbent substrate, such as primary particle or granular size, pore size and distribution, surface area and acid-basic properties. Higher adsorption capacity usually corresponds to the adsorbents of larger surface area, while the adsorption affinity associates with the microporosity and amount of surface chemical groups that are able to bind or attract the adsorbates.

Table 2.1: Reported experimental conditions and properties of the as-synthesized TNC via wet chemical impregnation

Studies	**Adsorbent properties**			**TiO_2 precursors**	**Hydrolysis conditions**			**Calcinations T [°C]** [a]	**TNC properties**		
	Type	BET [m^2/g]	Primary size [mm]		Solvent	pH	T [°C]		TiO_2 wt %	TiO_2 size [nm]	BET [m^2/g]
Sampath et al.[1]	Mordenite			$Ti[OCH(CH_3)_2]_4$	HCl	3		300	18, 56, 75		175
Takeda et al.[2]	Zeolum A-5	465		$Ti[OCH(CH_3)_2]_4$	HNO_3	3		300	53		381
	Zeolum F-9	548									367
	Mordenite	375									293
	Ferrierite	290									270
	AC	1130									623
Xu et al.[3]	Zeolite A	275		$Ti[OCH(CH_3)_2]_4$	Ethanol			450	5.1		177
	ZSM5	408			HNO_3				5		392
									14.3		308
Xu et al.[4]	Zeolite X and Y			$Ti[OCH(CH_3)_2]_4$	Ethanol		4	150-730	Up to 30		
	MCM-41	985-1109			HNO_3				10, 20,40		

Reddy et al.[5]	USY-zeolite	659		$Ti[OCH(CH_3)_2]_4$	Isopropanol			450	25		415
	β-zeolite	525		$(NH_4)_2TiO(C_2O_4)_2$							231
	MCM-41	941									669
Torimoto et al.[6]	Mordenite			$Ti[OCH(CH_3)_2]_4$	HNO_3	3		300	70		
	AC				NaOH						
Torimoto et al.[7]	AC	950		$Ti[OCH(CH_3)_2]_4$	HNO_3	3		300	65,80,90		
					NaOH						
Harada et al.[8]	AC-M	1050		$TiCl_3$			50	200-450	10		
	AC-S	1399		$(NH_4)_2TiO(C_2O_4)_2$					0.5		
Carpio et al.[9]	AC	1007	0.152	$Ti[OCH(CH_3)_2]_4$	Isopropanol			300, 325, 350	50	12	704
		688	5 o.d. and 10 long								780
Tao et al.[10]	AC		1.1-1.3	$Ti[OCH(CH_3)_2]_4$	2-propanol		25, 90, 175	300 in air and N_2	2.38-8.33		1018-1270
Liu et al. [11]	AC	1150		$TiCl_4$	HCl	8	98	500 in N_2	80	10.4	296.35
					$(NH_4)_2SO$				95	14.0	96.97

					$_4$			98	13.6	67.56
Zhu et al.[12]	AC	912	2.2	$Ti(OBu)_4$	Ethanol		200	1.7	4-5	912
					HNO_3					
Dai et al. [13]	AC	1466		$Ti(OBu)_4$	Ethanol	25	200			1128
		1065			HNO_3			4.6		962
Zou et al. [14]	AC	1000		$Ti(OBu)_4$			200			932.4
Zhu et al. [15]	AC	952	3	$Ti(OBu)_4$	Ethanol		200	1.4	4-5	894
		1053	3.35×1.68		HNO_3			1.5		983
		894	3.35×1.68					1.5		859
		912	3.35×1.68					1.7		906
		936	4					1.3		861

[a] Calcinations were carried out in air if not otherwise specified.

In terms of the types of adsorbent substrates, most recent literature in this regard is concentrated on AC, which are known for their characteristics of large surface area, low cost, and wide pore size distribution from micro- to macro-sized pore[17]. Earlier studies seemed more interested in zeolites or molecular sieves as a group of alternative adsorbents. These contain uniformly sized pores in the range of 0.4-1.3 nm, so the materials have the ability of recognizing, discriminating and organizing molecules with precision that can be less than 0.1nm[18]. Non-porous substrates, such as glass beads, fiberglass, silica sand, clay, etc., or less porous ones (surface areas <200 m^2/g), such as alumina ceramics and silica, were also studied among the early attempts. However, the results were far from being satisfactory in terms of photocatalytic efficiency, i.e. as-prepared TNCs possess less photocatalytic activity than the corresponding TiO_2 alone[19,20]. Pozzo et al. reviewed most of early works using non- or less porous substrates [21]. The present work (Table 1) is in turn mainly focused on recent efforts of utilizing AC and zeolites as promising adsorbents. For these two candidates, the clear advantages of one over another as the porous substrate for TNC are still non-conclusive at this stage. Some of the noteworthy considerations regarding a suitable adsorbent include:

1) The dissolved organic compounds pollutants in wastewater are often targeted to be of large molecular weight, so the favourable pore size range of adsorbents in these applications should fall into the lower range of meso-scale (2-50nmn). This renders most of zeolite adsorbents somewhat disadvantaged due to their small pore size, which could also result in undesirable plugging especially during high TiO_2 impregnation.

2) It would be true that, depending on the targeted dissolved organic compounds, the adsorbent may have different adsorption performances. In terms of adsorption selectivity on different dissolved organic compounds, zeolite adsorbents are more flexible than AC due to their uniform pore size distribution. Accordingly, the repeatability of as-synthesized TNC quality based on zeolites is also superior.

3) Dissolved organic compounds removal by a TNC is a complex interplay between adsorption and photocatalytic decomposition. In many cases, a compromise of the adsorbent selection need to be made between ones with higher adsorption capacity and ones with lower affinity. Some early studies conducted by Yoneyama

and his coworkers on various adsorbent substrates have shown that TNC based on AC have most adsorption on propyzamide due to AC adsorption capacity, whereas TNC based on zeolites (Tosoh TSZ-640NAA) has the highest photocatalytic decomposition rate due to its moderate adsorption affinity[22].

4) Adsorbents should have higher surface areas than that of loaded TiO_2 nanoparticles and should be inert with dissolved organic compounds. Both candidates are agreeable on this, whereas zeolites feature more desirable mechanical properties, such as attrition resistance, hardness and compressive strength.

5) Adsorbents should possess reasonable transparency to UV-Vis light sources, as light penetration to internal surfaces is one limiting factor for photocatalytic efficiency. On adsorbents side, this is dependent on pore size and its distribution. ACs featuring a wide range of macropores are more desirable in this sense as they provide easy access for the propagation of UV-Vis light.

Depending on the TNC size, there are two types of operations reported in the literature: 1) fixed bed system containing large-sized TNC pellets (mm) or 2) suspension solution containing small-sized TNC powders (μm). In the form of large size pellets, the primary size of resultant TNC is usually equal to its adsorbent substrate, as the TiO_2 nanoparticle loading only contributed little changes to the size of TNC in most of these studies. Evidently, low size ratio of porous adsorbent to TiO_2 nanoparticles could result in a decrease of resultant TNC surface area, but could significantly improve the TiO_2 coating dispersiveness on the adsorbent surface. In a study of Carpio et al., they prepared two types of TNC: large size pellets and small size powders[10]. The authors reported a negligible difference of surface area between the absorbent and the corresponding TNC resultant for the former, which, however, exhibited very poor dispertiveness under SEM characterization (see Fig. 2.2). On a more practical note, using small size TNCs in form of suspension for wastewater purification would result in the difficulty of removal and separation, whereas large granular size TNCs do eliminate this problem but, on the other hand, the large size TNCs may limit the mass transfer compared to the small size ones. Further to this complexity, the information on the primary size of the adsorbents reported in the TNC literature is largely missing in many of the studies (see Table 2.1),

which make it impossible to cross-examine and elucidate the reported photocatalytic activities.

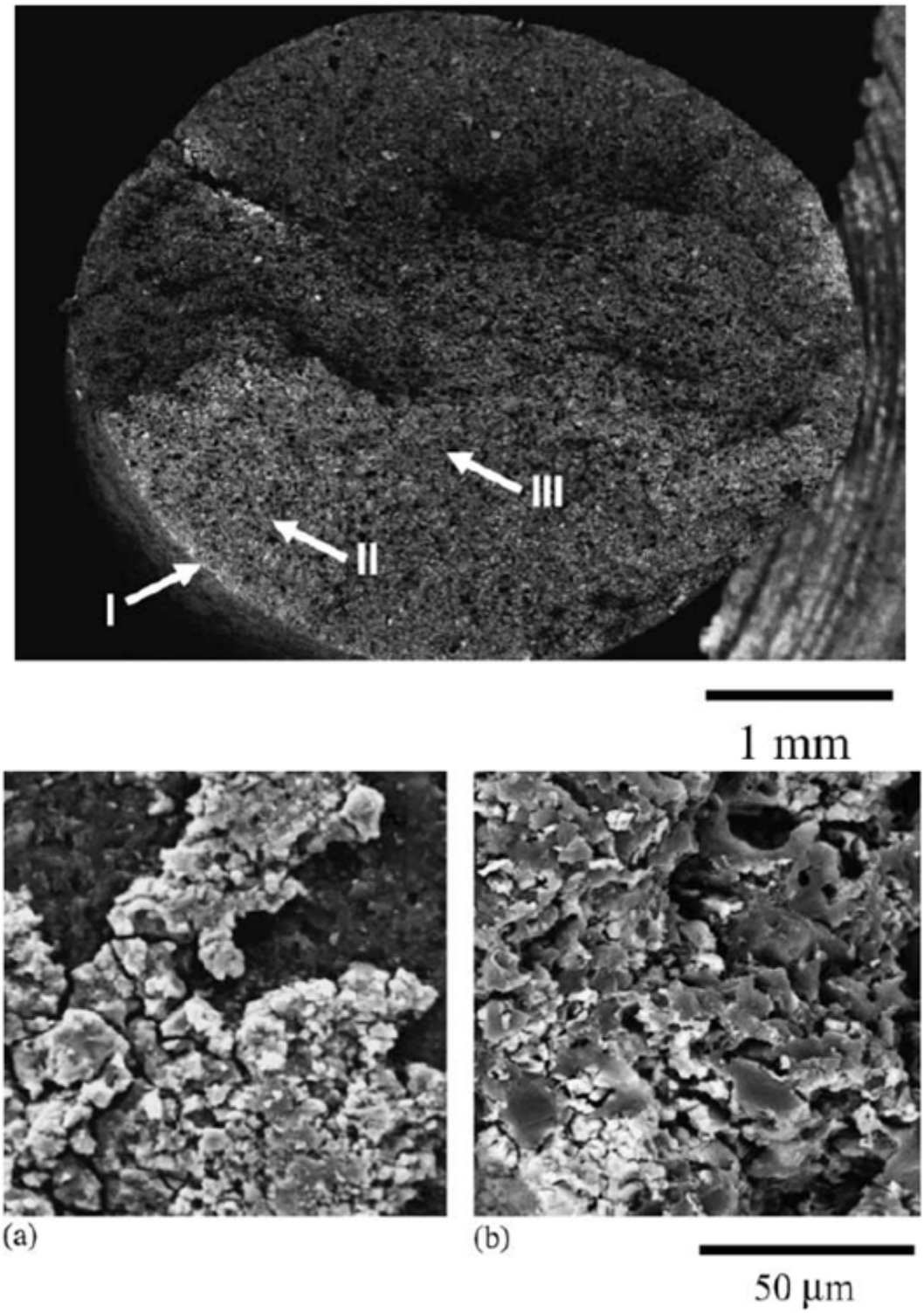

Figure 2.2: Cross sectional SEM of a TiO_2/AC pellet in which three different regions are pointed out. Ti wt% in Region I (a), II (b) and III is 76, 7 and 2 respectively[10].

Functional groups on the surface of adsorbents such as mineral matter and oxygen content may also influence the adsorption process through changing the hydrophilicity, as hydrophilic surface characteristics (like most zeolites compared with AC) can preferentially adsorb water or polar organic components. Therefore, competition of effective adsorption between different organic pollutants and solvent molecules implies the importance of selection of the adsorbents for target dissolved organic compounds. In the literature, the nature of the surface groups on adsorbents can be modified by thermal (under O_2, NH_3 or inert gases) or wet chemical impregnation (i.e. treated with acid or base). Most relevant studies reported utilizing the unmodified adsorbents, and yet the authors fail to characterize or specify the relevant information of surface group on their starting adsorbents before assessing the as-prepared TNC performance. These adsorbent surface characteristics could even have influences on the crystallization and size of TiO_2 species somehow during the impregnation of hydrolyzed TiO_2 precursors to the adsorbents.

2.3. Influence of TiO_2 precursors

Choosing different types of TiO_2 precursors plays an important role in preparation of TNC via wet chemical impregnation. Many mainly fall into two groups: titanium alkoxides and inorganic titanium, such as titanium chloride and titanium sulfate. In their study Harada et al. observed that the presence of Cl^- ions on the surface of AC promotes the aggregation of titanium oxides species, and the formation of rutile TiO_2 phase instead of anatase form. As one of two common TiO_2 species, rutile generates fewer charge carriers with lower lifetimes than that of an anatase type TiO_2, when in the same nano-sized particles form with the same crystalline quality and reactive surface properties[22]. On the other hand, the SO_4^{2-} presence on TiO_2 has been reported to show higher photocatalytic activity than pure TiO_2[23,24,25]. It is envisaged that using titanium sulfate as precursor could be advantageous, although this effect during the wet chemical impregnation to different adsorbents still needs further investigation.

2.4. Influence of TiO_2 loading and location

An increased amount of TiO_2 loading could also lead to augmentation of overall TNC photocatalytic activity. However, there is a bottleneck situation where penetrations of the light irradiation are blocked by excessive TiO_2 loading itself, and so are the adsorbent pores. Lu et al. reported a negligible effect of increasing TiO_2 loading on photocatalytic activity, after the loading exceeded 5 wt% in their as-prepared TNC[26]. This indicated an existence of optimal values of TiO_2 loading for maximized economical uses of TNC and energy. In the literature, there is a great discrepancy between TiO_2 loadings and their optimal values on photocatalytic activity of TNC reported in different studies, even when the same types of adsorbents are used. Apart from the missing information on the primary size of adsorbents they used, this was likely to arise from the failure to specify the TiO_2 loading dispersiveness of their as-prepared TNC in most studies. With the same TiO_2 loading, better dispersiveness (i.e. thinner TiO_2 layer) would reduce the blockage of light irradiation, and would improve the diffusion rate of adsorbates to the TiO_2 photoactive sites by shortening the diffusion length. This also signifies the necessity of the dispersiveness screening of TiO_2 loading after the TNC preparation, which can be done by microscopic characterization techniques, such as TEM and SEM. Finally, a note should be taken that an excessive thin TiO_2 layer could have an adverse effect on the crystallinity of TiO_2 nanoparticles formation on a TNC: for instance, Takahashi et al. observed an undesirable formation of amorphous TiO_2 occurring at a layer thickness of less than 50nm[27]. This would no doubt damage the photoactive quality of TNC resultants as well.

The location of TiO_2 loading, i.e. at the surface or in the bulk, is also anticipated to influence the photocatalytic activity to a certain extent. Due to the small size of TiO_2 nanoparticles, their loading could literally enter from macro-to micro-pores. Since penetration of either UV or Visible light into the inside pores is less likely, especially for small pores (<5nm), effective loading is preferably located on the surface, or in macropores in case of high TiO_2 loading. High loading in micropores also leads to plugging and will thus impair the adsorption capacity.

2.5. Influence of solvents and pH value

In some TNC preparations reported, alcohol solvents (such as 2-isoproponal, ethanol, etc.) or their aqueous solution, were chosen mainly due to volatility higher than that of

using water alone. This could facilitate the evaporation and the following drying treatments. Nevertheless, excessive use of alcohol or high alcohol-to-TiO_2 precursor volume ratio should be prevented, as it could shrink the body of colloidal formation and make it denser and less porous[28]. This could lead to poor crystallinity of TiO_2 nanoparticles formation at the later stage. As for using water alone, addition of a certain amount of acid is crucial to obtain a stable colloidal solution and to preserve the particles in their nano-sized form. This catalytic effect is brought about by the electrical charging of the hydroxide particles by proton adsorption, which hinders the gel agglomeration. Acid addition is also likely to have a potential linkage to the TiO_2 phase transition during the hydrolysis: Zhu et al. reported that high acid concentration (2.0M) favored the formation of rutile phase TiO_2 during the hydrolysis of $TiOSO_4 \cdot xH_2O$ (see Fig. 2.3) [29]. The follow-up investigations in this aspect are still coming. In terms of the acid type, HNO_3 is preferable to HCl due to avoiding the possible implication of an unfavorable Cl^- ion effect on TiO_2 crystal formation.

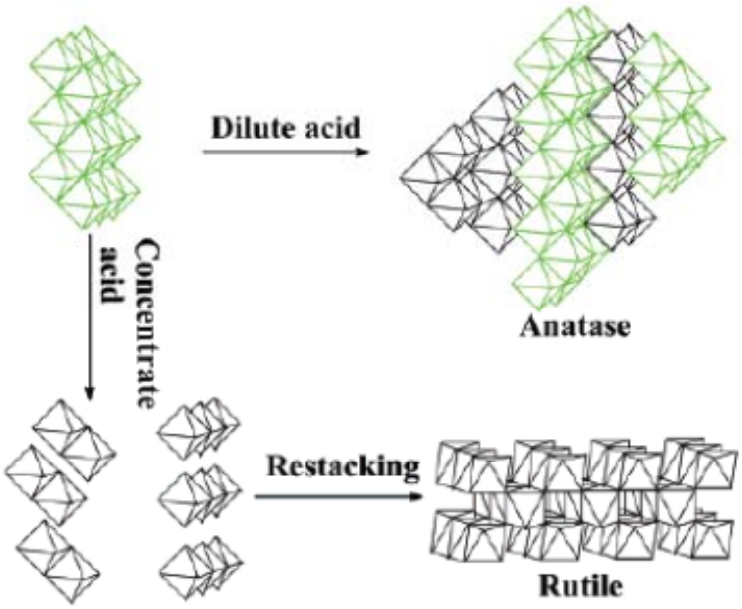

Figure 2.3 Structural features of hydrogen-titanate (top left), anatase (top right), and rutile (bottom right), as well as the phase transitions from the hydrogen-titanate to anatase and rutile, in dilute and concentrate acid solutions, respectively[44].

In parallel with its catalytic effect on TiO_2 colloidal formation, the addition of proper acids also manipulates the pH value of solvent. The pH requirement could vary to a great degree when impregnating the hydrolyzed TiO_2 precursor to different adsorbents.

For example, when preparing a TNC on a zeolite substrate, pH should not be kept too low to avoid the potential acid-leaching of the zeolite and thus destruction of its porous crystal structure[30]. The structural change could affect not only the adsorption but also the photocatalytic activities of a zeolite-based TNC resultant. Xu et al. reported a detrimental effect of lower zeolite crystallinity on the photocatalytic activity of their as-prepared zeolite TNC, although the adsorption of that alone was not significantly affected by the zeolite crystal change[31]. Detailed explanation of the former through structural investigation of the as-prepared TNC was absent in the study, though the authors speculated that it may be attributed to the lessen stabilizing effect of zeolite rigid framework on reactive species (i.e. OH^- and O_2^-), and decreased oxygen adsorption on TNC, of which the latter is believed to be essential to the electron accepting process on the TiO_2.

2.6 Influence of post assembly treatments

As discussed previously, the photocatalytic activities of TiO_2 nanoparticles are closely correlated to their electronic (i.e. amount of charger carrier and its lifetime) and morphological properties (i.e. particle size, surface area and crystal phase). Post assembly treatment, such as drying and calcinations, are necessary to remove most of the organic residues on the surface and moisture, and also most likely have an impact on the photocatalytic activities of the resultant TNC. Generally, the processes involving high-temperature steps (>500°C) would be considered unfavorable for the impaired photocatalytic performance of TiO_2, because their surface areas decrease with temperature due to the grain (i.e. crystallite size) growth or nanoparticles agglomerating effect throughout the treatment process. In addition, high temperature (>700°C in air) facilitates the phase transition of TiO_2 from anatase to rutile crystalline phase, which is also not preferable for the preparation of efficient TNC. As a result, the recommended temperature when calcining TiO_2 gel alone should not be higher than 400°C, where the anatase phase of TiO_2 is predominantly formed. However, a temperature that is too low (<200°C) would also be detrimental to the quality of TiO_2 crystallinity, which is deeply related to its electronic properties (i.e. less and shorter charger carrier lifetimes) and certainly should be prevented. Nevertheless, aforementioned standards could be varied to a certain degree in presence of absorbent substrates. For example, Xu et al. observed the presence of

zeolites substrate shifted the TiO_2 phase transition temperature to a higher range and inhibited the growth of TiO_2 crystallites[5]. The authors attributed it to the crystallinity of zeolite, although a detailed explanation of the effect was lacking. Relatively few investigations have been undertaken of this aspect so far, so it certainly merits further research.

High temperatures also induce the loss of adsorption capacity on adsorbent side through surface or structural alterations. This may cause more damages to the overall performance of a TNC on dissolved organic compounds removal since it is mainly driven by the adsorption capacity. Especially when preparing an AC-based TNC, in addition to the temperature control, general practices also require protective gases, such as nitrogen, to avoid unnecessary carbon loss. Some of the ambient gases are also likely to affect the calcination temperature on TiO_2 crystal phase transition. These effects deserve a more comprehensive investigation. For example, using protective hydrogen gas alone reportedly confined the complete anatase-to-rutile phase transition temperature of a TiO_2 between 525°C and 550°C, which is much lower than that (700°C) in the presence of air[32].

Compared to the investigations of calcination effects on the photocatalytic activities of TiO_2 nanoparticles, the drying process and its corresponding influence in the wet chemical preparation of TNC have received far less attention. However, as an improvement to the traditional procedure (i.e. air, <100°C, atmospheric pressure), some advantages of drying under the supercritical conditions were indeed addressed in the literature. Such changes mainly affected the specific surface of TiO_2 nanoparticle resultants. It is well known that supercritical conditions would contribute to the maintaining of a pore structure identical to that in the gel due to the absence of surface tension[33]. One instance is that Boujday et al. reported a 23 times surface areas enlargement of the TiO_2 resultants through hydrolyzing a titanium isopropoxide precursor within their drying conditions (supercritical CO_2, >35°C, 70bar)[34]. Nevertheless, the augmentative effects on electronic properties of the resultants were somewhat compromised, as the charger carriers generated on the samples dried under supercritical condition were fewer and had shorter lifetimes. In addition, these observations were obtained in the absence of adsorbent substrates. Future efforts are

needed on this particular aspect to justify this promising technique when preparing a TNC.

2.7 Current barriers and research opportunities in using titania/adsorbent composites for wastewater treatment

Among the concurrent efforts along with general practices of TNC preparations reviewed heretofore, several lab-scale testings of TNC photocatalytic activity using various dissolved organic compounds, such as phenol, methanol, dichloromethane, propyzamide, pyridine, propionaldehyde, 4-chlorophenol, etc, were also devised in these studies. Satisfactory results have been demonstrated, along with different adsorption and photocatalysis rates. However, due to non-identical operational conditions, i.e. light sources, intensity, concentration of the dissolved organic compounds, amount of TNCs used and apparatus design, these results do not allow a direct comparative cross-examining across different studies at this stage. Some other limitations regarding the TNC literature that needed to be addressed before TNC attains the commercial viability of TNC include:

1) The current experimental results are still a long way from continuous operation of adsorption and photocatalytic regeneration of TNC. In principle, photocatalytic regeneration of TNCs is a three-step process: dissolved organic compounds adsorbates desorption from the adsorbents, diffusion to the photoactive sites and the photocatalytic decomposition by TiO_2 photocatalysts. As discussed in section 2.1, photocatalytic decomposition process by TiO_2 requires much longer time compared to the adsorption of dissolved organic compounds by the absorbents, and such are the desorption and diffusion process of adsorbed dissolved organic compounds. These have affected its feasibility for commercial applications. Several possible improvements from the TNC design point of view has been suggested in section 2, including reduced size of adsorbent substrates and improved dispersiveness of TiO_2 coating. From the operation point of view, there are also some practical improvements regarding this issue, including the introduction of proper external heat[35] or ultrasonic waves[36] to enhance the desorption and diffusion rate of most dissolved organic compounds adsorbates, and the addition of oxidizing inorganics such as hydrogen peroxides, ozone, ammonium persulphate, potassium bromate and peroxydisulphate [37,38,39] to supply more beneficial radicals to the photo reaction

system. In addition, to inhibit the electron-hole recombination of TiO_2, oxygen and its steady-state concentration in the solution system will also have a profound effect on the photodecomposition rate under ambient conditions [40,41]. However, in the wake of these problems, the possible continuous operation would be more attractive for adsorbents with faster desorption properties and for those dissolved organic compounds with weak affinity to the adsorbents.

2) Compared with using TiO_2 photocatalyst alone, one advantage of TNC is found to be its large ability to collect photodecomposed intermediates and to prevent possible secondary pollution, as illustrated in Fig. 2.4. However, this also gives an uncertainty in modeling of TNC photocatalysis kinetics because the ongoing photocatalytic reaction by TiO_2 likely occurs with both adsorbed reactants and ones in the solution. Previously, several experimental results indicated that photocatalytic reaction rates of various dissolved organic compounds over illuminated TiO_2 fitted the Langmuir-Hinshelwood (L-H) model [42,43,44,45,46,47]:

$$r = \frac{\mathrm{d}C}{\mathrm{d}t} = \frac{kKC}{1+KC} \tag{1}$$

where r is the photocatalysis rate of the reactant (mg/l min), C the concentration of the reactant (mg/l), t the illumination time, k the reaction rate constant (mg/l min), and K the adsorption coefficient of the reactant (l/mg). In terms of a TNC photocatalysis model, not only does the adsorption coefficient of the reactant, K, have to adjust accordingly, but also the concentration of the reactant, C, should be replaced by a value with considerations of both adsorbed reactants and the ones left in solution. This value is also likely dependent on the diffusion rate from the adsorption sites to the photoactive sites. Given that most of current lab-scale TNC studies with dissolved organic compounds were empirical, a mechanistic model that can address the kinetics between different working processes (i.e. adsorption, diffusion and photocatalysis) is yet to be developed, as this is only explicable by understanding the underpinning science.

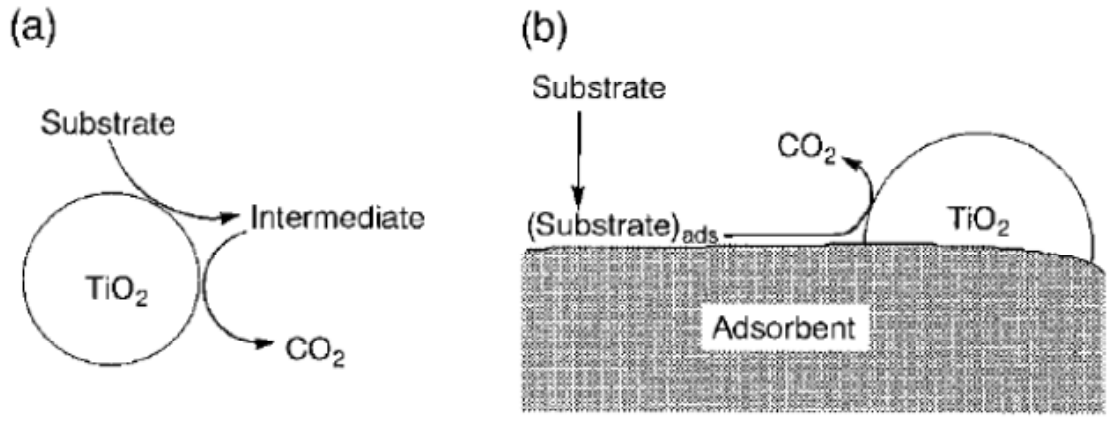

Figure 2.4: Reaction mode of photoinduced mineralization of propyzamide substrate over naked TiO_2 (a) and TiO_2-loaded adsorbent (b) [7].

3) It is well known that the band gap energy of TiO_2 is intrinsically wide, between 3.0 and 3.2eV (3.0 for rutile and 3.2 for anatase). This means plain TiO_2 semiconductors only absorb a small portion (5%) of the solar spectrum in the UV region. Currently, it is of great interest to find ways that TNC could possess the ability of directly utilizing visible sunlight through modification of TiO_2 photocatalysts. Early attempts on visible-light sensitization of TiO_2 mainly involved the doping of transition metal elements [48,49,50], which, however, has the drawbacks of requiring intensive energy and expensive ion implantation facilities. The processes increase free charge carrier trapping in bound electron-hole pairs and tend to form charge carrier recombination centers. As a result, doped TiO_2 resultants suffer from thermally instability, possible photo-corrosion and harmful nature of the dopants [51,52,53]. More importantly, most cationic dopants only result in limited band-gap changes, and in some cases, do increase the light absorption, but not the photocatalytic activity. As a consequence, more significant advances in this field were achieved on doping TiO_2 photocatalyst with non-metallic or anionic elements such as carbon, sulfur, halides, phosphor and boron. This has been reflected readily in several recent reviews [54,55,56]. Asahi et al. first recognized the visible light sensitivity of TiO_2 with a certain amount of nitrogen dopants[57] and attributed it to the band gap narrowing effect, which was resulted from the interaction between doped N (2p) and original O (2p) states (as illustrated in Fig. 2.5). Now nitrogen has proven to be the most effective dopant due to its similar size to oxygen and low ionization energy[58]. Most recently, Burda et al. developed N-doped TiO_2 via a wet chemical method (titanium isopropoxide and triethylamine as

Ti and N precursors) [59,60,61] and claimed it had no high-temperature induced surface property changes. Fine control of the nitrogen doping level was attained with the possibility of high N-content (reportedly up to 8%) compared with other methods, e.g. the sputtering and implantation [62.63,64], high temperature sintering TiO_2 under N-containing atmosphere [65,66,67], etc. More importantly, it is envisaged that the future visible-light sensitive TNC could be achieved within a single wet chemical procedure without any extra preparation complexity and cost, as illustrated in Fig. 2.6.

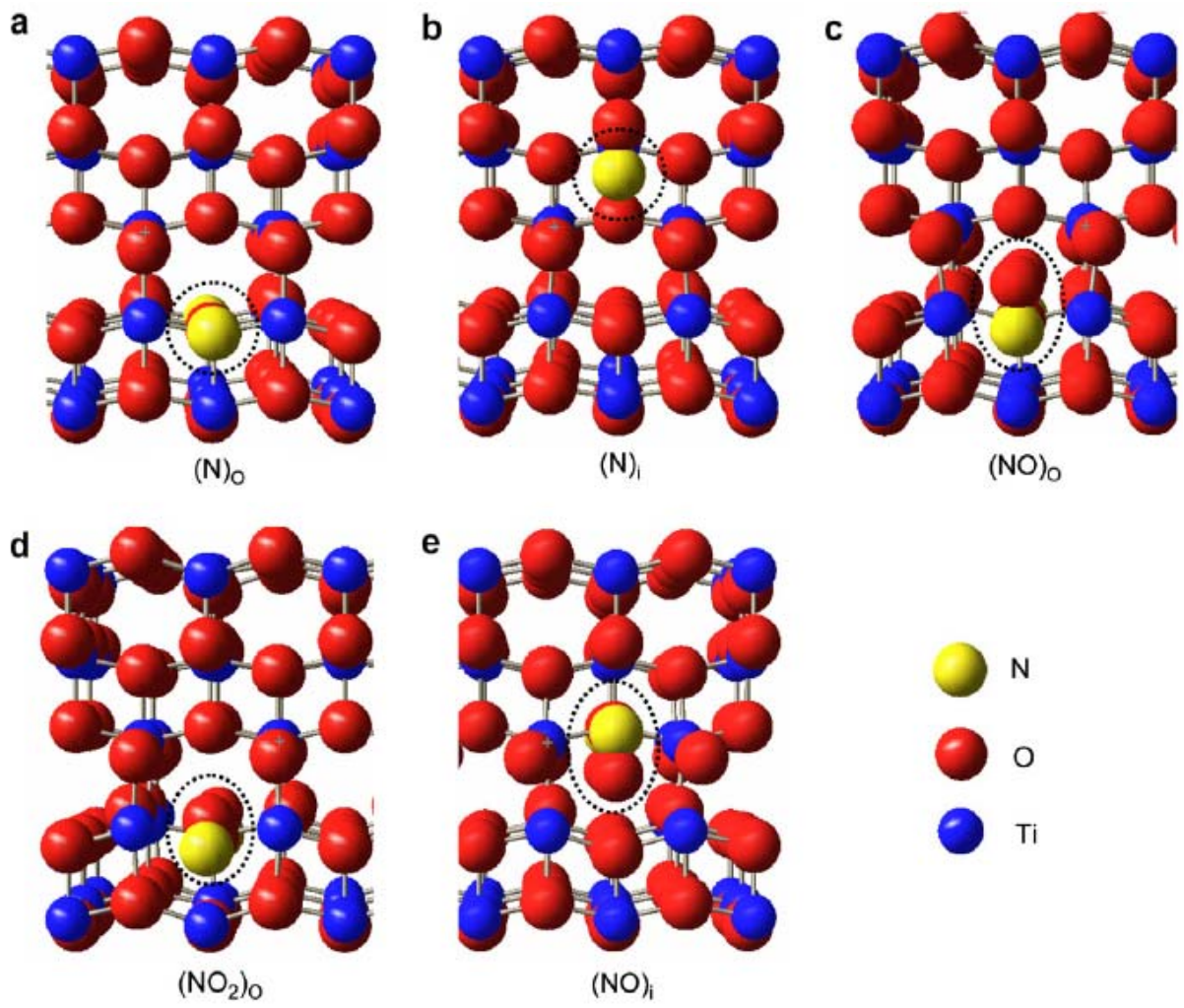

Figure 2.5: Schematic models for (a) substitutional N-doping, (b) interstitial N-doping, (c) substitutional NO-doping, (d) substitutional NO_2-doping, and (e) interstitial NO-doping. Each atom of the supercell (16 TiO_2 units) is fully relaxed to stabilize the system [57].

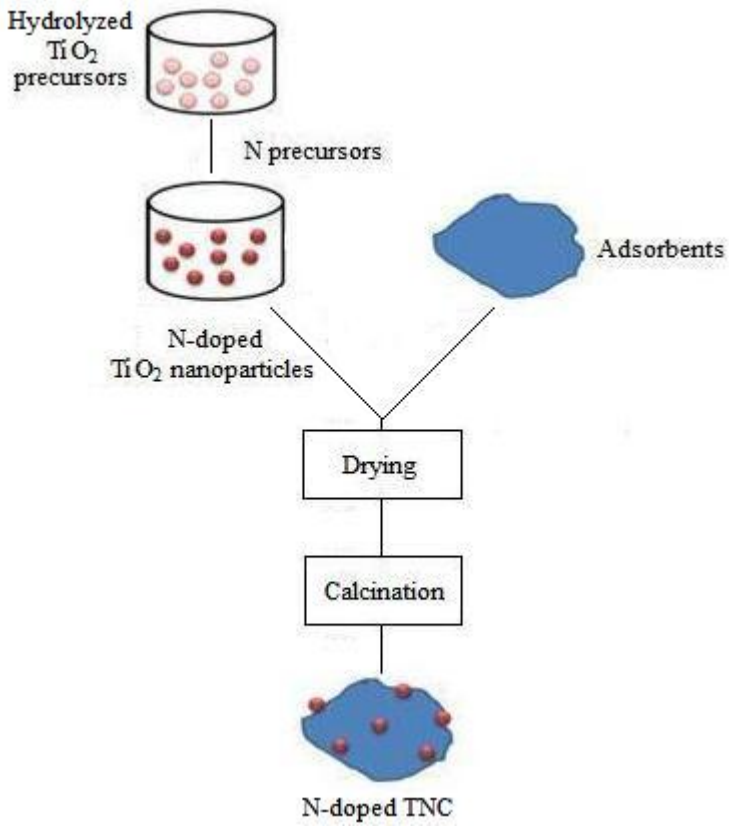

Figure 2.6: A conceptual N-doped TNC preparation via wet chemical impregnation

2.8. Some conclusive remarks

Development of TNC and its wastewater treatment applications are still in the very early infancy. Highlights of this technique include the higher level of overall photoactivity compared to using suspension mixture of TiO_2 photocatalysts and adsorbents, a large capability of scavenging degradation intermediates and potentials of directly utilizing the low-cost visible-light sources. For a TNC prepared via wet chemical impregnation, electronic properties (i.e. amount of charge carrier and its lifetime) and morphological properties (e.g. particle size, surface area and crystal phase) of TiO_2 in as-prepared resultants are largely dependent on the experimental conditions available during the synthesis. Collectively, efforts of TNC preparation and its potential TiO_2 visible-light sensitization via wet chemical impregnation carried out in the literature thus far have formed a useful database for developing future visible-light sensitive TNC. Based upon the literature available from this review, recommendations regarding future efforts can be mainly two-fold. On the

experimental front, visible-light sensitive TNC prepared via a wet chemical procedure, especially N-doping, should be demonstrated in a timely fashion; On the theoretical front, given that most of lab-scale TNC studies with dissolved organic compounds were empirical, a mechanistic model that can address the kinetics between different working processes (i.e. adsorption, diffusion and photocatalysis) within a TNC system is yet to be developed. The optimal design of TNC is only achievable by understanding the underpinning mechanisms of these processes and their synergistic interactions. The following chapters are targeting some of those issues from both experimental and theoretical directions in order to shed some lights on the future application of this technology.

References

[1] C.Perego, P. Villa, Catalyst preparation methods, Catalyst preparation methods, Catal.Today 34 (1997) 281-305.

[2] S. Sampath, H. Uchida, H. Yoneyama, Photocatalytic degradation of gaseous pyridine over zeolite-supported titanium dioxide, J. Catal. 149 (1994) 189-194.

[3] N. Takeda, T. Torimoto, S. Sampath, S. Kuwabata, H. Yoneyama, Effect of inert supports for titanium dioxide loading on enhancement of photodecomposition rate of gaseous propionaldehyde, J. Phys. Chem. 99 (1995) 9986-9991.

[4] Y. Xu, C. H. Langford, Enhanced photoactivity of a titanium (IV) oxide supported on ZSM5 and zeolite A at low coverage, J. Phys. Chem. 99 (1995) 11501-11507.

[5] Y. Xu, C. H. Langford, Photoactivity of titanium dioxide supported on MCM41, Zeolite X, and Zeolite Y, J. Phys. Chem. B 101 (1997) 3115-3121.

[6] E. P. Reddy, L. Davydov, P. Smirniotis, TiO_2-loaded zeolites and mesoporous materials in the sonophotocatalytic decomposition of aqueous organic pollutants: the role of the support, Appl. Catal. B 42 (2003) 1-11.

[7] T. Torimoto, S. Ito, S. Kuwabata, H. Yoneyama, Effects of adsorbents used as supports for titanium dioxide loading on photocatalytic degradation of propyzamide, Environ. Sci. Technol. 30 (1996) 1275-1281.

[8] T. Torimoto, Y. Okawa, N. Takeda, H. Yoneyama, Effect of activated carbon content in TiO_2-loaded activated carbon on photodegradation behaviours of dichloromethane, J. Photochem. Photobiol. A: Chem. 103 (1997) 153-157.

[9] M. Harada, M. Honda, H. Yamashhita, M. Anpo, Preparation of titanium oxide photocatalysts loaded on activated carbon and their photocatalytic reactivity for the degradation of 2-propanol diluted in water, Res. Chem. Intermed. 25 (1999) 757-768.

[10] E. Carpio, P. Zúñiga, S. Ponce, J. Solis, J. Rodriguez, W. Estrada, Photocatalytic degradation of phenol using TiO2 nanocrystals supported on activated carbon, J. Molecular Catal. A 228 (2005) 293-298.

[11] Y. Tao, S. Schwartz, C. Wu, D. W. Mazyck, Development of a TiO/AC composite photocatalyst by dry impregnation for the treatment of methanol in humid air streams, Ind. Eng. Chem. Res. 44 (2005) 7366-7372.

[12] S. X. Liu, X. Y. Chen, X. Chen, A TiO_2/AC composite photocatalyst with high activity and easy separation prepared by a hydrothermal method, J. Hazard. Mater. 143 (2007) 257-263.

[13] B. Zhu, L. Zou, Removal of color compounds from recycled water using combined activated carbon adsorption and AOP decomposition, J. Adv. Oxid. Technol. 12 (2009) 1-8.

[14] X. Dai, L. Zou, Z. Yan, M. Millikan, Adsorption characteristics of N-nitrosodimethylaine from aqueous solution on surface-modified activated carbons, J. Hazard. Mater. 168 (2009) 51-56.

[15] L. Y. Zou, Y. Luo, E. J. Hu, Using titania photocatalysts to degrade toluene in a combined adsorption and photocatalysis process, J. Adv. Oxid. Technol.,10 (2007) 31-36.

[16] B. Zhu, L. Zou, Trapping and decomposing of color compounds from recycled water by TiO_2 coated activated carbon, J. Environ. Manag. (2009), doi:10.1016/j.jenvman.2009.04.008.

[17] C. B. Roop, G. Meenakshi, Activated carbon adsorption, CRC press, Taylor and

Francis Group, New York USA, 2005, pp. 69-74.

[18] D.W. Beck, Zeolite Molecular Sieves. Wiley, New York,1974.

[19] R. W. Matthews, Purification of water with near-u.v. illuminated suspensions of titanium dioxide, Water Res. 24 (1990) 653-660.

[20] J. Sabate, M. A. Anderson, M. A. Aguado, Comparison of TiO_2 powder suspensions and TiO2 ceramic membranes supported on glass as photocatalytic systems in the reduction of chromium (VI), J. Mol. Catal. 71 (1992) 57-68.

[21] R. L. Pozzo, M. A. Baltanás, A. E. Cassano, Supported titanium oxide as photocatalyst in water decontamination: state of art, Catal. Today 39 (1997) 219-231.

[22] C. Colbeau-Justin, M. Kunst, D. Huguenin, Structural influence on charge-carrier lifetimes in TiO_2 powders studied by microwave absorption, J. Mater. Sci. 38 (2003) 2429–2437.

[23] S. Yamazaki, N. Fujinaga, K. Araki, Effect of sulfate ions for sol-gel synthesis of titania photocatalysts, Appl. Catal. A: Gen. 210 (2001) 97-102.

[24] H. J. Kim, K. H. Nam, Y. G. Shul, Preparation TiO_2 fiber and its photocatalytic properties, Mater. Sci. For. 439 (2003) 271.

[25] Y. Huang, B. Zhao, Y. Xie, A novel way to prepare silica supported sulfated titania, Appl. Catal. A: Gen. 171 (1998) 65-73.

[26] M. C. Lu, J. N. Chen, K. T. Chang, effect of adsorbents coated with titanium dioxide on the photocatalytic degradation of propoxur, Chemosphere, 38 (1999) 617-627.

[27] M. Takahashi, K. Mita, H. Toyuki, M. Kume, Pt-TiO_2 thin films on glass substrates as efficient photocatalysts, J. Mater. Sci. 24 (1989) 243-246.

[28] J. A. Montoya, T. Viveros, J. M. Dominguez, L. A. Canales, I. Schifter, On the effects of the sol-gel synthesis parameters on textural and structural characteristics of TiO_2,Catal. Lett. 15 (1992) 207-217.

[29] H. Y. Zhu, Y. lan, X. P. Gao, S. P. Ringer, Z. F. Zheng, D. Y. Song, J. C. Zhao,

Phase transition between nanostructure of titanate and titanium dioxides via simple wet-chemical reactions, J. Am. Chem. Soc. 127 (2005) 6730-6736.

[30] A. Dyer, An introduction to zeolite molecular sieves, John Wiley& Sons, New York, 1988.

[31] Y. Xu, C. H. Langford, Enhanced photoactivity of a titanium (IV) oxide supported on ZSM5 and zeolite A at low coverage, J. Phys. Chem. 99 (1995) 11501-11507.

[32] Y. Hamasaki, S. Ohkubo, K. Murakami, H. Sei, G. Nogami, Photoelectrochemical properties of anatase and rutile films prepared by the sol-gel method, J. Electrochem. Soc. 141 (1994) 660-663.

[33] V. Gourinchas, F. Bocquet, K. Chhor, C. Pommier, Modelling of a continuous reactor for TiO_2 powder synthesis in a supercritical fluid-experimental validation, J. Supercrit. Fluids 9 (1996) 222-226.

[34] S. Boujday, F. Wnsch, P. Portes, J. Bocquet, C. Colbeau-Justin, Photocatalytic and electronic properties of TiO_2 powders elaborated by sol-gel route and supercritical drying, Sol. Energy Mat. Sol. Cell 83 (2004) 421-433.

[35] F. Salvador, C. S. Jimenez, Effect of regeneration treatment with liquid water at high pressure and temperature on the characteristics of three commercial activated carbons, Carbon 37 (1999) 577-583.

[36] V. Augugliaro, M. Litter, L. Palmisano, J. Soria, The combination of heterogeneous photocatalysis with chemical and physical operation: a tool for improving the photoprocess performance, J. Photochem, Photobiol. C: Photochem. Rev. 7 (2006) 127-144.

[37] S. Mario, Some working principles of heterogeneous photocatalysis by semiconductors, Electrochem. Acta. 38 (1993) 1056-1062

[38] L. Zou, B. Zhu, The synergistic effect of ozonation and photocatalysis on color removal from reused water, J. Photochem. Photobiol. A: Chem. 196 (2008) 24-32.

[39] M. Saquiba, M. A. Tariqa, M. Faisala, M. Muneer, Photocatalytic degradation of

two selected dye derivatives in aqueous suspensions of titanium dioxide, Desalination 219 (2008) 301-311.

[40] H. Gerischer, A. Heller, The role of oxygen in photooxidation of organic molecules on semiconductor particles, J. Phys. Chem. 95 (1991) 5261-5267.

[41] G. N. Scharauzer, T. D. Guth, Photocatalytic reactions. 1. Photolysis of water and photoreduction of nitrogen on titanium dioxide, J. Am. Chem. Soc. 99 (1977) 7189-7193.

[42] A. Houas, H. lachheb, M. Ksibi, E. Elaloui, C. Guillard, J. M. Hermann, Photocatalytic degradation pathway of methylene blue in water, Appl. Catal. B: Environ. 31 (2001) 145-157.

[43] Y. Xu, C. H. Langford, UV- or visible-light-induced degradation of X3B on TiO2 nanoparticles: the influence of adsorption, Langmuir 17 (2001) 897-902.

[44] T. Sauer, G. C. Neto, H. J. Jose, R. F. P. M. Moreira, Kinetics of photocatalyitc degradation of reactive dyes in a TiO_2 slurry reactor, J. Photochem. Photobiol. A: Chem. 149 (2002) 147-154.

[45] C. Galindo, P. Jacques, A. Kalt, Photodegradation of the aminoazobenzene acid orange 52 by three advanced oxidation processes: UV/H_2O_2, UV/TiO_2 and VIS/TiO_2: comparative mechanistic and kinetic investigations, J. Photochem. Photobiol. A: Chem. 130 (2000) 35-47.

[46] L. B. Reutergarth, M. Langphasuk, Photocatalytic decolourization of reactive azo dye: A comparison between TiO_2 and us photocatalysis, Chemosphere 35 (1997) 585-596.

[47] W. Z. Tang, H. An, UV/TiO_2 photocatalytic oxidation of commercial dyes in aqueous solutions, Chemosphere 31 (1995) 4157-4170.

[48] M. R. Hoffmann, S. T. Martin, W. Choi, D. W. Bahnemannt, Environmental applications of semiconductor photocatalysis, Chem. Rev. 95 (1995) 69-96.

[49] W. Choi, A. Termin, M. R. Hoffmann, Einflüsse von Dotierungs-Metall-Ionen auf die photokatalytische Reaktivität von TiO_2-Quantenteilchen**,** Angew. Chem. 106 (1994) 1148-1149.

[50] C. Wang, D. W. Bahnemann, J. K. Dohrmann, A novel preparation of iron-doped TiO_2 nanoparticles with enhanced photocatalytic activity, Chem. Commun. (2000) 1539-1540.

[51] Y. Wang, H. Cheng, Y. Hao, J. Ma, W. Li, S. Cai, Photoelectrochemical properties of metal-ion-doped TiO_2 nanocrystalline electrodes, Thin Solid Films 349 (1999) 120-125.

[52] H. Yamashita, M. Honda, M. Harada, Y. Ichihashi, M. Anpo, T. Hirao, N. Itoh, N. Iwamoto, Preparation of titanium oxide photocatalysts anchored on porous silica glass by a metal ion-implantation method and their photocatalytic reactivities for the degradation of 2-propanol diluted in water, J. Phys. Chem. B 102 (1998) 10707-10711.

[53] W. Choi, A. Termin, M. R. Hoffmann, The role of metal ion dopants in quantum-sized TiO_2: correlation between photoreactivity and charge carrier recombination dynamics the role of metal ion dopants in quantum-sized TiO_2: correlation between photoreactivity and charge carrier recombination dynamics, J. Phys. Chem. 98 (1994) 13669-13679.

[54] J. Zhao, C. Chen, W. Ma, Photocatalytic degradation of organic pollutant under visible light irradiation, Top. Catal. 35 (2005) 269-278.

[55] D. Chatterjee, S. Dasgupta, Visible light induced photocatalytic degradation of organic pollutant, J. Photochem. Photobiol. C: Photochem. Rev. 6 (2005) 186-205.

[56] F. Han, V. S. R. Kambala, M. Srinivasan, D. Rajarathnam, R. Naidu, Tailored titanium dioxide photocatalysts for the degradation of organic dyes in wastewater treatment: a review, Appl. Catal. A: Gen 359 (2009) 25-40.

[57] R. Asahi, T. Morikawa, T. Ohwaki, K. Aoki, Y. Taga, Visible-light photocatalysis in nitrogen-doped titanium oxides, Science 293 (2001) 269-271.

[58] C.H. Park, S. B. Zhang, S. H. Wei, Origin of p-type doping difficulty in ZnO:

The impurity perspective, Phys. Rev. B 66 (2002) 073202-1-3.

[59] C. Burda, Y. Lou, X. Chen, A. C. S. Samia, J. Stout, J. L. Gole, Enhanced nitrogen doping in TiO nanoparticles, Nano Lett. 3 (2003) 1049-1051.

[60] X. Chen, C. Burda, Photoelectron spectroscopic investigation of nitrogen-doped titania nanoparticles, J. Phys. Chem. B 108 (2004) 15446-15449.

[61] X. Qiu, C. Burda, Chemically synthesized nitrogen-doped metal oxide nanoparticles, Chem. Phys. 339 (2007) 1-10.

[62] M. Batzil, E. H. Morales, U. Diebold, Phys. Influence of nitrogen doping on the defect formation and surface properties of TiO_2 rutile and anatase, Rev. Lett. 96 (2006) 026103-1-4.

[63] O. Diwald, T. L. Thompson, E. G. Grolaski, S. D. Walck, J. T. Yates, Photochemical activity of nitrogen-doped rutile TiO_2(110) in visible light, J. Phys. Chem. B 108 (2004) 52-57.

[64] M. Kitano, K. Funatsu, M. Matsuoka, M. Ueshima, M. Anpo, Preparation of nitrogen-substituted TiO thin film photocatalysts by the radio frequency magnetron sputtering deposition method and their photocatalytic reactivity under visible light irradiation, J. Phys. Chem. B 110 (2006) 25266-25272.

[65] O. Diwald, T. L. Thompson, T. Zubkov, E. G. Goralski, S. D. Walck, J. T. Yates, Photochemical activity of nitrogen-doped rutile TiO_2(110) in visible light,J. Phys. Chem. B 108 (2004) 6004-6008.

[66] R. Nakamura, T. Tanka, Y. Nakato, Mechanism for visible light response in anodic photocurrents at N-doped TiO_2 film electrodes, J. Phys. Chem. B 108 (2004) 10617-10620.

[67] H. Irie, S. Washizuka, N. Yoshinob, K. Hashimoto, Visible-light induced hydrophilicity on nitrogen-substituted titanium dioxde films, Chem. Commun. (2003) 1298-1299.

CHAPTER 3

A PARAMETRIC STUDY OF VISIBLE-LIGHT SENSITIVE TITANIA PHOTOCATALYSTS SYNTHESIS VIA A WET CHEMICAL N-DOPING METHOD

Abstract

In present chapter, a brief literature review on the recent attempts of titania visible-light sensitization via wet chemical N-doping was conducted first. Then it was followed by a parametric study of visible-light sensitive TiO_2 via a facile wet chemical N-doping method was carried out in order to understand the experimental factors on obtaining the optimal photocatalytic ability. Visible-light activity of as-prepared products was assessed using solutions of methylene blue (MB) as model pollutants. Optimal visible light activity was achieved at equal N-to-Ti precursor molar ratio and 350˚C calcinations. Characterization of structural, chemical and optical properties of synthesized TiO_2 photocatalysts was also undertaken to elucidate the effects of N-to-Ti precursor molar ratio and calcinations temperature on the resulting photocatalytic activity. The pH value of N-doped TiO_2 sol during the preparation was also found to be an effective indicator of N-doping quality without using any post-synthesis analysis. These findings could be utilized in the successful development of TiO_2 photocatalysts or its nanocomposites for cost effective solar-driven environmental friendly technology.

3.1. Introduction

Nano-sized TiO_2 photocatalyst has become a strong candidate for environmental clean-up, which can effectively oxidize a wide range of dissolved organic compounds, more to this advantage, at ambient or moderate room conditions [1,2]. Other reported benefits include low cost, greatly enhanced surface area, tunable properties which can be modified by particle size reduction, doping, sensitizer, etc., no substantial loss of photocatalytic activity after repeated process cycles, enhanced photo-induced charge transport and no depletion layer formation on the surface. [3] However, it is well known that the band gap energy of TiO_2 is intrinsically wide, i.e. between 3.0 and 3.2eV (3.0 for rutile and 3.2 for anatase). This means plain TiO_2 semiconductors only absorb a small portion (5%) of solar spectrum in the UV region. Early attempts on visible-light sensitization of TiO_2 mainly involved the doping of transition metal elements which, however, has the drawbacks of requiring intensive energy and expensive ion implantation facilities, thermally unstable, increasing free charge carrier trapping in bound electron-hole pairs, tending to form charge carrier recombination centres, possible photo-corrosion and harmful nature of the dopants [4]. More importantly, these cationic dopants only result in limited band-gap changes, and in some cases, do increase the light absorption, but not the photocatalytic activity. As a consequence, more significant advances in this field were achieved on doping TiO_2 photocatalysts with non-metallic or anionic elements such as carbon, sulfur, halides, phosphor and boron [5]. Among the available, nitrogen has become the most effective dopant due to its similar size to oxygen, and small ionization energy [6,7]. The origin of visible light activity, i.e. N dopants or O vacancies [8], substitoinal N or interstitial N [9,10], enhanced magnetic properties [11,12], band gas narrowing or new mid-band creation [13,14] and its photocatalytic mechanism (i.e. whether or not through OH radicals) arising from N-doping are still subject to debate. Most recently, Burda et al. developed N-doped TiO_2 via a sol-gel method (i.e. hydrolysis of titanium tetraisoproxide, TTIP with triethylamine) and claimed that it did not have high-temperature induced surface property change and have fine control of the nitrogen doping level of up to 8% compared with other methods, e.g. the sputtering and implantation [15,16,17], high temperature sintering TiO_2 under N-containing atmosphere [18,19,20], etc.

Previously, many experimental parameters of sol-gel synthesized undoped TiO_2 photocatalysts and their effects were investigated, including water/alkoxide molar ratio, pH, type, and amount of solvent, reaction temperature, and mixing conditions [21,22]. For example, increased water/alkoxide ratio would lead to smaller TiO_2 particle size. Collectively, science behind sol-gel synthesis of pure TiO_2 photocatalysts has become quite established. In contrast, recent studies on N-doped TiO_2 photocatalysts preparation via sol-gel methods are still lacking of similar investigations on N-doping related experimental parameters (i.e. N-to-Ti precursor ratio and calcinations temperature), and more importantly their influences on the visible light photoactivity. It is evident to speculate that the optical and photocatalytic properties of as-prepared products are sensitively dependent on these parameters during the synthesis. In this work, a visible-light activity optimisation of N-doped TiO_2 photocatalysts synthesized via a sol-gel method was carried out in order to provide some useful insights in near term development of TiO_2 photocatalysts or its composites for solar-driven environmental clean-up[23,24]. The visible light activity of as-prepared N-doped TiO_2 was assessed using aqueous methylene blue (MB) as a model pollutant, which is often considered to be one major dye pollutant in the textile industry effluent and difficult to be degraded by the conventional biological treatment.

3.2. Effects of N-doping on TiO_2 visible-light sensitivity

An attempt to summarize the latest literature on visible-light sensitive N-doped TiO_2 nanoparticles synthesized by wet chemical methods is undertaken (Table 3.1), of which key experimental variables are listed for comparison. Optimal values of the experimental parameters in each study are also underlined where possible. Despite the viability of TiO_2 visible light sensitization through wet chemical N-doping, there are still several discrepancies in the literature regarding the promoting effect of N-doping on the visible-light sensitivity of TiO_2:

1) It is still subject to a debate that whether doped nitrogen or oxygen vacancies are responsible for the photocatalytic activity shift towards visible-light range. Whilst most of works in this area agreed upon the necessity of N presence in N doped TiO_2, Ihara et al. claimed that the visible light sensitivity of N-TiO_2 nanoparticles arise from the oxygen-deficient sites, as the existence of N-dopants was only necessary to retard the reoxidation of oxygen-deficient TiO_2, which authors considered to be essential for

visible-light sensitization[42]. The recent development on this subject provided by Lin et al. further suggested that N dopants can only affect the absorption below 500nm wavelength, whereas the O vacancies are responsible for the visible light sensitization at wavelength above 500nm[25].

2) N dopants in the TiO_2 resultants can exist as either substitutional in form of Ti-N-Ti bond or interstitial in form of Ti-O-N or Ti-N-O bond as illustrated in Fig. 3.1. For the former, literature agreed that the binding energy (BE) of N 1s peaks is fingerprinted at 396-398eV; for the later, that is 400-406eV. This dispute can be dated back to the heated debate over the originality of Asahi's work, as Sato challenged the first discovery of N-doped TiO_2 and its visible light sensitivity to his credit[26]. This was later cleared up by the fact that the N-doped TiO_2 obtained by Asahi belonged substitutional group, whereas the one reported by Sato et al. 15 years earlier was more interstitial like. Based on some theoretical densities-of-states (DOS) calculations of different substitutional doping (i.e. C, N, F, S for O) Asahi maintained the critical role of Ti-N bond on visible light sensitivity of N-TiO_2 in his famous work, although their samples in absence of any Ti-N bond were indicative of visible light activities as well [7]. Almost at the same time, Sakatani and Koike suggested that the nitrogen atoms were doped at the interstitial sites and that these interstitial nitrogen atoms were responsible for visible light response[27]. The latest progress on this subject contributed by Peng et al. explained that both interstitial and substitutional N dopants can enable the visible light sensitivity of TiO_2 nanoparticles, whereas only the former is higher than the later in terms of visible light activity[28].

It is estimated that the existence of these two N doping states would vary according to the different preparation techniques, in many cases, both coexisted. However, larger proportion of N dopants in TiO_2 nanoparticles prepared by wet chemical methods should more likely belong to the interstitial doping group (see Table 3.1), as it is a consensus that Ti-O bond is quite stable at the mild conditions, which make it very difficult for nitrogen to replace the oxygen sites during the diffusion-controlled wet chemical preparation. Plus, N containing amino substances would undergo serious oxidation during the calcinations treatment. This could result in the existence of various NO_x species, such as NO, NO_2, NO^{2-}, NO_2^-, NO_2^{2-}, $NO_3^-$and $N_2O_2^{2-}$, etc. in N-doped TiO_2 resultants, which has been observed widely in the literature [29,30,31,32].

Finally, it is noteworthy that the radius of these N-containing species are usually too large to dope into the TiO_2 bulk, so they more likely exist at the surface of the catalysts particles through formed chemical bonds or be adsorbed at the meso-pores. This, however, should barely hinder its application of water treatment at all, as the photoactive surface of an N-doped TiO_2 photocatalyst is generally considered to be sufficient during photodegradation of dissolved organic compounds.

3) Asahi ascribed the visible light absorbance in N-doped TiO_2 to the band gap narrowing effect, which was resulted from the interaction between N_{2p} and O_{2p} state [7]. Later on, several other researcher in their follow-up studies on N-doped TiO_2 suggested that the creation of new mid-bands localized within the band-gap of TiO_2 is the origin of visible light activity based on density-functional-theory (DFT) calculations [33,34,35,36,37,38].For example, Di Valentin et al. suggested that the single-atom nitrogen impurities form either diamagnetic (N_b^-) or paramagnetic ($N_b^\bullet$) bulk centres. Both types of N_b centres give rise to localized N_{2p} states within the band gap of the oxide, as illustrated in Fig. 4, rather than mixing with O_{2p} states for both rutile and anatase TiO_2. To clarify, Payne and his co-workers further claimed that the hybridization between N_{2p} and O_{2p} states is only possible when the N-doping level exceeds 20% in anatase TiO_2[25]; Yang et al. found that the interaction between N_{2p} and O_{2p} states is less pronounced when N-doping is the substitutional type[38]. In a most recent paper, Sun et al. attempted to correlate the concentration of NO_2^{2-} with the visible light activity of as-prepared N-doped TiO_2 photocatalysts, as their DFT calculations supported a NO_2^{2-} induced formation of new mid-band energy levels near conduction band (CB)[52].

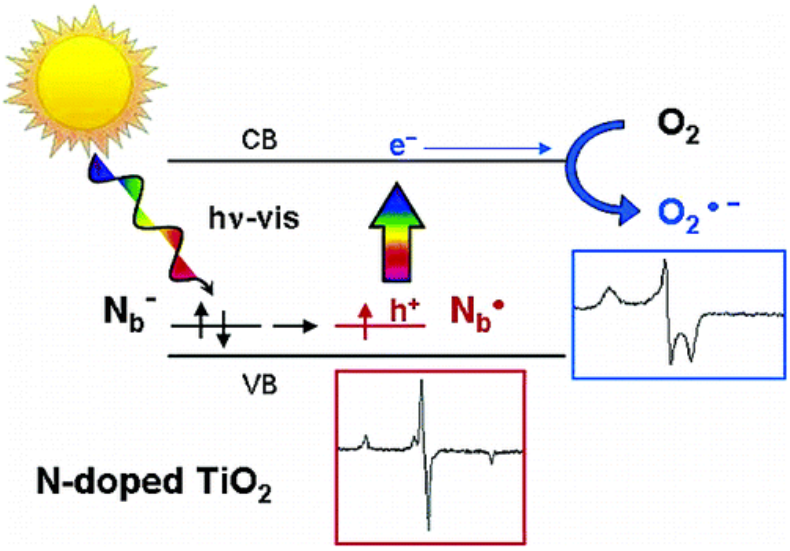

Figure 3.1: Sketch of the proposed mechanism for the processes induced by vis-light irradiation of the N-doped sample in O_2 atmosphere [32].

Other promoting effects of N-doping on the photocatalytic activity of TiO_2 observed in the literature include the increase in resultant surface area and the number of surface hydroxyl groups[53], of which the later would in turn increase the concentration of beneficial free hydroxyl radicals for the TiO_2 photodecomposition [39]. The nitrogen content in the N-doped TiO_2 resultants is one major indicator of the doping quality, provided that the visible light absorbance generally increases with it, ceteris paribus. The N content reported in each study varies from 0.08 to 8% (even reported a 20% sample) along with different degree red-shift towards the visible light range. Apart from different preparation conditions, other factors to the uncertainty could arise from the content of other visible-light induced dopants (such as C, S, etc) as impurities from organic precursors or simply the chemisorbed N-containing molecules on as-prepared TiO_2 nanoparticles surface that are non-active, such as NH_3.

To test N-doped TiO_2 photocatalytic activity, some lab-scale investigations on the degradations of dissolved organic compounds under simulated environmental conditions were carried out. Various decomposition degree and rates were reported, of which most claimed to be satisfactory, and yet not directly comparable between studies. Other limitations of the current literature include:

1) Most of the works were carried out in simulated or artificial visible-light irradiation, while reported activities under natural sunlight are still rare.

2) Photocatalytic decomposition of large molecular weight organics in solution by N-doped TiO_2 nanoparticles has not yet been reported. This is mainly due to the fact that depending on different dissolved organic compounds, the degree and rate of total mineralization, i.e. decomposition of organic pollutants into harmless products, varies. Further investigations in this aspect are certainly of great interests, especially in terms of water treatment applications. At the current stage, the feasibility of their applications is still restricted to dilute synthetic solutions.

3) Furthermore, it should be noted that there is not yet a clear correlation between N-doping level and overall photocatalytic activity, since the latter is affected by many other factors, such particle size, surface area and functionlization. This has also made it very difficult to provide a universal guidance at this stage with a certainty for each variable of N-doping preparation. Instead of one-factor-at-a-time style investigation, a statistically valid parameter optimization investigation for general optima of photocatalytic activity will be certainly useful. Optimization of the preparation technique is envisaged to be beneficial to the near term development of TiO_2 photocatalysts or its nanocomposites for solar-driven environmental clean-up, i.e. dissolved organic compounds removal in wastewater treatment.

Table 3.1: experimental conditions and properties as-synthesized N-doped TiO_2 via wet chemical methods

Studies	**TiO_2 precursors**	**N precursors**	**N-doping conditions**			**Calcinations T [°C]**	**N-doped TiO_2 properties**		
			pH	**T [°C]**	**solvent**		**N wt%**	**N doping state**	**size [nm]**
Gole et al.[40]	$Ti[OCH(CH_3)_2]_4$	Triethylamine Hydrazine	2		Aqueous isopropanol		5.1, 17.3	Substitutional	10
Sathish et al.[41]	$TiCl_3$	Ammonia	8.5		Na_2S solution	400*, 500, 600		Substitutional	14
Ihara et al. [42]	$Ti(SO_4)_2$	Ammonia 28%	7			400	0.2		13*
Liu et al. [43]	$Ti[OCH(CH_3)_2]_4$	Ammonia		85	Aqueous ethanol	400			
Sakthivel et al.[44]	$TiCl_4$	Ammonia Ammonium carbonate Ammonium bicarbonate	5.5			400	0.08-0.13		7-10
Sakthivel et al.[45]	1). $Ti[OCH(CH_3)_2]_4$	Thiourea			Ethanol	500	0.07	Interstitial	22
	2). $TiCl_4$					600*	0.3		7

Sano et al.[46]	$TiCl_4$	2,2'-bipyridine			300 in air, 380 in N_2		Interstitial	7.7-8.7
Wang et al.[47]	$Ti(OBu)_4$	Ammonia 25%		HNO_3 and ethanol	400-800		Interstitial	13.9-63.7
Kobayakawa et al.[48]	$Ti(OH)_4$	Urea			400			
Ananpattarachai et al.[49]	$Ti[OCH(CH_3)_2]_4$	Diethanolamine	4	HNO_3 and ethanol	800	4.11	Interstitial	
		Triethylamine				0.64		
		Urea				5.01		
Wang et al.[50]	$TiCl_3$	Diethylamine			140	0.24-0.29	Interstitial	
		Triethylamine				0.34-0.44		
		Ethylenediamine				0.23-1.70		
Sun et al.[51]	$Ti(OBu)_4$	Ammonia			450	1.76		14
Sun et al.[52]	$TiCl_4$	Mixture of ammonia and hydrazine hydrate*	5.5	~ 0	400	0.45	Interstitial	
		Ammonia				0.21		
		Hydrazine hydrate				0.24		

Xu et al.[53]	$Ti(OBu)_4$	Ethylamine	1.5	Isopropanol			Substitutional	3.5
Wang et al.[54]	$Ti(OBu)_4$	Ammonia 25%		HNO_3 and ethanol	350		Interstitial	9
Sato et al.[55]	1).$Ti[OCH(CH_3)_2]_4$ 2). $TiCl_4$	Ammonia	0		>330		Interstitial	
Livraghi et al.[56]	$Ti[OCH(CH_3)_2]_4$	NH_4Cl		Isopropanol	497		Interstitial	50
Belver et al.[57]	$Ti[OCH(CH_3)_2]_4$	2-methyoxyethylaimne N,N,N',N'-tetramethylethyl-enediamine 1,2-phenylenediamine		Isopropanol		0.03-0.53		
Sathish et al.[58]	$Ti[OCH(CH_3)_2]_4$	melamine	50	Aqueous ethanol	400,500*,600,700		Interstitial	25-50

*indicates the optimum of the variable within reported experimental conditions; Calcinations were carried out in air if not otherwise specified

3.3. Experimental

3.3.1. N-doped TiO_2 preparation

All reagents in this work were of analytical grade and used as received. In a typical N-doped TiO_2 preparation, 40ml of titanium (IV) butoxide ($Ti(OC_4H_9)_4$) (Sigma Aldrich) were first dissolved in 160ml of ethanol (C_2H_5OH) by 30 mins stirring at room temperature to obtain solution A. In addition, 400 ml of deionised water was mixed with a certain amount of nitric acid (HNO_3) by 10 mins stirring at room temperature to obtain solution B. Solution B was then added drop-wise into solution A under vigorous stirring, and this was then followed by the hydrolysis of $Ti(OC_4H_9)_4$ under stirring conditions at room temperature until a transparent sol was formed. Different ratio of N-doping was achieved by dropwise addition of a certain amount of triethylamine (Sigma Aldrich) to the formed TiO_2 sol under continuous stirring (24hr). The resulting mixture was subsequently dried by evaporation at 100°C in 2-3hrs, followed by calcinations at designated temperatures (250°C, 350°C, 450°C and 550°C) for 2 hr. Temperature ramp during the calcinations was set at 5°C /min. In addition, commercially available TiO_2 nanoparticles, P25 from Sigma Aldrich, were also used for comparison.

3.3.2. Characterization of the experimental materials

For characterization of the as-prepared N-doped TiO_2, the Brunauer-Emmett-Teller (BET) specific surface area measurement was obtained based on the N_2 adsorption-desorption isotherms, determined at 77K via a Belsorp apparatus, Japan. Before each measurement, samples were degassed at 200°C for 15hr. Optical properties of N-doped TiO_2 were obtained using UV-Vis diffusion reflectance spectroscopy (UV-Vis DRS) in the range 200-800nm, which was conducted by a Varian Cary 100 UV-Vis spectrophotometer equipped with diffuse reflectance accessories. The crystalline structure of N-doped TiO_2 was investigated by powder XRD technique on an X-ray diffractometer (Mini Material Analyser, Diffraction Technology) using Cu Kα radiation (λ=0.154056 nm) and operating in the angle range of 20-80 degree. The scan speed was $0.5°min^{-1}$. The amount of $OH^{\cdot}$ radicals generated on N-doped TiO_2 photocatalysts surface under visible light irradiation was investigated using a fluorescence spectrometer (Cary Eclipse) with a setting of the excitation wavelength

at 312nm and emission wavelength at 426nm. In typical test, about 20mg of N-doped TiO_2 photocatalysts was added to 30ml of terephthalic acid (TA) solution with a concentration of 1g/L and pH=12 adjusted by 0.1M NaOH. In each case, the visible light irradiation over the TiO_2-TA suspension which was supplied by a Newport Oriel series Q solar simulator with a 100W Xe lamp was kept for 4 hr to generate high fluorescence hydroxyterephthalic acid (TAOH), which is the only product with significant fluorescence [59].

$$OH^{\cdot} + TA \rightarrow TAOH \quad (1)$$

Zeta potentials were measured at different N-to-Ti ratio by micro-electrophoresis on a Malvern ZetaSizer Nano ZS. The instrument can calculate zeta potentials by determining the migration distance of colloid in electric field with microscopy observation. It is imperative that the final results were obtained from statistical analyses of multiple sampling. The data of zeta potentials were the mean values of 10 particles. As charges density and nature on TiO_2 nanoparticles has close relation with pH values, zeta potentials were measured at different pH, which was adjusted by 0.1M NaOH solution.

3.3.3. Photocatalytic experiment

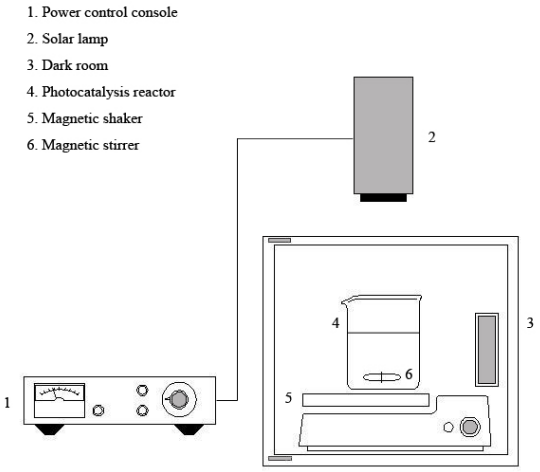

Figure 3.2: A schematic set-up of the experimental photocatalysis reactor

To evaluate the visible-light activity of as-prepared N-doped TiO_2, the photodegradation of MB (Sigma Aldrich) was carried out in a 200ml cylindrical glass vessel under a visible light irradiation, which is supplied by a Newport Oriel series Q

solar simulator with a 100W Xe lamp. A dichoic mirror (NewSpec 66219) was mounted on the lamp to eliminate infrared and UV irradiation. The schematic experimental set-up was shown in Fig. 3.2. As a result, the total collimated cut-off irradiance between 420 and 630nm was measured approximately 570mW on the surface of sample by a Newport optical power meter 1918-C. In a typical test, 30 mg N-TiO_2 photocatalysts were added into 100 ml of 15 mg/L MB solution (a typical concentration observed in wastewater), respectively. For all cases, 2.5ml suspension was retrieved with a filter syringe at a defined time interval and then centrifuged. The concentration of MB was analysed using a Varian Cary 100 UV-Vis spectrophotometer at 648nm, of which the decrease in absorption could indicate the degradation of aromatic structures in MB molecules.

Photocatalytic reaction rates are also calculated using a pseudo-first-order kinetics [60]:

$$\ln[A_0/A]=kt \quad (2)$$

where k is the apparent rate constant, A_0 is taken as the equilibrium absorbance of MB at 254nm and A is that at time t. In a series of blank experiments conducted, no self-decomposition of MB was found to occur in the absence of TiO_2 photocatalysts with visible-light illumination at ambient experimental conditions or vice versa.

3.4. Results and discussion

3.4.1. Effect of calcinations temperature

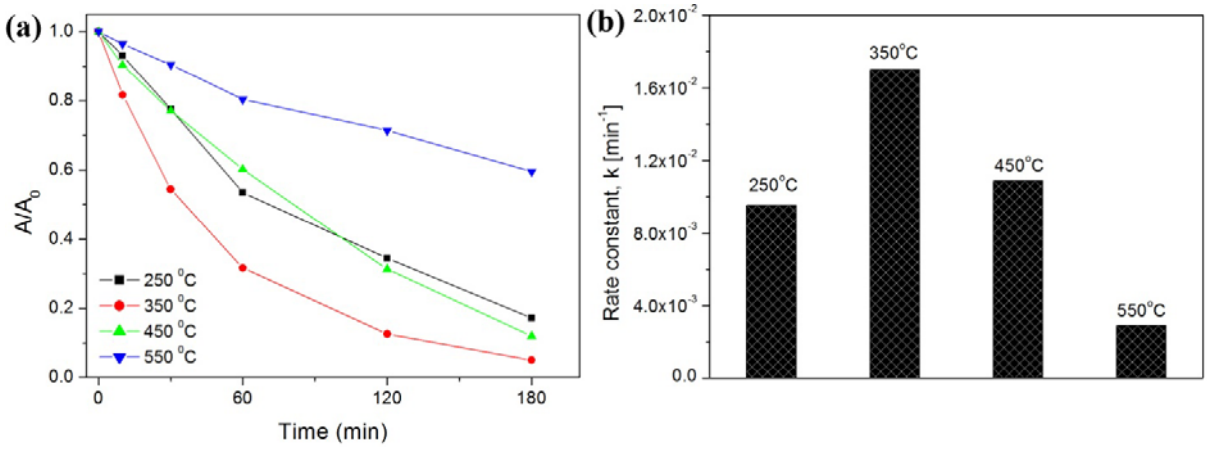

Figure 3.3: Visible-light photocatalytic activities of N-TiO_2 photocatalysts under calcinations temperature

Generally, the photocatalytic activity of TiO_2 photocatalysts increases with calcinations temperatures in the relative lower range (<200°C), as sufficient calcinations temperature is required to initiate the proper crystallinity of the TiO_2 photocatalysts and thus essential for the formation of photocatalytic activity. Nevertheless, high temperature calcinations were reported to have adverse effects on TiO_2 photocatalysttic ability. As Fig. 3.3 shows in this work, visible-light photocatalytic activities of N-TiO_2 photocatalysts prepared under calcinations temperature rose first (250˚C ~350˚C) and then dropped dramatically as the calcinations temperature increased above 350˚C. The potential reason behind the adverse effects of high calcinations temperature could be multi-fold, which could be better elucidated by interpreting several characterizations.

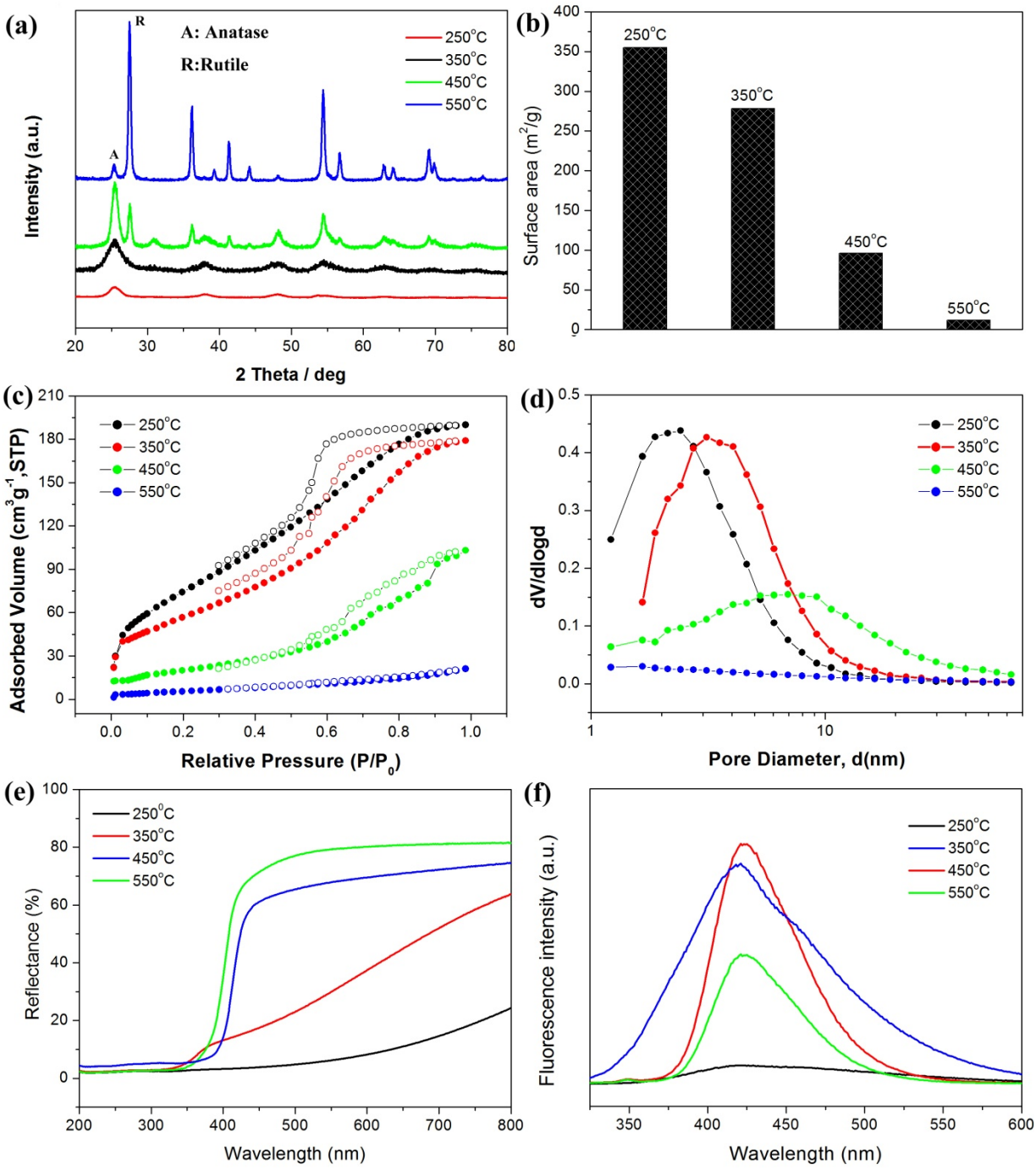

Figure 3.4: XRD patterns (a), surface area (b), nitrogen adsorption-desorption isotherm (c), pore size distribution (d), UV-Vis DRS spectra (e), and fluorescence spectra (f) of N-doped TiO_2 under different calcinations temperatures

First of all, one major factor that affects the TiO_2 photocatalytic ability is the crystallinity. The N-TiO_2 crystal structure under calcinations temperature can be interpreted from XRD pattern in Fig. 3.4 (a), where the major anatase (1 0 1) and rutile (1 1 0) characteristic peaks are marked at 25.4° and 27.5°. It can be observed

that anatase crystal feature become more noticeable when calcinations temperature increased from 250°C to 350°C. Upon further increase of calcinations temperature (up to 450°C), rutile phase begin to appear. As one of two common TiO_2 species, rutile form generates fewer charge carriers with lower lifetimes than that of an anatase type TiO_2, when in the same nano-sized particles form with the same crystalline quality and reactive surface properties[61]. Therefore, N-TiO_2 crystal phase transformation induced by high temperature is one factor that account for the decrease of photocatalytic ability after the calcinations temperature reach 350°C.

Based on the XRD results, the crystal size of the N-TiO_2 microspheres are usually estimated using the Scherrer formula:

$$L=K\lambda/\beta\cos\theta \quad (2)$$

Where L is the crystalline size in nm, λ (0.154056nm) the wavelength of the X-ray radiation, K the usually taken as 0.89, θ is the diffraction angle, λ is the X-ray wavelength corresponding to the Cu Kα irradiation, and β is the line width at half-maximum height after subtraction of equipment broadening for the peak at 2θ=25.4°for anatase and 27.5 for rutile (the highest intensity peak of each phase). As calcinations temperature increases, the crystal sizes of as-prepared N-TiO_2 photocatalysts were estimated to be 4 (anatase) nm for 250°C, 5(anatase) nm for 350°C, 8.5(anatase) and 17(rutile) nm for 450°C, 18.5(anatase) and 24(rutile) nm for 550°C, respectively. It is clear that high temperatures increased the TiO_2 crystal size for both anatase and rutile phase, which could lead to surface area loss to various extents. As confirmed in Fig. 3.4 (b), surface areas of the N-doped TiO_2 consistently decreased with calcinations temperature with a near quantitative loss from 350°C to 450°C. Since higher surface areas could draw more contaminant molecules to the vicinity of photocatalytic active sites and thus increase the photocatalytic rate, high-temperature-induced surface area loss in N-doped TiO_2 is detrimental to the N-doping quality as well.

To understand the surface structure of the as-prepared N-doped TiO_2 better, nitrogen adsorption-desorption data was also obtained and analysed. Fig.3.4 (c) represent the nitrogen adsorption-desorption isotherm for N-TiO_2 photocatalysts prepared under

different calcinations temperatures. It can be seen from Fig. 3.4 (c) that the N-TiO_2 prepared under 250˚C, 350˚C and 50˚C calcinations all features type IV isotherm according to the BDDT classification [62]. This phenomenon is usually associated with the capillary condensation and suggestive of the presence of mesopores. Nevertheless, the appearances of hysteresis loop at the high pressure are quite different, where the N-TiO_2 prepared under 250˚C and 350˚C calcinations belong to H2 type and that under 450˚C calcinations is more like H3 type. For the N-TiO_2 prepared under 550˚C calcinations, the isotherm shape was somewhat transited to type II isotherm, which is usually typical of non-porous or macroporous particles. The pore size distribution pattern of N-TiO_2 photocatalysts prepared under different calcinations temperatures was obtained via the BJH approach, which are depicted in Fig. 3.4 (d). For the N-TiO_2 prepared under 250˚C and 350˚C calcinations, the shape of pore size distribution profile is much similar with narrow peaks, whereas the pore volume for 350˚C sample is predominantly concentrated around the pore size of 2nm and that for 250˚C sample is slightly shifted left to the microporous region. As the calcinations temperature increased to 450˚C and 550˚C, the peak of pore size distribution became broader with significantly reduced total pore volume.

Another aspect in the adverse effect of elevated calcinations temperature is the visible-light absorbance reduction of N-doped TiO_2. This was usually observed by the fading of the colour intensity of the products, and also reflected on the red shift of optical absorbance towards visible light range in Fig. 3.4 (e). The optical absorbance and reflectance was commonly used to study the capability to visible-light sensitize the TiO_2 nanoparticles. Fig. 3.4 (e) demonstrates that the reflectance within visible-light range (400-800nm) was getting higher as calcinations temperature increased. In extreme, the UV-Vis DRS profile under 550˚C calcinations could be very similar to that of the undoped TiO_2 photocatalysts with a nearly vertical shoot of light reflectance at around 400nm. This is probably due to the thermal release of the doped nitrogen and its re-substitution by oxygen atoms under high temperature calcinations. Given that retaining sufficient visible-light absorbance within TiO_2 nanoparticles is essential for effective visible-light sensitization, high calcinations temperature is also unfavourable for N-doping quality.

During the TiO_2 photocatalysis process, it is widely acknowledged that superoxide species and, specifically, $OH^{\cdot}$ radicals, are active reagents for the mineralization of the organic compounds into nontoxic form such as carbon dioxide and water, which is realized through the surface contact of $OH^{\cdot}$ radicals and C-H bonds. As reported previously, the $OH^{\cdot}$ radicals generated by means of visible light irradiation can react with TA to produce high fluorescence TAOH, which is the only product with significant fluorescence. This offered a more direct approach to investigate and compare the generation of $OH^{\cdot}$ radicals over the TiO_2 surface. Fig. 3.4 (f) illustrates the fluorescence spectra produced by TAOH for N-TiO_2 photocatalysts prepared under different calcinations temperatures. It can be observed that the wavelength of maximum emission were similar for N-TiO_2 samples to be at 426nm, whereas the shapes of the spectra characteristics to the reaction product varies. The peak area of N-doped TiO_2 under high temperatures (450°C and 550°C) calcinations appear to be narrower, which was probably accompanied by the phase transition to rutile. The peak area is also known to be associated with the total amount of $OH^{\cdot}$ radicals generated over the TiO_2 surface. As a result, it can be seen that N-TiO_2 photocatalyst under 350°C calcinations generated the highest amount of $OH^{\cdot}$ radicals. As calcinations temperature increased above 350°C, the amount of $OH^{\cdot}$ produced over the TiO_2 surface began to decline. This also confirms that rutile phase is less active than anatase phase in term of photocatalytic capacity. In addition, it is also found that the peak area for N-doped TiO_2 under 250°C calcinations is minimal probably due to its poor crystallinity, however, with much higher photocatalytic rate than that under 550°C calcinations (Fig. 2(b)). Researchers have established that the oxidizing species ($^{\cdot}OH$) generated by the photocatalyst, does not migrate very far from the active centers of the TiO_2 and thus degradation takes place virtually on the catalyst surface [63]. It can be concluded that higher surface area is more of a deciding factor during the TiO_2 photocatalysis process.

In summary, moderate range of calcinations temperature (around 350˚C) appeared to be the optimal for N-doping quality, which can be ascribed to the anatase phase of N-doped TiO_2 products, high surface area, sufficient visible-light absorbance, and highest production of $OH^{\cdot}$ radicals.

3.4.2. Effect of N-to-Ti precursor molar ratio

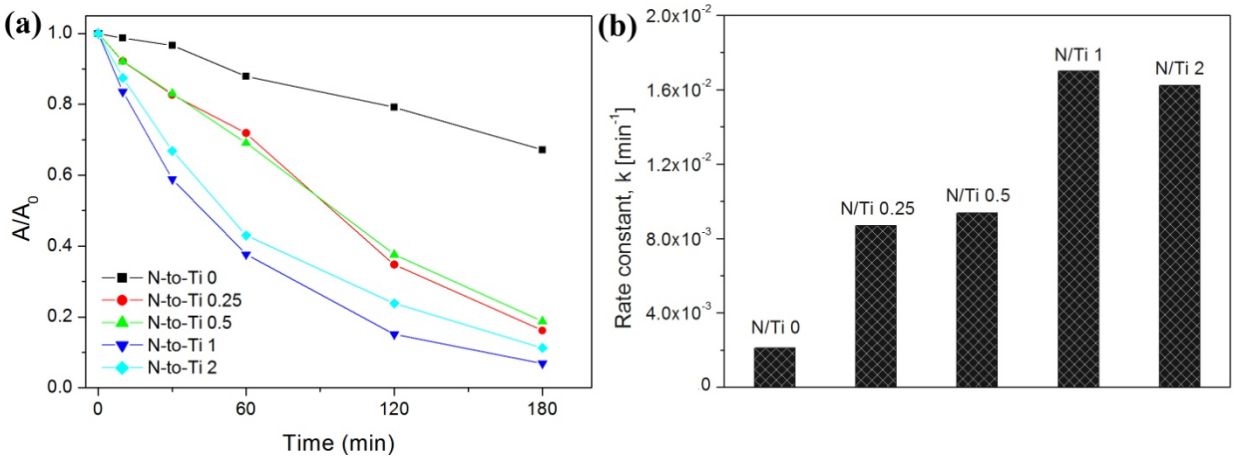

Figure 3.5: Visible-light photocatalytic activities of N-TiO_2 photocatalysts prepared under different N-to-Ti precursor molar ratio

During the sol-gel preparation of N-doped TiO_2, N-to-Ti precursor molar ratio is another important aspect that could influence the resulting doping quality, provided that the nitrogen content would generally increase with N-to-Ti precursor molar ratio in the final N-doped TiO_2 products. Fig. 3.5 (a) illustrates the visible-light photocatalytic activities of N-doped TiO_2 prepared under different N-to-Ti precursor molar ratio, which was also evaluated by the photocatalytic rate constant, k in Fig. 3.5 (b). It can be seen that visible-light photocatalytic activities increased with the N-to-Ti precursor molar ratio until it reached 1.

XRD pattern of N-doped TiO_2 prepared under different N-to-Ti precursor molar ratio are shown in Fig. 3.6 (a), where the major anatase (1 0 1) and rutile (1 1 0) characteristic peaks are marked at 25.4° and 27.5°. Apparently, all the TiO_2 photocatalysts with N dopant belong to anatase phase. It seems that increasing the N precursor ratio did not have significant effect on TiO_2 crystal size, which was estimated to be around 5nm based on the Scherrer formula. However, when the N precursor ratio dropped down to zero (N-to-Ti 0), the major peak of rutile phase begins to show up in Fig. 5(a). It can be concluded that N-doping has some hindering effects on TiO_2 crystal formation of rutile phase under the same calcinations temperature. For the bare TiO_2 (N-to-Ti 0), crystal sizes of anatase and rutile phase were estimated to be 6.6 and 12.9 nm, respectively.

Increasing the N precursor ratio also seemed to increase the surface area of N-TiO_2 products as illustrated in Fig. 3.6 (b). As we discussed, this could certainly be

beneficial to the resulting photocatalytic activity as well. However, it is noteworthy that the surface area augmentation also became less pronounced when N-to-Ti precursor molar ratio exceeded 1. Nitrogen adsorption-desorption data of N-TiO_2 photocatalysts prepared under different N-to-Ti precursor molar ratio was also obtained and analysed, which is shown in Fig. 3.6 (c). The shapes of their nitrogen adsorption isotherm were all similar, which is typical of type IV with an apparent hysteresis loop. These suggest mesoporous structure, which was also confirmed by BJH plot of their pore size distribution in Fig. 3.6 (d).

UV-Vis DRS results in Fig. 3.6 (e) represent the red shift of TiO_2 photocatalyst absorbance towards the visible-light range1 resulted from N-doping. Bare TiO_2 (N-to-Ti 0) has minimal light absorbance after the wavelength exceeds 400nm. With N doping, visible-light absorbance (<800nm) begin to pick up and also increased with the increase of N-to-Ti precursor molar ratio. This probably is due to that higher N precursor usage could potentially contribute to higher content of nitrogen dopant in the TiO_2 products. It is noteworthy that this effect also reaches a plateau after N-to-Ti precursor molar ratio became 1.

Fig. 3.6 (f) illustrates the by N-doped TiO_2 prepared under different N-to-Ti precursor molar ratio. The shapes of the spectra characteristics to the reaction product TAOH and wavelength of maximum emission are similar, whereas only the intensity of these spectra is changed. This is probably due to the similar crystal phase of N-doped TiO_2 prepared under different N-to-Ti precursor molar ratio. It can be seen that amount of the $OH^{\cdot}$ radicals generated increase with N precursor ratio. This is likely responsible for the fact the photocatlaytic ability increased with N precursor ratio. Nevertheless, excessive usage of N precursor (N-to-Ti molar ratio 2) appeared to reduce the $OH^{\cdot}$ production. One possible reason using oversupplied N precursors is that some chemisorbed N containing species on TiO_2 surface might be left after the thermal treatment, which was not doped into the TiO_2 lattice. These species could cover the photoactive sites and capture photo-induced holes [64]. Oversupplied N precursors might amplify this adverse effect and thus be detrimental to the oxidative degradation. This might diminish the overall photoactive promoting effect of the N doping.

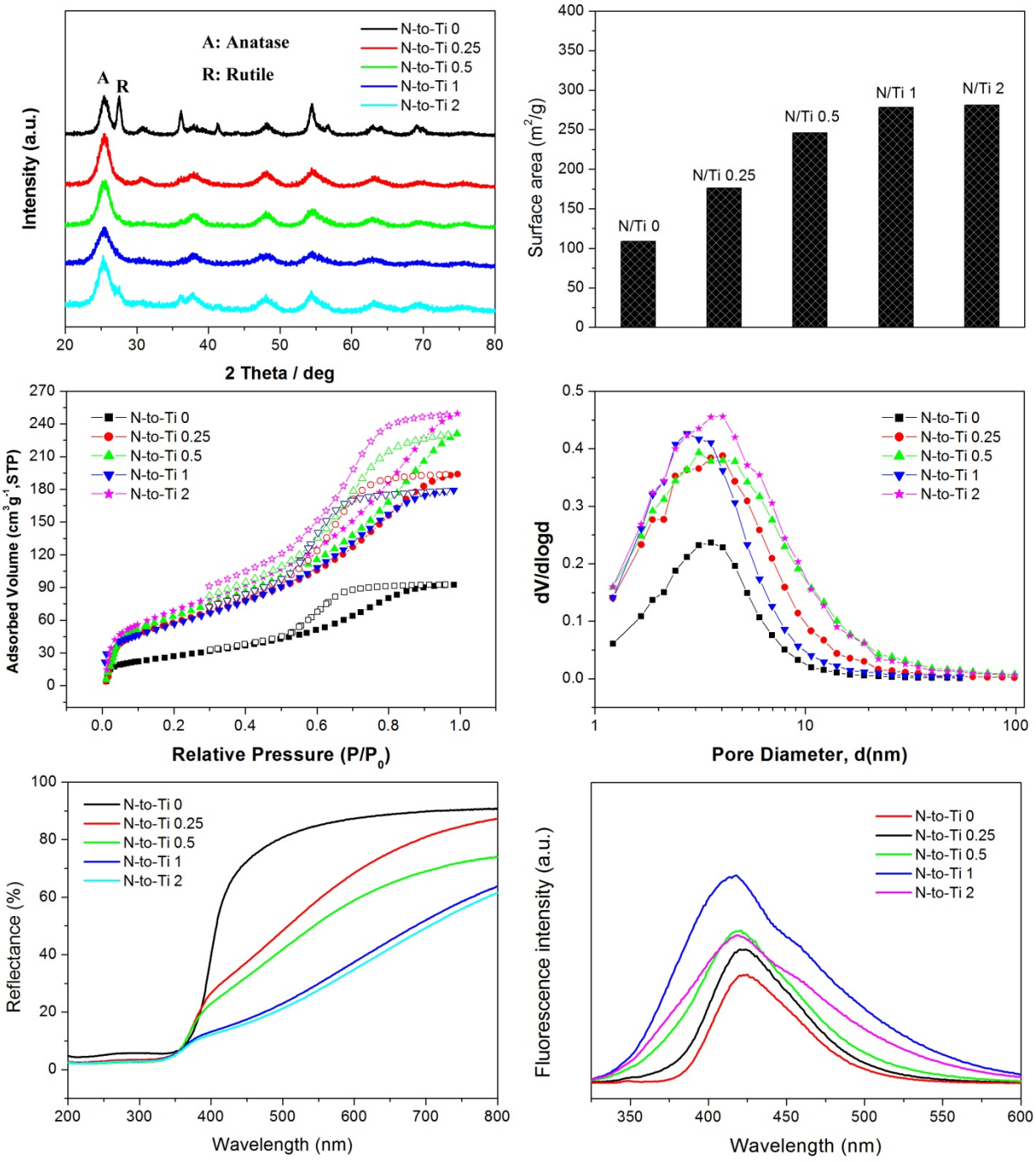

Figure 3.6: XRD patterns (a), surface area (b), nitrogen adsorption-desorption isotherm (c), pore size distribution (d), UV-Vis DRS spectra (e) and fluorescence spectra (f) of N-TiO_2 photocatalysts prepared under different N-to-Ti precursor molar ratio

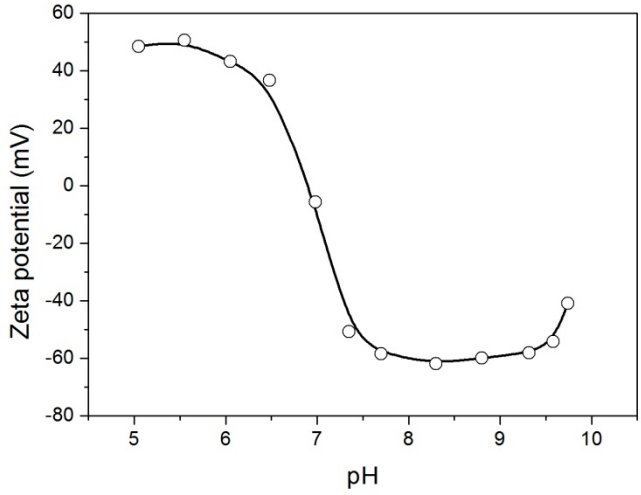

Figure 3.7: Zeta-potentials of N-TiO_2 sol as a function of pH

Fig. 3.7 shows the zeta potential variation as function of pH value of colloidal N-TiO_2 nanoparticles, where the isoelectric point appears to be around 6.8. This is also consistent with the reported value of pure TiO_2 colloidal suspension in the literature. During the preparation, N-doped TiO_2 sol turned basic when N-to-Ti precursor molar ratio reached 1 (pH≈8). From Fig.6, it can also be observed that the zeta potential of colloidal TiO_2 nanoparticles approached the maximum value (-60mV) under the same pH value and then began to drop after pH value turned 9. As the N-to-Ti precursor molar ratio increased to 2, pH value of colloidal N-TiO_2 nanoparticles continued to rise to around 10. At the mean time, the colour of colloidal N-TiO_2 changed to be white and non-transparent. This probably resulted from the reduced zeta potential of suspended N-TiO_2 nanoparticles and thus induced intraparticle agglomeration. Based on the MB removal test and $OH^{\cdot}$ radical measurement, this could undermine resulting photocatalytic ability of N-TiO_2. As a result, highest photocatalytic of N-TiO_2 nanoparticles appeared to be consistent with maximum zeta potential of their colloidal suspension (pH value between 8 and 9). This is also indicated that pH values of N-doped TiO_2 sol could be used as an indicator of effective N-doping during the sol-gel preparation.

In summary, increasing N-to-Ti precursor ratio during the preparation could contribute to higher photocatalyitc ability. However, excessive usage (N-to-Ti molar

ratio > 1) should be prevented as this could potentially be detrimental to the overall N-TiO_2 photacatalytic activity.

3.5. Conclusion

A multi-parameter investigation of sol-gel synthesized N-doped TiO_2 was carried out. N-to-Ti molar ratio and calcinations temperature influenced on optical and photocatalytic properties of the products greatly. Optimal visible light activity of N-doped TiO_2 was obtained at N-to-Ti precursor molar ratio of 1 and 350˚C calcinations, and was of 5nm particle size and single anatase phase. Except the bare TiO_2 samples synthesized without any nitrogen doping, all TiO_2 achieved better photocatalytic rate of MB than commercial P25 ($k=2.57\times10^{-3}$) under the visible light irradiation. In addition, the pH value of N-doped TiO_2 sol during the preparation was found to be an effective indicator of N-doping quality without using any post-synthesis analysis. These findings could help develop viable TiO_2 photocatalysts or their composites for cost effective solar-driven environmental technology in the near term.

References

[1] O. Legrini, E. Oliveros, A. M. Braun, Photochemical processes for water treatment, Chem. Rev. 93 (1993) 671-698.

[2] M. Gratzel, Photoelectrochemical cells, Nature 414 (2001) 338-344.

[3] L. Zou, B. Zhu, Enhancing the reuse of treated effluent by photocatalytic process, J. Adv. Oxid. Technol. 10 (2007) 273-281.

[4] F. Han, V. S. R. Kambala, M. Srinivasan, D. Rajarathnam, R. Naidu, Tailored titanium dioxide photocatalysts for the degradation of organic dyes in wastewater treatment: a review, Appl. Catal. A: Gen. 359 (2009) 25-40.

[5] J. Zhao, C. Chen, W. Ma, Photocatalytic degradation of organic pollutant under visible light irradiation, Top. Catal. 35 (2005) 269-278.

[6] C. H. Park, S. B. Zhang, S. H. Wei, Origin of p-type doping difficulty in ZnO: The impurity perspective, Phys. Rev. B 66 (2002) 073202-1-3.

[7] R. Asahi, T. Morikawa, T. Ohwaki, K. Aoki, Y. Taga, Visible-light photocatalysis in nitrogen-doped titanium oxides, Science 293 (2001) 269-271.

[8] H. H. Lo, N. O. Gopal, S. C. Ke, Origin of photoactivity of oxygen-deficient TiO_2 under visible light, Appl. Phys. Lett. 95 (2009) 083126.

[9]F. Peng, L. Cai, H. Yu, H. Wang, J. Yang, Synthesis and characterization of substitutional and interstitial nitrogen-doped titanium dioxides with visible light photocatalytic activity, J. of Solid State Chem. 181 (2008) 130-136.

[10] J. Ananpattarachai, P. Kajitvichyanukul, S. Seraphin, Visible light adsorption ability and photocatalytic oxidation activity of various interstitial N-doped TiO_2 prepared from different nitrogen dopants, J. Hazard. Mater. 168 (2009) 253-261.

[11] K. S. Yang, Y. Dai, B. Huang, M. Whangbo, Density functional studies of the magnetic properties in nitrogen doped TiO_2, Chem. Phys. Lett. 481(2009) 99-102.

[12] M. D'Arienzo, R. Scotti, L. Wahba, Hydrothermal N-doped TiO_2: Explaining photocatalytic properties by electronic and magnetic identification of N active sites, Appl. Catal. B: Environ. 93 (2009) 149-155.

[13]K.Yang, Y. Dai, B. Huang, S. Han, Theoretical study of N-doped TiO_2 rutile crystals, J. Phys. Chem. B. 110 (2006) 24011-24014.

[14]C. D. Valentin, G. Pacchioni, A. Selloni, S. Livraghi, E. Giamello, Characterization of paramagnetic species in N-doped TiO_2 powders by EPR spectroscopy and DFT calculations, J. Phys. Chem. B. 109 (2005) 11414-11419.

[15]M. Kitano, K. Funatsu, M. Matsuoka, M. Ueshima, M. Anpo, Preparation of nitrogen-substituted TiO thin film photocatalysts by the radio frequency magnetron sputtering deposition method and their photocatalytic reactivity under visible light irradiation, J. Phys. Chem. B 110 (2006) 25266-25272.

[16]O. Diwald, T. L. Thompson, E. G. Grolaski, S. D. Walck, J. T. Yates, The effect of nitrogen ion implantation on the photoactivity of TiO_2 rutile single crystals, J. Phys. Chem. B 108 (2004) 52-57.

[17]M. Batzil, E. H. Morales, U. Diebold, Influence of nitrogen doping on the defect formation and surface properties of TiO_2 rutile and anatase, Phys. Rev. Lett. 96 (2006) 026103-1-4.

[18]R. Nakamura, T. Tanka, Y. Nakato, Mechanism for visible light response in anodic photocurrents at N-doped TiO_2 film electrodes, J. Phys. Chem. B 108 (2004) 10617-10620.

[19]H. Irie, S. Washizuka, N. Yoshinob, K. Hashimoto, Visible-light induced hydrophilicity on nitrogen-substituted titanium dioxde films, Chem. Commun. (2003) 1298-1299.

[20]O. Diwald, T. L. Thompson, T. Zubkov, E. G. Goralski, S. D. Walck, J. T. Yates Photochemical activity of nitrogen-doped rutile TiO_2(110) in visible light, J. Phys. Chem. B 108 (2004) 6004-6008.

[21] I. A. Montoya, T. Viveros, J. M. Domínguez, L. A. Canales, I. Schifter, On the effects of the sol-gel synthesis parameters on textural and structural characteristics of TiO_2, Catal. Letters, 15 (1992) 207-217.

[22] J. Kim, K. C. Song, S. E. Pratsinis, The effect of hydrolysis temperature on synthesis of bimodally nanostructured porous titania, J. Nano. Res. 2 (2000) 419-424.

[23]W. Zhang, L. Zou, L. Wang, Photocatalytic TiO_2/adsorbent nanocomposite prepared via wet chemical impregnation for wastewater treatment: a review, Appl. Catal. A: Gen. 371(2009) 1-9.

[24] W. Zhang, L. Zou, L. Wang, Visible-light assisted methylene blue (MB) removal by novel TiO_2/adsorbent nanocomposites, Water Sci. Technol. 61 (2010) 2863-2871.

[25]Z. Lin, A. Orlov, R. M. Lambert, M. C. Payne, New insights into the origin of visible light photocatalytic activity of nitrogen-doped and oxygen-deficient anatase TiO_2, J. Phys. Chem. B. 109 (2005) 20948-10952.

[26]S. Sato, Photocatalysts sensitive to visible light, Science 295 (2002) 626-627.

[27] Y. Sakatani, H. Koike, Japanese Patent2001072419 (March 21, 2001).

[28] F. Peng, L. Cai, H. Yu, H. Wang, J. Yang, Synthesis and characterization of substitutional and interstitial nitrogen-doped titanium dioxides with visible light photocatalytic activity, J. of Solid State Chem. 181 (2008) 130-136

[29] X. B. Chen, Y. Lou, A. C. S. Samia, C. Burda, J. L. Gole, Formation of oxynitride as the photocatatlytic enhancing site in nitrogen-doped titania nanocatalysts: comparison to a commercial nanopowder, Adv. Funct. Mater. 15 (2005) 41-49.

[30] Y. Sakatani, J. Nunoshige, H. Ando, K. Okusako, H. Koike, T. Takata, J. N. Kondo, M. Hara, K. Domen, photocatalytic decomposition of acetaldehyde under visible light irradiation over La3+ and N co-doped TiO_2, Chem. Lett. 32 (2003) 1156-1157.

[31] S. Joung, T. Amemiya, M. Murabayashi, K. Itoh, Relation between photocatalytic activity and preparation conditions for nitrogen-doped visible light-driven TiO_2 photocatalysts, Appl. Catal. A: Gen. 312 (2006) 20-26.

[32] S. Livraghi, M. C. Paganini, E. Giamello, A. Selloni, C. Di Valentin, G. Pacchioni, Origin of photoactivity of nitrogen-doped titanium dioxide under visible light, J. Am. Chem. Soc. 128 (2006) 15666-15671.

[33] C. D. Valentin, G. Pacchioni, A. Selloni, S. Livraghi, E. Giamello, Characterization of paramagnetic species in N-doped TiO_2 powders by EPR spectroscopy and DFT calculations, J. Phys. Chem. B. 109 (2005) 11414-11419.

[34] C.D. Valentin, G. Pacchioni, A. Selloni, Origin of the different photoactivity of N-doped anatase and rutile TiO_2, Phys. Rev. B: Solid State, 70 (2004) 85116.

[35] C.D. Valentin, G. Pacchioni, A. Selloni, Theory of carbon doping of titanium dioxide, Chem. Mater. 17 (2005) 6656-6665.

[36] H. Wang, J. P. Lewis, Second-generation photocatalytic materials: anion-doped TiO_2, J. Phys. Condens. Matter 18 (2006) 421.

[37]J. Lee, J. Park, J. Cho, Electronic properties of N- and C-doped TiO_2, Appl. Phys. Lett. 87 (2005) 11904-1-3.

[38]K. Yang, Y. Dai, B. Huang, S. Han, Theoretical study of N-doped TiO_2 rutile crystals, J. Phys. Chem. B. 110 (2006) 24011-24014.

[39]J. Yang, J. Dai, C. Chen, J. Zhao, Effects of hydroxyl radicals and oxygen species on the 4-chlorophenol degradation by photoelectrocatalytic reactions with TiO_2-film electrodes, J. Photochem. Photobiol. A: Chem. 208 (2009) 66-77.

[40] J. L. Gole, J. D. Stout, C. Burda, Y. Lou, X. Chen, Highly efficient formation of visible light tunable TiON photocatalysts and their transformation at the nanoscale, J. Phys. Chem. B, 108 (2004) 1230-1240.

[41] M. Sathish, B. Viswanathan, R. P. Viswanath, C. S. Gopinath, Synthesis, characterization, electronic structure, and photocatalytic activity of nitrogen-doped TiO nanocatalyst, Chem. Mater., 17 (2005) 6349-6353.

[42] T. Ihara, M. Miyoshi, Y. Iriyama, O. Matsumoto, S. Sugihara, Visible-light-active titanium oxide photocatalyst realized by an oxygen-deficient structure and by nitrogen doping, Appl. Catal. B: Environ. 42 (2003) 403-409.

[43] Y. Liu, X. Chen, J. Li, C. Burda, Photocatalytic degradation of azo dyes by nitrogen-doped TiO_2 nanocatalysts, Chemosphere, 61 (2005) 11-18.

[44] S. Sakthivel, H. Kisch, Photocatalytic and photoelectrochemical properties of nitrogen-doped titanium dioxide, Chemphyschem, 4 (2003) 487.

[45] S. Sakthivel, M. Janczarek, H. Kisch, Visible light activity and photoelectrochemical properties of nitrogen-doped TiO, J. Phys. Chem. B. 108 (2004) 19384-19387.

[46] T. Sano, N. Negishi, K. Koike, K. Takeuchi, S. Matsuzawa, Preparation of a visible light-responsive photocatalyst from a complex of Ti4+ with a nitrogen-containing ligand, J. Mater. Chem. 14 (2004) 380-384.

[47] Y. Wang, X. Yu, D. Sun, Synthesis, characterisation, and photocatalytic activity of TiO_2-xNx nanocatalyst, J. Hazard. Mater., 144 (2007) 328-33.

[48] K. Kobayakawa, Y. Murakami, Y. Sato, Visible-light active N-doped TiO_2 prepared by heating of titanium hydroxide and urea, J. Photochem. Photobiol. A:

Chem. 170 (2005) 177-179.

[49] J. Ananpattarachai, P. Kajitvichyanukul, S. Seraphin, Visible light absorption ability and photocatatlytic oxidation activity of various interstitial N-doped TiO_2 prepared from different nitrogen dopants, J. Hazard. Mater. (2009)

[50] Z. Wang, F. Zhang, Y. Yang, J. Cui, Q. Sun, N. Guan, One-pot synthesis of visible-light-responsive TiO_2 in the presence of various amines, Chin. J. Catal., 27 (2006) 1091-1095.

[51] J. Sun, L. Qiao, S. Sun, G. Wang, Photocatalytic degradation of Orange G on nitrogen-doped TiO_2 catalysts under visible light and sunlight irradiation, J. Hazard. Mater., 155 (2008) 312-319.

[52] H. Sun, Y. Bai, H. Liu, W. Jin, N. Xu, Photocatalytic decomposition of 4-chlorophenol over an efficient N-doped TiO_2 under sunlight irradiation, J. Photochem. Photobiol. A: Chem. 201 (2009) 15-22.

[53] J. Xu, Y. Ao, D. Fu, C. Yuan, A simple route to synthesize highly crystalline N-doped TiO_2 particles under low temperature, J. Crystal Growth, 310 (2008) 4319-4324.

[54] Z. Wang, W. Cai, X. Hong, X. Zhao, F. Xu, C. Cai, Photocatalytic degradation of phenol in aqueous nitrogen-doped TiO_2 suspensions with various light sources, Appl. Catal. B: Environ. 57 (2005) 223-231.

[55] S. Sato, R. Nakamura, S. Abe, Visible-light sensitization of TiO_2 photocatalysts by wet-method N doping, Appl. Catal. A: Gen. 294 (2005) 131-137.

[56]S. Livraghi, A. Votta, M. C. Paganini, E. Giamello, The nature of paramagnetic species in nitrogen doped TiO_2 active in visible light photocatalysis, Chem. Commun. (2005) 498-500.

[57] C. Belver, R. Bellod, A. Fuerte, M. Fernandez,-Garcia, Nitrogen-containing TiO_2 photocatalysts Part 1. Synthesis and solid characterization, Appl. Catal. B: Environ. 65 (2006) 301-308.

[58] M. Sathish, B. Viswanathan, R. P. Viswanath, Characterization and photocatalytic activity of N-doped TiO_2 prepared by thermal decomposition of Ti-melamine complex,

Appl. Catal. B: Environ. 74 (2007) 307-312.

[59] T. Hirakawa, Y. Nosaka, Properties of $O_2^{\cdot-}$ and OH formed in TiO_2 aqueous suspensions by photocatalytic reaction and the influence of H_2O_2 and some ions, Langmuir 18 (2002) 3247-3254.

[60] I. K. Konstantinou, T. A. Albanis, TiO_2-assisted photocatalytic degradation of azo dyes in aqueous solution: kinetic and mechanistic investigations, Appl. Catal. B: Environ. 49 (2004) 1-14.

[61] C. Colbeau-Justin, M. Kunst, D. Huguenin, Structural influence on charge-carrier lifetimes in TiO_2 powders studied by microwave absorption, J. Mater. Sci. 38 (2003) 2429–2437.

[62] K. S. W. Sing, D. H. Everett, R. A. W. Haul, L. Moscou, R. A. Pierotti, J. Rouquerol, T. Siremieniewska, Reporting physisorption data for gas/solid systems with special reference to the determination of surface area and porosity, Pure Appl. Chem. 57 (1985) 603-621.

[63] C. Minero, F. Catozzo, F. Pelizzetti, Role of adsorption in photocatalyzed reaction of organic molecules in aqueous titania suspensions, Langmuir, 8 (1992) 481-486.

[64] R. A. Young, P, Desai, Archiwum Nauki o Materialach (Archives of Materials Science) 10 (1989) 71-90.

CHAPTER 4

WET CHEMICAL PREPARATION OF DIFFERENT TITANIA/ADSORBENT COMPOSITES AND THEIR VISIBLE-LIGHT ASSISTED METHYLENE BLUE (MB) REMOVAL*

Abstract

In present chapter, visible light sensitive TiO_2/adsorbent composites (TNC) were prepared via a facile wet chemical method. Three types of adsorbents including zeolites (F-9, HSZ-690 and HSZ-930), mesoporous silica (MPS-2.7 and 4) and activated carbon, were used as the porous substrates for nanocomposites. Visible light sensitivity was incorporated to TNCs by nitrogen doping of TiO_2, which is obtained through the addition of a nitrogen precursor, triethylamine, within the same wet chemical procedure. The photocatalytic and adsorption ability of as-prepared TNC resultants were studied using solutions of methylene blue (MB) as a model pollutant. Synergistic interactions between adsorption and visible-light photocatalysis were observed, as under the assistance of visible-light irradiation, all TNCs achieved higher MB removal rates than those by adsorption process alone. The better performance of the as-prepared N-doped TNC reveals its potential to be used in cost effective solar photocatalytic degradation of dissolved organic compounds.

* This chapter has been adapted from: Water Science & Technology, 61 (2010) 2863-2871.

4.1. Introduction

In recent decades, heterogeneous photocatalysis has become a strong candidate for environmental clean-up, especially water treatment, which can effectively oxidize a wide range of organic compounds, at ambient or moderate room conditions [1]. Among those available, nano-sized TiO_2 photocatalysts have proven to be most promising [2], due to its low cost, greatly enhanced surface area, tunable properties which can be modified by size reduction, doping, sensitizer, etc., and good stability i.e. no substantial loss of photocatalytic activity after repeated process cycles. Besides, due to the intensive research on the photocatalytic activity of TiO_2, the mechanism of its purification on various dissolved organic compounds is well understood as a consequence. It is widely acknowledged that superoxide species and, specifically, hydroxyl radicals, as active reagents for the mineralization of the organic compounds into nontoxic form such as carbon dioxide and water, which is realized through the surface contact of OH radicals and C-H bonds.

One promising area of TiO_2 based photocatalytic applications is the regeneration of spent porous adsorbents. The adsorption process has been used as industrial treatments of wastewater containing low level of dissolved organic compounds for decades due to the reasonable efficacy and comparatively low costs. Nevertheless, the spent adsorbents saturated with dissolved organic compounds at the end of treatments have posed an environmental problem as they need to be disposed properly. Early attempts of this nature were to utilize TiO_2 heterogeneous photocatalysis as a separate procedure, that is, to mix the spent adsorbents with TiO_2 powders mechanically after the wastewater treatment [3]. However, the process was intrinsically mass transfer limited. Later on, research interests were shifted into coating TiO_2 photocatalysts on the surface of adsorbents, which was found to combine the advantages of both adsorption and photocatalytic techniques. On one hand, adsorbents with large surface-area work as the support of nano-sized TiO_2 photocatalyst and concentrate the pollutants and intermediates around the TiO_2; on the other hand, the coated photocatalyst can decompose the pollutants thus regenerating the adsorbents in situ. A variety of coating methods for the preparation of TiO_2/adsorbent composites (TNC) have been reported. Some are chemical methods, such as carbonization of coal and TiO_2 mixture [4], ionized cluster beam deposition [5] and chemical vapour deposition

[6]. Others are physical methods, such as impregnation–desiccation [7], boil and dip-coating deposition [8].Wet chemical method, i.e. hydrolysis of TiO_2 precursors and their subsequent impregnation to adsorbents is of particular interests at the moment [9,10]. Their advantages include facile nature, continuous process ability, low temperature and energy costs, uniform coating with good reproducibility and adhesion, and the simplicity in controlling crystal structure/morphology and particle size by simple variations in experimental conditions, such as hydrolysis rate, solution pH and solvent systems. In addition, Mazyck's group reported several improvements to the traditional wet chemical impregnation method in attempts to couple the TiO_2 with AC, including dry impregnation and microwave-assisted impregnation [11,12,13]. Better TiO_2 coating on the external surface of carbon and photocatalytic ability with methanol were obtained. Currently, all of these research are limited to incorporate UV sensitive TiO_2 (band energy 3.0-3.2ev) with the adsorbent [14], although the visible-light capability has been successfully introduced to TiO_2 nanoparticles [15].

Asahi et al. first recognized the visible light sensitivity of TiO_2 with a certain amount of N-dopants and proposed that in an N-doped TiO_2 system, the oxygen sites were substituted by nitrogen atoms, which contribute to the band gap narrowing by mixing N_{2p} and O_{2p} states [16]. At the moment, the origin of visible light activity i.e. N dopants or O vacancies [17], substitoinal N or interstitial N [18], band gas narrowing or new mid-band creation [19,20,21] and its photocatalytic mechanism (i.e. whether or not through OH radicals) arising from N-doping are still subject to debate. However, these have not prevented nitrogen from becoming the most effective dopant due to its similar size to oxygen, and small ionization energy [22]. Reported doping methods include the sputtering and implantation [23,24,25], high temperature sintering TiO_2 under N-containing atmosphere [26,27,28], etc. Different synthesis methods also likely play a role on the types and level of doped nitrogen ipurities. Most recently, Burda and his co-workers demonstrated an N-doping TiO_2 via wet chemical method and obtained up to 8% N-content in their as-prepared TiO_2 nanoparticles [29]. This has led to the possibility of incorporating visible light sensitivities to a TNC within a single wet chemical procedure.

In this work, it is the first attempt to incorporate visible light sensitive TiO_2 with three different types of adsorbents which were used as the substrates including zeolites (F-9,

HSZ-690 and HSZ-930), mesoporous silica (MPS-2.7 and 4), and activated carbon (AC). The formed TiO_2/adsorbent nanocomposites will have dual capacities of adsorbing dissolved organic compounds, and self-regenerating by decomposing of the adsorbed pollutants. Following the material preparation, overall adsorption and photocatalytic degradation performance of the novel TNC systems were assessed using aqueous methylene blue (MB) as model organic pollutant, which is often considered to be one of the major dye stuff used in the textile industry and is difficult to be degraded by the conventional biological wastewater treatment.

4.2. Experimental

4.2.1 Preparation of N-doped titania/adsorbent composites

AC samples (activated from coconut shell powder) and two types of mesoporous silica (MPS-2.7 and MPS-4) were obtained from Activated Carbon Technologies PTY Ltd. and Taiyo Kagaku CO., Ltd., respectively. Three types of zeolites (F-9, HSZ-690 mordenite and HSZ-930 beta) were purchased from Tosoh, Japan. TiO_2 precursor, titanium (IV) butoxide (97%), and N precursor, triethylamine, were purchased from Sigma Aldrich. In a typical N-doped TNC preparation, 40ml of titanium (IV) butoxide ($Ti(OC_4H_9)_4$) were first dissolved in 160ml of ethanol (C_2H_5OH) by 30 mins magnetic stirring at room temperature to obtain solution A. In addition, deionised water was mixed with nitric acid (HNO_3) by magnetic stirring at room temperature to obtain solution B. Solution B was then added drop-wise into solution A under vigorous stirring, and this was then followed by the hydrolysis of $Ti(OC_4H_9)_4$ under stirring conditions at room temperature until a transparent sol was formed. The N-doping was achieved by drop-wise addition of a certain amount of triethylamine to the formed TiO_2 sol under continuous stirring (24 hr), where the precursor molar ratio of N to Ti was controlled at 1. In the last, 0.42g of each type of adsorbent powder was added to 5ml N-doped TiO_2 sol respectively with magnetic stirring for 1 hr. Prior to the addition, all types of adsorbents was dried in oven at 398K overnight to avoid any moisture content. The resulting mixture was subsequently dried and calcined at 623K for 2 hr. Due to the likely carbon loss under calcinations in air, AC-based TNC was calcinated under N_2 protection. In all cases, temperature ramp during the calcinations was 5K /min.

4.2.2. Characterization of the experimental materials

For characterization of the as-prepared TNC samples, the textural properties were obtained based on the N_2 adsorption-desorption isotherms, determined at 77K via a Belsorp apparatus, Japan. Before each measurement, samples were degassed at 423K for 5hr. Surface texture of as-prepared TNCs was characterized by a field emission scanning electron microscopy (SEM) analysis (Philips XL 30). Surface chemical charateristics of as-prepared TNCs were investigated by transmission Fourier transform infrared spectroscopy (FTIR) analysis in 4000-500 cm^{-1} frequency, which was conducted on a Shimadzu FTIR-8400s using KBr pellets for sample preparation. In each preparation, 1-2mg of catalyst was ground with 100mg of KBr.

4.2.3. Adsorption and photocatalytic experimental set-up

To evaluate the overall performance of the TNC resultants, the removal of MB (Sigma Aldrich) was carried out in a 200ml cylindrical glass vessel under a controlled visible light source, which was supplied by a Newport Oriel series Q solar simulator with a 100W Xe lamp. A dichroic mirror (NewSpec 66219) was mounted on the lamp to eliminate infrared and UV portion of the irradiation, which help avoid any MB self-decompositionin in near UV light range as interference. As a result, the total collimated cut-off irradiance between 420 and 630nm was measured approximately 570mW on the surface of sample by a Newport optical power meter 1918-C. For further assessment of as-prepared TNC adsorption ability and that assisted by visible-light photocatalysis separately, MB removal tests were carried out in two modes without and with light. In a typical test, 30mg MPS-2.7, MPS-4 and F-9, 10mg HSZ-690 and HSZ-930, 3mg AC supported TNC samples were added into 100 ml of 15mg/L MB solution, respectively. For all cases, 0.5ml suspension was retrieved at a defined time interval, and the concentration of MB was then centrifuged and analysed using a Varian Cary 100 UV-Vis spectrophotometer at 650nm.

To evaluate as-prepared TNCs separation performance, 100ml of an aqueous solution of TNCs at a concentration of 1g/L was placed in a 200mL graduated cylinder and magnetic-shaken vigorously for 30 min before all the TNCs were allowed to settle.

4.3. Results and discussion

4.3.1. Characterizations of the as-prepared titania/adsorbent composites

Fourier transform infrared spectroscopy (FTIR). The FTIR spectra of different TNCs are presented in Fig. 4.1. The main absorption peaks at 3447, 1382, 1640cm^{-1} are related to the stretching and bending vibrations of surface OH- and H_2O. It is of particular interests that the peak located at 1059cm^{-1} could be discerned in all as-prepared TNCs, which was attributed to Ti-O-N bond [30]. In addition, peaks appeared at 960cm-1 for mesoporous silica and zeolite-supported TNCs indicate antisymmetric stretching vibration of Ti-O-Si bond [31]. This could have more profound impact on the surface structural alteration of these TNCs resultants.

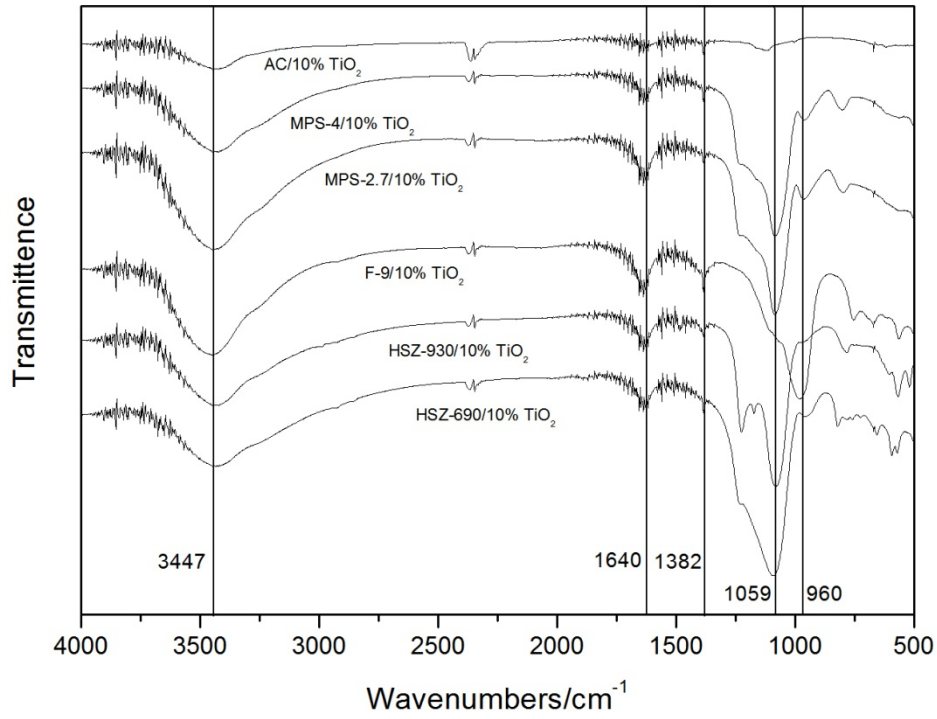

Figure 4.1: FTIR spectra of different as-prepared TNCs

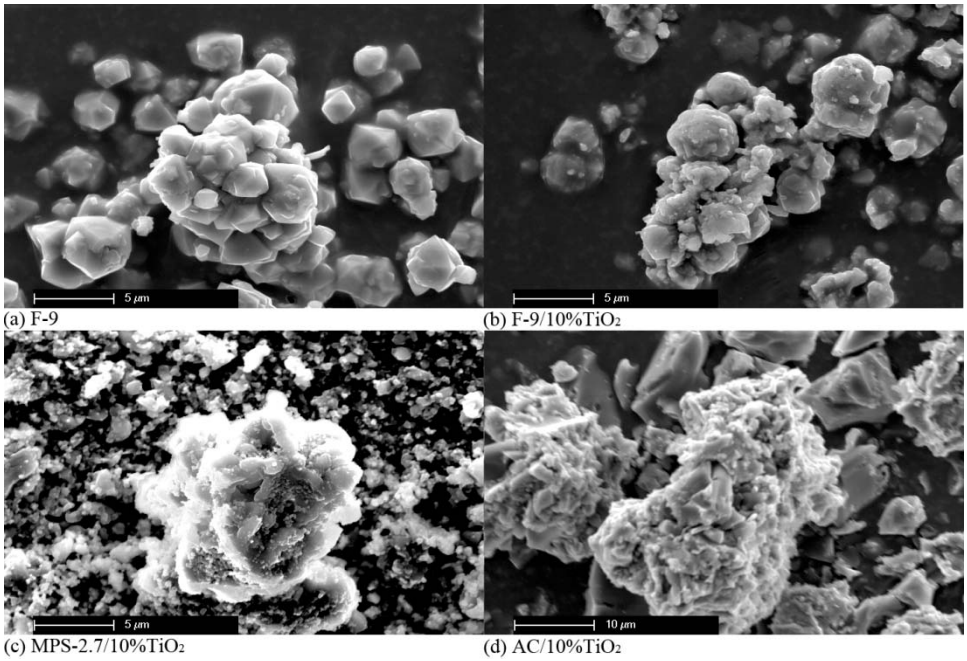

Figure 4.2: Typical SEM images of different as-prepared TNCs

Scanning electron microscopy (SEM) images. Typical SEM images of different as-prepared TNCs are shown in Fig. 4.2. The surface morphology of F-9 zeolites showed spherical like crystals in Fig. 4.2a, whereas its crystallinity was less pronounced with more surface roughness after the TiO_2 loading in Fig. 4.2b. It can also be observed that AC-supported TNCs features some macropores (~μm) in Fig. 4.2d, which could be seriously blocked by TiO_2 loading. In cases of mesoporous silica, strong agglomeration was observed in Fig. 4.2c. As a result, they formed large agglomerates rather than stayed as individual crystals. Interestingly, some macropores of the size similar to those of AC were also formed on these large porous agglomerates, which were predominately occupied by TiO_2 nanoparticles as well.

4.3.2. Adsorption and photodegadration of MB by as-prepared TNCs

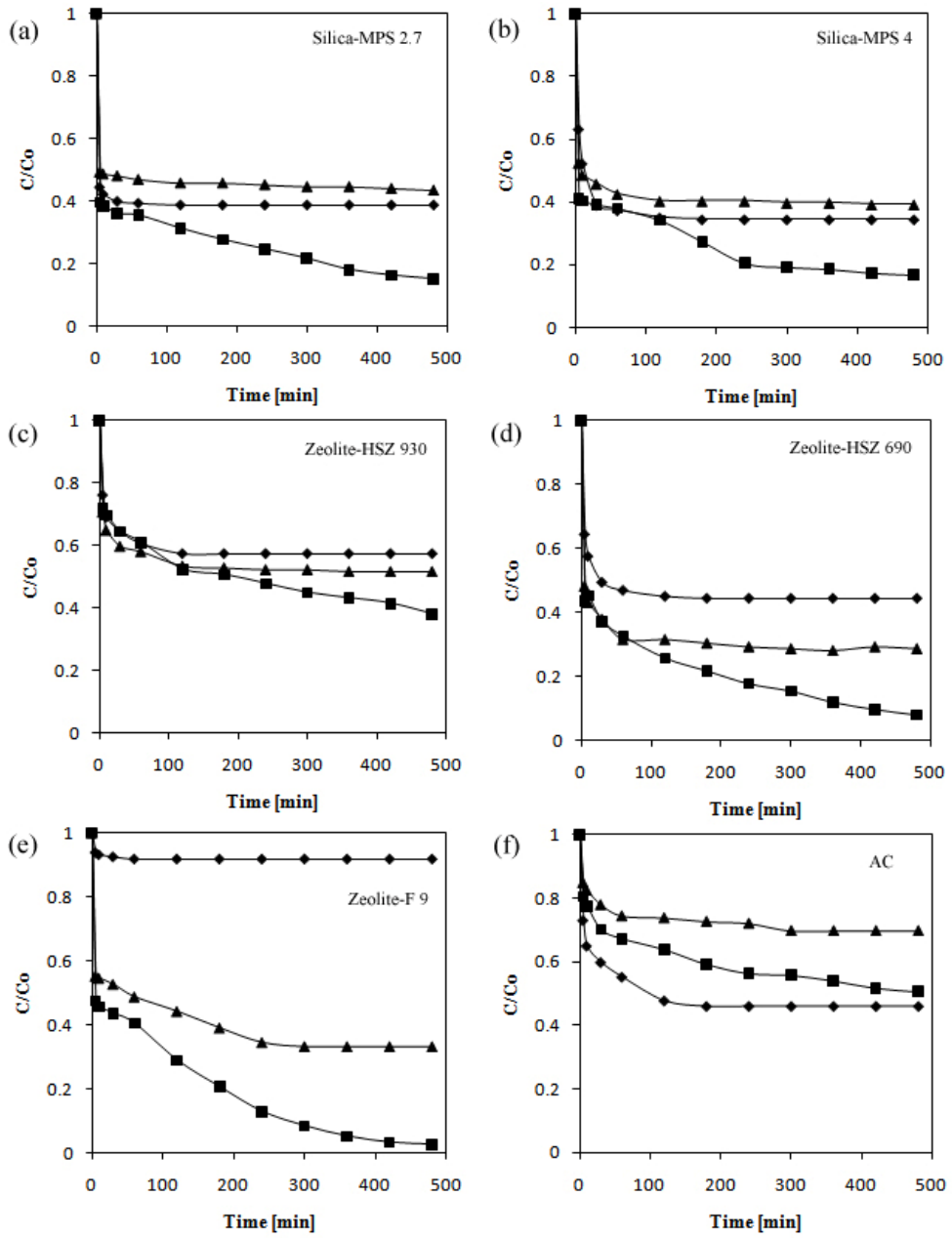

Figure 4.3: MB removal rate (C/C_0) as a function of time using different adsorbent-based TNCs, where ♦ represents the result using bare adsorbent, ▲ is that using its TNC without light and ■ is that using its TNC with light.

In a series of blank experiments conducted, no self-decomposition of MB was observed in the dark with TNCs or in the presence of visible-light illumination without TNCs at ambient experimental conditions. The time series of MB removal by different adsorbent-supported TNCs under visible light and no visible light conditions are compiled in Fig. 4.3.

Table 4.1: Physical properties of experimental materials

	BET [m^2/g]	**Total pore volume [cm^3/g]**	**Mean pore diameter [nm]**
AC	1666	0.731	1.76
AC/10% TiO_2	739	0.369	1.99
MPS-2.7	844	0.788	2.8
MPS-2.7/10% TiO_2	778	0.629	3.23
MPS-4	821	0.699	3.74
MPS-4/10% TiO_2	809	0.576	3.46
F-9	489	0.217	1.78
F-9/10% TiO_2	462	0.24	2.08
HSZ-690	393	0.328	3.33
HSZ-690/10% TiO_2	315	0.235	4.39
HSZ-930	538	0.247	1.84
HSZ-930/10% TiO_2	481	0.252	2.09

4.3.2.1. Adsorption characteristics of different adsorbent-supported titania/adsorbent composites.

Adsorption capacity of each adsorbent has been summarised in Fig. 4.4. Before loaded with TiO_2, MB adsorption capacity order of the adsorbents used in this work is AC>HSZ-690>HSZ-930>MPS-4≈MPS-2.7>F-9. Generally, TiO_2 loading on adsorbents could affect the adsorption of TNC resultants in two ways: 1) plugging some pores of the adsorbents and 2) modifying surface characteristics. The former effect could be reflected on in Table 4.1, where all the TNCs resultants suffered from some loss of surface area compared with their parent adsorbents. It was found that the surface area of AC-based TNC was only less than half of that before the TiO_2 modification. This is likely due to the fact that AC features some macropores (~μm) in their porous structure, which are more easily to be plugged by the TiO_2 nanoparticles and their agglomerates. As a result, the adsorption capacity of AC-supported TNC was severely diminished. The adsorption capacity of MB by two types of mesoporous silica-based TNCs were lower than their parent absorbents but the differences were negligible. In cases of three types of zeolites, adsorptions of MB by their supported TNCs were improved to various degrees (see Fig. 4.4), of which the Z-9 composite achieved the highest MB removal rate via sole adsorption process (almost 9 times higher than the bare F-9). The probable reasons are two-folds. Firstly, due to the crystalline structure of the zeolite with uniform micropores, the TiO_2 photocatalysts were mainly lodged onto the outer surface of zeolites instead of inside of their micropores (<2nm), TiO_2 colloidal particles size (about 2-4nm) is often too big to reach the micropores. As a result, the negative effect of TiO_2 loading resulted from pores plugging (i.e. surface area decrease) could be reduced to a minimal. Secondly, there is a relationship of zeolite surface hydrophobicity with its adsorption towards dissolved organic compounds [32,33,34]. As zeolites surface hydrophobicity usually increases with their SiO_2/Al_2O_3 ratio [35], the surface hydrophobic order of zeolites in current work should be HSZ-690(240)>HSZ-930(27)>F-9(2.5). Since more hydrophobic surface characteristics are favourable for MB adsorption, this order was also consistent with that of their adsorption capacity illustrated in Fig. 4.4. After the TiO_2 modification, the surface characteristics of all zeolites supported TNCs became more hydrophobic, which in turn contributed to the various degrees of enhancement of MB adsorption. For instance, the uptake of MB increased most significantly on F-9

zeolites, which are well-known of being strongly selective as water adsorbents due to its extremely high hydrophilicity.

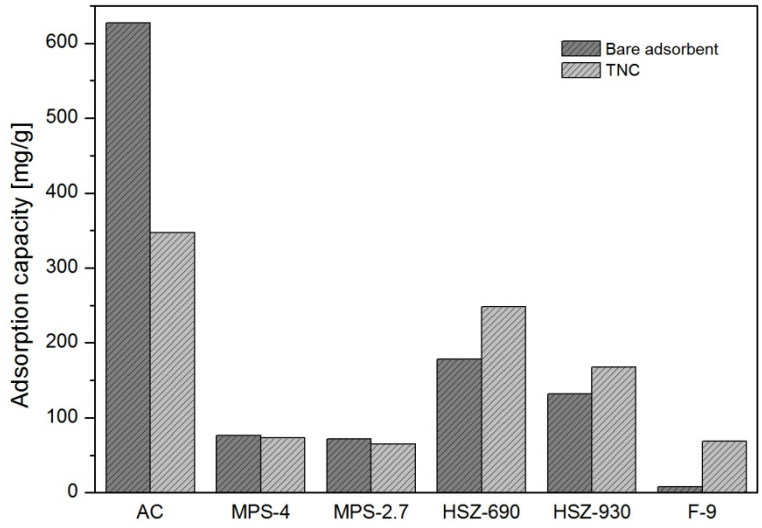

Figure 4.4: Adsorption capacity of different adsorbents and their supported TNCs

4.3.2.2. Visible-light photocatalysis assisted MB removal by different adsorbent-supported titania/adsorbent composites.

A synergistic interaction between the adsorption and photocatslysis was observed for all types of TNCs, as higher MB removal rates than that in the dark conditions were achieved when combined with visible-light irradiation (see Fig. 4.3). This is contributed by the incorporation of visible-light photocatalysis. Furthermore, this coupled photocatalytic-adsorptive ability is also proven to be quite sustainable, as there was a continuous decrease of MB concentrations until zero for all TNCs given the sufficient treatment time (maximum overnight in case of AC-supported TNC). In addition, a series of separation experiments conducted on TNC suspensions showed that, all the TNCs can be easily separated by gravity sedimentation on the bottom of a graduate cylinder within 3 min. This is due to their larger particle sizes.

In order to further investigate the interaction between the adsorption and photocatalysis, a separate assessment of the part of MB removal by photocatalytic degradation process was also carried out. Figure 4.5 illustrates the part of MB removal rate by photocatalytic degradation as a function of time for each TNC, which is obtained by subtracting the amount of MB removal in no light condition from that under the light in Fig. 4.3. Before comparing the photocatalytic activity of each TNC,

it should be noted that the initial amount of photocatalysts used could affect the photocatalytic rate significantly. In cases of 10mg TNCs used for HSZ-690 and HSZ-930, HSZ-690 degraded MB faster than HSZ-930 (see Fig. 4.5a). This was attributed to the higher adsorption capacity of HSZ-690 supported TNC (see Fig.4.4), as this could draw more MB molecules to the proximity of TiO_2 photocatalytic active sites located on the TNC surface. In cases of 30mg TNCs used for F-9, MPS-2.7 and MPS-4 supported TNCs, all of them possessed similar adsorption capacity (see Fig. 4.4), and accordingly their photodegradation rate of MB was also comparable (see Fig. 4.5b). These together signify the synergistic relationship between adsorption and photocatalytic process of TNCs, which have been discussed previously [15]. Another note should be taken that it is the adsorption capacity of as-prepared TNCs rather than their parent adsorbents was used to assess the adsorption effect on the photocatalysis. Furthermore, photocatalytic kinetics studies of all TNCs were also carried out using a pseudo-first-order equation:

$$\text{In } [Co/C] = kt \qquad (1)$$

where k is the pseudo-first-order rate constant, Co is taken as the initial concentration of MB (mg/L) and C is the concentration at time t (mg/L). Nevertheless, photocatalytic kinetics of all TNCs fit the pseudo-first-order reaction poorly, which indicates the photocatalytic reaction kinetics of TNCs in presence of simultaneous adsorption is somewhat different from that of the unsupported TiO_2 photocatalysts [36]. A better devised model study is needed to understand the interaction mechanism of simultaneous adsorption and photoassisted degradation of TNCs fully.

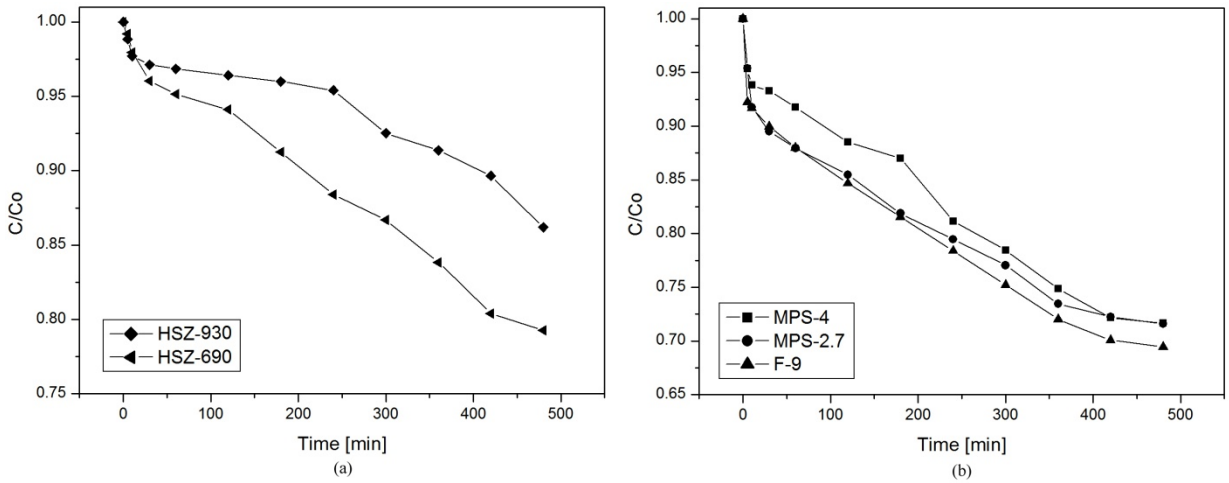

Figure 4.5: The part of MB removal rate by photocatalytic degradation for different TNCs

4.4. Conclusion

In present study, a series of visible-light sensitive TiO_2/adsorbent composites (TNC) have been successfully prepared via a facile wet chemical method. Viability of this technique has been demonstrated to various types of adsorbents, i.e. AC, mesoporous silica (MPS-2.7 and MPS-4) and zeolites (F-9, HSZ-690 and HSZ-930). In case of AC and mesoporous silica as substrates, the TNC resultants underwent some loss of adsorption capacity compared with their parent adsorbents; in cases of zeolites-based TNCs, however, the adsorption capacity was improved to different degrees due to chemical changes on their surfaces. Under visible light irradiations, all TNCs reached the higher removal rate of MB than their parent adsorbent at the end of treatment. Photocatalytic abilities of TNCs were found to increase with their adsorption capacities of their substrate, which suggests the most adsorptive and low cost AC is favourable to be utilized as substrate in near-term practical application. Furthermore, easy separating ability and good photocatalytic sustainability were also obtained. Overall, the performance of as-prepared N-doped TNCs has revealed its promising potential in the field of solar photocatalytic degradation of low level dissolved organic compounds such as colour and other pollutants in the water and wastewater. On a final note, dyes can serve in a different way as visible light photosensitizer to TiO_2 photocatalysts. This might give rise to an uncertainty that minor part of photodecomposition may proceed via non-N-doping induced visible light activity. Further studies are recommended to assess the visible light photocatalytic performance of as-prepared TNCs fully using non-colored dissolved organic compounds, such as 4-chlorophenol, phenol, 2-proponal, benzoic acid, trichloroethylene (TCE), etc.

References

[1] O. Legrini, E. Oliveros, A. M. Braun, Photochemical processes for water treatment, Chem. Rev. 93 (1993) 671-698.

[2] M. Gratzel, Photoelectrochemical cells, Nature 414 (2001) 338-344.

[3] J. Matos, J. Laine, J.M. Herrmann, Synergy effect in the photocatalytic degradation of phenol on a suspended mixture of titania and activated carbon, Appl. Catal. B: Environ. 18 (1998) 281-291.

[4] J. Przepiorski, N. Yoshizawa, Y. Yamada, Activated carbons containing TiO_2: characterization and influence of a preparation method on the state of supported TiO_2, J. Mater. Sci. 36 (2001) 4249-4257.

[5] H. Yamashita, M. Haraha, A. Tanii, M. Honda, M. Takeuchi, Y. Ichihashi, M. Anpo, N. Iwamoto, N. Itoh, T. Hirao, Preparation of efficient titanium oxide photocatalysts by an ionized cluster beam (ICB) method and their photocatalytic reactivities for the purification of water, Catal. Today 63 (2000) 63-69.

[6] Z. Ding, X. Hu, Q.L. Gao, P. L. Yue, P. F. Greenfield, Novel silica gel supported TiO_2 photocatalyst synthesized by CVD method, Langmuir 16 (2000) 6216-6222.

[7] S. X. Liu, C. L. Sun, S. R. Zhang, Photocatalytic regeneration of exhausted activated carbon saturated with phenol, Bull. Environ. Contam. Toxicol. 73 (2004) 1017-1024.

[8] M. Lu, J. Chen, K. Chang, Effect of adsorbents coated with titanium dioxide on the photocatalytic degradation of propoxur. Chemosphere 38 (1999) 617-627.

[9] B. Zhu, L. Zou, Removal of color compounds from recycled water using combined activated carbon adsorption and AOP decomposition, J. Adv. Oxid. Technol. 12 (2009)1-8.

[10] B. Zhu, L. Zou, Trapping and decomposing of color compounds from recycled water by TiO_2 coated activated carbon, J. Environ. Manag. 90 (2009) 3217-3225.

[11] Y. Tao, S. Schwartz, C.Y. Wu, D.W. Mazyck, Development of a TiO_2/AC composite photocatalysty dry impregnation for the treatment of methanol in humid airstreams, Ind. Eng. Chem. Res. 44 (2005) 7366-7372.

[12] Y. Tao, C.Y. Wu, D.W. Mazyck, Removal of methanol from pulp and paper mills using combined activated carbon adsorption and photocatalytic regeneration, Chemosphere, 65 (2006) 35-42.

[13] Y. Tao, C.Y. Wu, D.W. Mazyck, Microwave-assisted preparation of TiO_2/Acitivated carbon composite photocatalyst for removal of methanol in humid air streams, Ind. Eng. Chem. Res. 45 (2006) 5110-5116.

[14] F. Han, V.S. R. Kambala, M. Srinivasan, D. Rajarathnam, R. Naidu, Tailored titanium dioxide photocatalysts for the degradation of organic dyes in wastewater treatment: a review, Appl. Catal. A: Gen. 359 (2009) 25-40.

[15] W. Zhang, L. Zou, L. Wang, Photocatalytic TiO_2/adsorbent nanocomposite prepared via wet chemical impregnation for wastewater treatment: a review, Appl. Catal. A: Gen., 371 (2009) 1-9.

[16] R. Asahi, T. Morikawa, T. Ohwaki, K. Aoki, Y. Taga, Visible-light photocatalysis in nitrogen-doped titanium oxides, Science 293 (2001) 269-271.

[17] T. Ihara, M. Miyoshi, Y. Iriyama, O. Matsumoto, S. Sugihara, Visible-light-active titanium oxide photocatalyst realized by an oxygen-deficient structure and by nitrogen doping, Appl. Catal. B. 42 (2003) 403-409.

[18] F. Peng, L. Cai, H. Yu, H. Wang, J. Yang, Synthesis and characterization of substitutional and interstitial nitrogen-doped titanium dioxides with visible light photocatalytic activity, J. of Solid State Chem. 181 (2008) 130-136.

[19] K. Yang, Y. Dai, B. Huang, S. Han, Theoretical study of N-doped TiO_2 rutile crystals, J. Phys. Chem. B. 110 (2006) 24011-24014.

[20] J. Lee, J. Park, J. Cho, Electronic properties of N- and C-doped TiO_2, Appl. Phys. Lett. 87 (2005) 11904-1-3.

[21] C.D. Valentin, G. Pacchioni, A. Selloni, S. Livraghi, E. Giamello, Characterization of paramagnetic species in N-doped TiO_2 powders by EPR spectroscopy and DFT calculations, J. Phys. Chem. B. 109 (2005) 11414-11419.

[22] C.H. Park, S.B. Zhang, S. H. Wei, Origin of p-type doping difficulty in ZnO: The impurity perspective, Phys. Rev. B 66 (2002) 732021-732023.

[23] M. Batzil, E.H. Morales, U. Diebold, Influence of nitrogen doping on the defect formation and surface properties of TiO_2 rutile and anatase, Phys. Rev. Lett. 96 (2006) 026103-1-4.

[24] O. Diwald, T.L. Thompson, E.G. Grolaski, S.D. Walck, J.T. Yates, The effect of nitrogen ion implantation on the photoactivity of TiO_2 rutile single crystals, J. Phys. Chem. B 108 (2004) 52-57.

[25] M. Kitano, K. Funatsu, M. Matsuoka, M. Ueshima, M. Anpo, Preparation of nitrogen-substituted TiO thin film photocatalysts by the radio frequency magnetron sputtering deposition method and their photocatalytic reactivity under visible light irradiation, J. Phys. Chem. B 110 (2006) 25266-25272.

[26] O. Diwald, T.L. Thompson, T. Zubkov, E.G. Grolaski, S.D. Walck, J.T. Yates, Photochemical activity of nitrogen-doped rutile TiO_2(110) in visible light, J. Phys. Chem. B 108 (2004) 6004-6008.

[27] H. Irie, S. Washizuka, N. Yoshinob, K. Hashimoto, Visible-light induced hydrophilicity on nitrogen-substituted titanium dioxde films, Chem. Commun. (2003) 1298-1299.

[28] R. Nakamura, T. Tanka, Y. Nakato, Mechanism for visible light response in anodic photocurrents at N-doped TiO_2 film electrodes, J. Phys. Chem. B 108 (2004)10617-10620.

[29] C. Burda, Y. Lou, X. Chen, A.C.S. Samia, J. Stout, J. L. Gole, Enhanced nitrogen doping in TiO nanoparticles, Nano Lett. 3 (2003) 1049-1051.

[30] S.X. Liu, X.Y. Chen, X. Chen, N-doped visible light response nanosize TiO_2 photocatalyst prepared by acid catalyzed hydrolysis method, J. Chin. Catal. 27 (2006) 697-702.

[31] D.L. Petkowicz, R. Brambilla, C. Radtke, C. D. S. da Silva, Z. N. da Rocha, S. B.C. Pergher, J. H.Z. dos Santos, Photodegradation of methylene blue by in situ generated titania supported on a NaA zeolite, Appl. Catal. A, 357 (2009) 125-134.

[32] C. Ooka, H. Yoshida, M. Horio, K. Suzuki, T. Hattori, Adsorptive and photocatalytic performance of TiO_2 pillared montmorillonite in degradation of endocrine disruptors having different hydrophobicity, Appl. Catal. B: Environ. 41 (2003) 313-321.

[33] E.P. Reddy, L. Davydov, P. Smirniotis, TiO_2-loaded zeolites and mesoporous materials in the sonophotocatalytic decomposition of aqueous organic pollutants: the role of the support, Appl. Catal. B: Environ. 42 (2003) 1-11.

[34] H. Yamashita, K. Ikeue, T. Takewaki, M. Anpo, *In situ* XAFS studies on the effects of the hydrophobic-hydrophilic properties of Ti-Beta zeolites in the photocatalytic reduction of CO_2 with H_2O, Top. Catal. 18 (2002)95-100.

[35] M. Takauchi, T. Kimura, M. Hidaka, D. Rakhmawaty, M. Anpo, Photocatalytic oxidation of acetaldehyde with oxygen on TiO_2/ZSM-5 photocatalysts: Effect of hydrophobicity of zeolites, J. Catal. 246 (2007) 235-240.

[36] I.K. Konstantinou, T.A. Albanis, TiO_2-assisted photocatalytic degradation of azo dyes in aqueous solution: kinetic and mechanistic investigations, Appl. Catal. B: Environ., 49 (2004) 1-14.

CHAPTER 5

A PARAMETRIC STUDY ON ADSORPTIVE AND PHOTOCATALYTIC ACTIVITIES OF TITANIA/ZEOLITE COMPOSITES UNDER VISIBLE LIGHT IRRADIATION*

Abstract

In present chapter, a series of $TiO_{2-x}N_x$/Beta composite samples were prepared by coating the nitrogen doped titania on the Beta zeolite using the same wet chemical method. Samples were characterized by nitrogen adsorption desorption, XRD, TEM, UV-vis, XPS and FTIR techniques. The photocatalytic activities were evaluated by the degradation of methylene blue under visible light irradiation. The synergistic effect between absorption and photocatalysis of the $TiO_{2-x}N_x$/Beta composite materials was found in terms of methylene blue removal efficiency under visible light irradiation, since the assisting adsorption ability from H-Beta zeolite could supply a concentrated pollutant environment around titania active sites. The highest photocatalytic efficiency was obtained on the 10% $TiO_{2-x}N_x$-coated composite sample, which was probably due to the better dispersion of titania on the support. Furthermore, the $TiO_{2-x}N_x$/Beta-10% catalyst was consistent to be the most efficient composite material tested for the photocatalytic degradation of methylene blue even in different pH environment.

* This chapter has been adapted from: Chemical Engineering Journal, 165 (2010) 301-309.

5.1. Introduction

In recent years, industrialization and agricultural development, together with rapid urbanisation, have caused ever increasing pollution especially on water resources. Various kinds of contaminants enter into our water sources, most of them through industrial wastewater discharge. Developing effective wastewater treatment technologies is a challenging task to most researchers [1,2]. Recently, extensive efforts have been made to investigate the use of photocatalysis for the destruction and removal of highly toxic organic compounds in wastewater purification. Titanium oxides as photocatalysts have attracted a great deal of attention, due to its high photocatalytic activity, resistance to photocorrosion, photo-stability, low cost and non-toxicity [3]. It is generally accepted that fine nano-sized TiO_2 particles are favourable for attaining higher photoactivity compared to bulky large particles. Therefore, many attempts have been made to prepare the photocatalyst with finer particle size and narrower size distribution. However, in practical applications, dispersing photocatalysts in the form of fine particles in water is difficult, and such is separation or recovery [4]. On the other hand, pollutants in the wastewater often exist in low concentration (order of ppm or below) and the low concentration contaminants near TiO_2 catalyst is not favourable for surface contact-based photocatalytic reaction [5]. In order to achieve rapid and efficient decomposition of organic pollutants and put it to the practical use, great efforts have been made to design composite materials of TiO_2 powder immobilized on inert and suitable porous materials, such as mesoporous silica [6,7,8,9], activated carbon [10,11,12,13] and zeolite [14,15,16,17,18,19,20,21]. Among many porous materials, zeolites exhibit several specific features, which make them suitable for being used as host candidates for photocatalysts. These are (i) more photochemical stability and thermal and chemical inertness; (ii) reasonable transparency to UV-vis radiations above 240 nm allowing light of certain wavelength to reach the catalysts and pollutants at intraparticle positions; (iii) high adsorptive capacity for concentrating the organic compounds from solution to the active sites of the photocatalysts on the substrate.; (iv) the ability of the zeolite framework to participate actively in the electron-transfer process, either as an electron acceptor or an electron donor [22]. However, so far most of the composite materials reported in the literatures were only photocatalytically activibe under UV light irradiation [23]. It is well known in the overall solar radiation reaching the

earth's surface, ultraviolet light only contribute to <5% [24]. Therefore, this with no doubt would restrict the practical application of these kinds of composite materials in future use.

Recently researchers found that pure TiO_2 modified by metal [25,26] and non-metal doping processes [24,27,28,29,30,31,32,33,34] could lead to visible light photocatalysis. However, metal doping has several drawbacks, such as thermal instability and high cost. Therefore, anionic dopant seems to be more attractive than metal ions at the moment. Furthermore, latest efforts on calculated densities of states (DOSs) of the doped anion in the anatase TiO_2 crystal revealed that nitrogen doping could be the most effective choice for inducing photocatalytic activity under visible light irradiation, which was also confirmed by several experiment results [5,29,34]. To the best of our knowledge, only few literatures about titania/adsorbent composite photocatalysts via sol-gel nitrogen doping preparation are reported [35,36,37], which certainly deserve more research attention. Therefore, in this article we developed a series of $TiO_{2-x}N_x$/Beta composite photocatalyst with different titania loading. The obtained composite photocatalysts were characterized by nitrogen adsorption-desorption, XRD, UV-vis reflectance, XPS, FTIR and TEM. In addition, we studied the photocatalytic activities of the $TiO_{2-x}N_x$/Beta composite under visible light irradiation by using methylene blue as a model pollutant. The influence of H-Beta zeolite involvement as porous support on the structure and photocatalytic activities of N-doped TiO_2 nanoparticles was also discussed.

5.2. Experimental

5.2.1. Materials and chemicals

Commercial Beta zeolite (Si/Al= 10.8) was purchased from Sinopec Co (Tianjin, China) and it was calcined at 500 ^oC for 4h before being used in the sample preparation. The chemicals used for the synthesis were titanium butoxides ($Ti(OC_4H_9)_4$, 97%, Aldrich), HCl (65.5%, BDH Chemicals, Australia), ethanol (100%, Scharlau). Methylene blue was obtained from Sigma-Aldrich. All the chemicals were used as supplied without further purification. Deionized water, purified with a water purification system (Diamond, Barnstead), was used for preparing solutions in the experiments.

5.2.2. Preparation of N-doped TiO_2/Beta composite catalysts

The TiO_2 nanoparticles were synthesized by hydrolysis of precursor chemicals to form a transparent sol using the following method: 50 ml of titanium butoxide ($Ti(OC_4H_9)_4$, 97%) was dissolved in ethanol (200 ml). The solution was stirred for 30 min at room temperature followed by addition of a mixture of deionized water and nitric acid under vigorous stirring. The solution was then successively stirred at room temperature till a clear transparent sol was obtained. To introduce the nitrogen dopant into the titanium nanoparticles, triethylamine (N/Ti=1.0) was added drop-wise into the above titanium solution. Sol was formed immediately and vigorously stirred for another 10 hours. Depending on the (wt. %) loading of TiO_2 on the catalyst, certain amount of H-Beta zeolite was added to the titanium sol. The resulting mixed suspension was continuously stirred for 5h. Finally, the resulting N-doped titania zeolite catalyst samples were dried at 105 ^oC for 10h and calcined in an air atmosphere at 350 ^oC with temperature ramping at 5 ^oC min^{-1} and maintained for 2h. The synthesized samples were denoted as $TiO_{2-x}N_x$/Beta-x%, where x is the titania content. The bare $TiO_{2-x}N_x$ sample without the addition of Beta zeolite, were also prepared under the same experimental conditions as a reference.

5.2.3. Catalysts characterization

The specific surface area of all the composite catalysts and the bare $TiO_{2-x}N_x$ sample was determined from nitrogen adsorption-desorption isotherms at 77K using volumetric adsorption equipment (BELSORP mini). The surface area was determined using the BET equation. X-ray powder diffraction (XRD) patterns of all samples were collected in the range 20-80° at ambient temperature using a Mini Material Analyser (Cu Kα radiation, λ=1.54065 Å), operated at 1 kV and 35 mA. The scan speed was 0.5^o min^{-1}. The crystallite size was estimated by using the Scherrer equation:

$$L=K\lambda/\beta\cos\theta \quad (1)$$

Where β is the full-width at half-maximum (FWHM) of the diffraction peak, K =0.89 is a coefficient, Θ is the diffraction angle, and λ is the X-ray wavelength corresponding to the Cu Kα irradiation. Optical properties of the $TiO_{2-x}N_x$/Beta composite samples were studied by a Cary 100 UV-visible spectrometer in diffuse reflectance mode over the spectral range of 200-800 nm. Surface analysis of the

composite materials and the bare N-doped TiO_2 catalysts was carried out by using X-ray photoelectron spectroscopy (XPS). The instrument employed for XPS studies was a SPECS SAGE spectrometer with a Phoibos 150 hemi-spherical analyser, and an MCD-9 detector. The radiation source used was Mg Kα, and was run at 10kV and 20mA (200W). Samples were placed on carbon tape and then inserted directly to the sample stage. Fourier transform infrared (FTIR) spectra were recorded with KBr disks containing the powder sample with the FTIR spectrometer (Shimadzu FTIR 84005). Transmission electron microscopy (TEM) analysis was conducted using H-7500 microscopy operating with an acceleration voltage of 80 kV. The samples were prepared by ultrasonication in ethanol, and then evaporating a drop of the resultant suspension onto a carbon support grid.

5.2.4. Photocatalytic activity test

The photocatalytic activities of $TiO_{2-x}N_x$/Beta composite catalysts were evaluated by measuring the concentration decrease of methylene blue dye (MB) in the solution under visible light irradiation. In order to eliminate the influence of adsorption, prior to the illumination, a suspension containing the catalyst (30 mg) and 100 ml of aqueous solution with 15 ppm of MB was stirred continuously for 2h in the dark in order to establish the adsorption/desorption equilibrium. Thereafter, the photocatalytic reaction proceeded under visible light irradiation, during which an 80-W Xe lamp equipped with a UV cut-off filter (λ>460 nm) was used as a visible light source. At the given time intervals, a *ca.* 2 ml of sample was withdrawn by a syringe from the suspension. The catalyst was separated by centrifugation from the aqueous solution prior to the analysis. The concentration of MB was determined by a Cary 100 UV-visible spectrometer at 650 nm wavelength. For the photocatalytic degradation at different pH value solutions, the pH was adjusted using either NaOH or HNO_3 solution.

5.3. Results and discussion

5.3.1. Characterization

Table 5.1: The physicochemical properties of the bare $TiO_{2-x}N_x$ and the composite samples

Samples	Titanium crystallite size from XRD (nm)	S_{BET} (m^2g^{-1})	1 st $E_{band\ gap}$ (eV)	2 st $E_{band\ gap}$ (eV)
H-Beta	-	523.6	-	-
$TiO_{2-x}N_x$/Beta-10%	-	315.6	3.28	2.66
$TiO_{2-x}N_x$/Beta-40%	5	274.8	3.28	2.40
$TiO_{2-x}N_x$/Beta-90%	5	228.3	3.28	2.53
Bare $TiO_{2-x}N_x$	5	272.1	3.26	2.57

The specific surface areas of all samples are listed in Table 5.1. Compared to the parent H-Beta zeolite, 10% titania coated on the zeolite lead to a great decrease on the BET specific surface area. A higher loading of titania would result in a further decease. However, this tendency alleviated when titania loading increased to 40% and 90%. As for the $TiO_{2-x}N_x$/Beta-90% catalyst, the surface area was even smaller than that of the bare N-doped TiO_2 sample. The decreasing trend on the specific surface area indicated that the zeolite support and naked N-doped TiO_2 was not simply a mechanical mixing. Instead, N-doped TiO_2 nanoparticles were dispersed on or inside the support and blocked the zeolite's pore channels partially, which may lead to the apparent decrease of the BET specific surface area.

The XRD patterns of $TiO_{2-x}N_x$/Beta-x% catalysts with 10%, 40%, 90% titania loading and the bare $TiO_{2-x}N_x$ sample are displayed in Fig. 5.1. For the bare N-doped TiO_2 sample the diffraction peaks were all assigned to the anatase crystalline phase, and no other crystal phase (rutile or brookite) was detected. As for the $TiO_{2-x}N_x$/Beta-x% catalysts with 40%, 90% titania loadings, besides the anatase crystalline phase, the diffraction peaks assigned to the Beta zeolite were clearly observed. This proves that

the zeolite structure was well preserved in the preparation process. For the $TiO_{2-x}N_x$/Beta-10% sample, except the diffraction peaks of zeolite support, no obvious anatase peaks could be seen. This may imply that the titania nanoparticles may be small enough and evenly dispersed on Beta zeolite support. The average crystalline sizes of the photocatalysts were determined according to Scherrer's equation and the results are listed in Table 1. The average crystalline sizes were estimated to be 5 nm for the $TiO_{2-x}N_x$/Beta-x% catalysts with 40%, 90% titanium loadings, which was close to that of the bare N-doped TiO_2 sample.

The TEM images of the bare N-doped TiO_2, $TiO_{2-x}N_x$/Beta-10% and $TiO_{2-x}N_x$/Beta-90% samples are shown in Fig. 5.2. From Fig. 5.2 (A, B), it seems that for the bare TiO_2 sample, the size of TiO_2 nano-particles is *ca.* 5 nm, which is in good accordance with the XRD calculation. However, the particle aggregation was so severe that massive bulk of titania can be seen in the image. For the image of $TiO_{2-x}N_x$/Beta-10% sample in Fig. 5.2 (C, D), it indicates that the titania particles were in small size and well dispersed on the support. While for the $TiO_{2-x}N_x$/Beta-90% sample in Fig. 5.2 (E, F), except a small part of the titania particles spread on the zeolite surface, most of them are aggregated like the bare N-doped TiO_2. From the TEM results, it can be conclude that 10% titania loading was suitable to obtain a good dispersion on the zeolite support.

X-ray photoelectron spectroscopy (XPS) was carried out for the surface characterization of the bare N-doped TiO_2 and the $TiO_{2-x}N_x$/Beta composite samples. In Fig. 5.3 (a), it can be seen that a tiny peak is present in the N1s spectra region of the bare N-doped TiO_2 sample and enlarged in the insert of Fig. 5.3 (a). With a suitable spectral deconvolution the peak could be separated into two peaks at ca. 400 eV and ca. 397 eV. It is well known that precise identification of nitrogen species with the banding energy at ca. 400 eV is still a challenging topic in the field of nitrogen-doped material, but it is generally accepted that the peak at ca. 400 eV may be attribute to the presence of the N atom from adsorbed nitrogen containing compounds on the surface of the samples. As for the peaks in the region of 396-398 eV, they probably arose from O-Ti-N linkages when N atoms replaced the oxygen in the TiO_2 crystal lattice [33,38,39]. Therefore, it is believed that during the sol-gel preparation some nitrogen has been successfully incorporated into the titania lattice

and substituted oxygen in the bare N-doped TiO_2 sample. The nitrogen content in the product is estimated to be 0.25%.

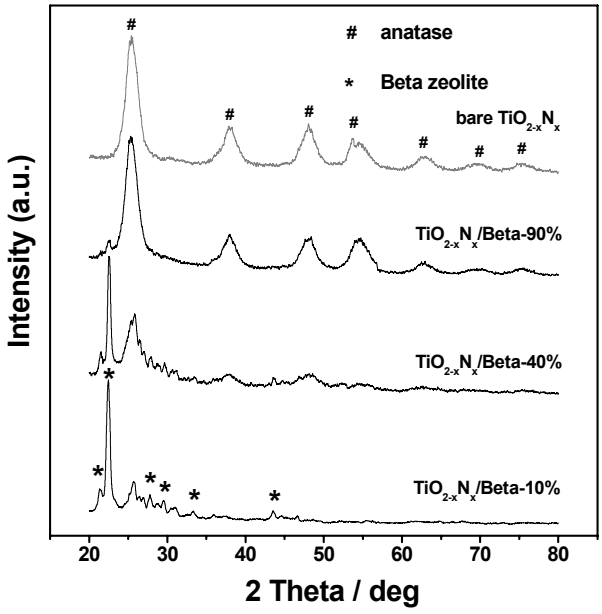

Figure 5.1: XRD patterns of the naked $TiO_{2-x}N_x$ and $TiO_{2-x}N_x$/Beta-x% composites samples coated with 10%, 40% and 90% titania loading.

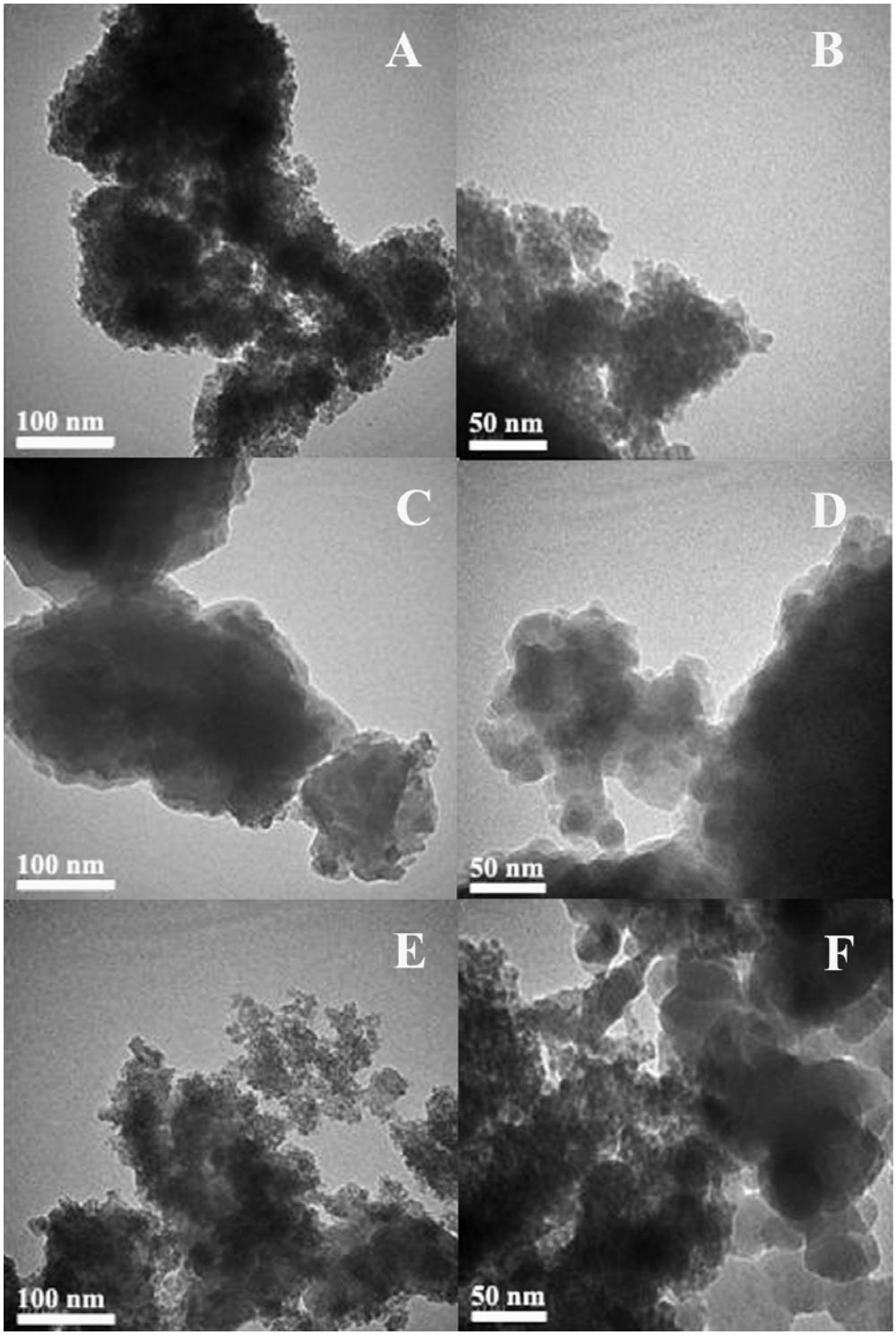

Figure 5.2: TEM images of the bare N-doped TiO_2 (A, B), $TiO_{2-x}N_x$/Beta-10% (C, D) and $TiO_{2-x}N_x$/Beta-90% (E, F) samples.

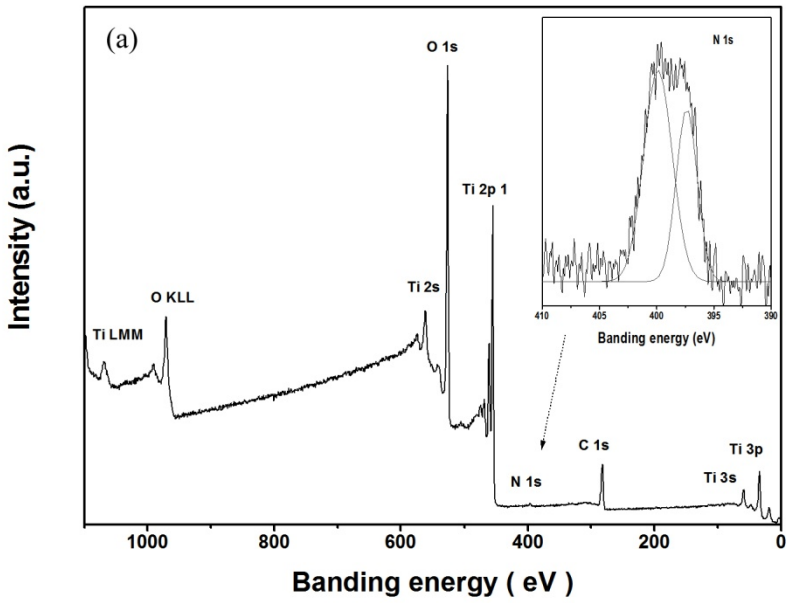
(a)
O 1s
Ti 2p 1
Ti 2s
O KLL
Ti LMM
N 1s
C 1s
Ti 3p
Ti 3s
Intensity (a.u.)
Banding energy (eV)
1000
800
600
400
200
0
Banding energy (eV)

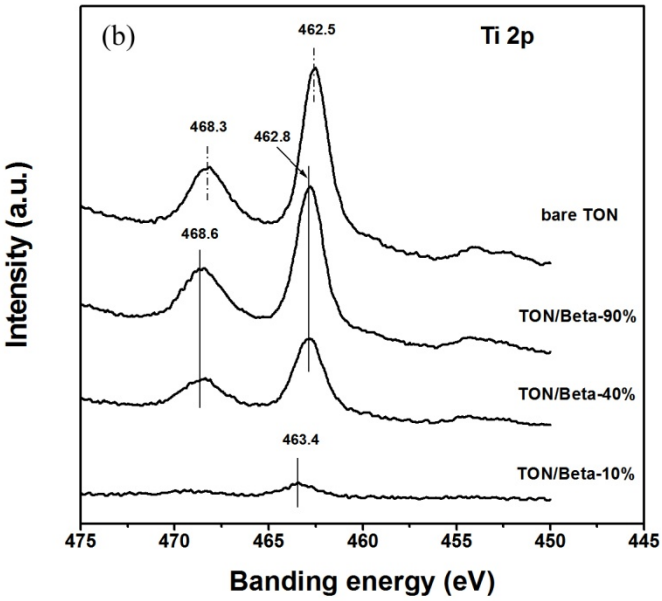
(b)
Ti 2p
462.5
468.3
462.8
468.6
463.4
bare TON
TON/Beta-90%
TON/Beta-40%
TON/Beta-10%
Intensity (a.u.)
475
470
465
460
455
450
445
Banding energy (eV)

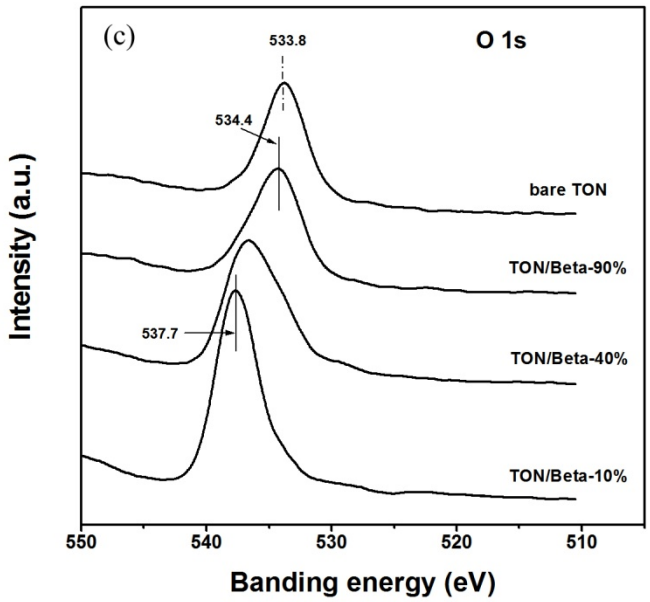
(c)
O 1s
533.8
534.4
537.7
bare TON
TON/Beta-90%
TON/Beta-40%
TON/Beta-10%
Intensity (a.u.)
550
540
530
520
510
Banding energy (eV)

Figure 5.3: (a) XPS spectra of the bare N-doped TiO_2 sample in the whole banding energy region and the banding energy region for N1s; The Ti 2p region (b) and O 1s region (c) of XPS spectra from different samples: the bare N-doped TiO_2 and $TiO_{2-x}N_x$/Beta-x% composites samples with different titania loadings.

Fig. 5.3 (b) shows the Ti 2p region of the XPS spectra collected from the composite samples with different Ti loading. The bare N-doped TiO_2 acts as a reference sample. The binding energy (BE) of the Ti $2p^{3/2}$ and Ti $2p^{1/2}$ for the bare N-doped TiO_2 sample appear at 462.5 eV and 468.3 eV. While for the $TiO_{2-x}N_x$/Beta-90% and $TiO_{2-x}N_x$/Beta-40% samples, the Ti 2p peak is shifted to the higher banding energy region, which is about 462.8 eV and 468.6 eV respectively. Furthermore, more obvious shift can be observed for the $TiO_{2-x}N_x$/Beta-10% sample, for which the $2p^{3/2}$ peak is at *ca.* 463.4 eV and no peak for Ti $2p^{1/2}$ can be clearly found. This result was similar to that observed by Petkowicz *et al*. [18,40]. Petkowicz *et al*. think that the shift was caused by the bonding configuration existing between TiO_2 and zeolite, with Ti-O-Si and Ti-O-Al bonds acting as bridges between two materials. In other words, chemical links were thought to exist between TiO_2 and Beta zeolite. From the TEM image in Fig. 5.2, it can be see that in the $TiO_{2-x}N_x$/Beta-10% sample titania particles were not tend to aggregate but to evenly dispersed on the support. Therefore, it is believed that the chemical link between TiO_2 and Beta zeolite were more pronounced in the $TiO_{2-x}N_x$/Beta-10% sample, which contributed the apparent shift to higher banding energy region in the Ti 2p peaks. Further investigation was conducted on the O1s region of XPS spectra for the same samples which are shown in Fig. 5.3 (c). It is believed that for the composite samples, the O1s signals come from two main contributions: first signal around 533.8 eV, related to the O in the formation of nitrogen doped TiO_2 anatase and second signal at higher banding energy region, related to the O bonded to Si and Al in the zeolite moiety [18]. From Fig. 5.3 (c), it seems that for the composite samples, the peaks of O 1s are all moved to the high banding energy region, compared to the N-doped TiO_2 sample, especially for the $TiO_{2-x}N_x$/Beta-10% sample. It means that for all the composite samples, the O 1s signal from the zeolite structure made contributions to the overall O 1s peak more or less. Petkowicz *et al.* [18] found that no signal of O 1s from the zeolite support could be detected if the layer of Ti completely covers the zeolite surface in the composite samples. Therefore, it can be inferred that

in our composite samples, the surface of zeolite was not covered by the Ti compound completely, even when the Ti loading was 90%.

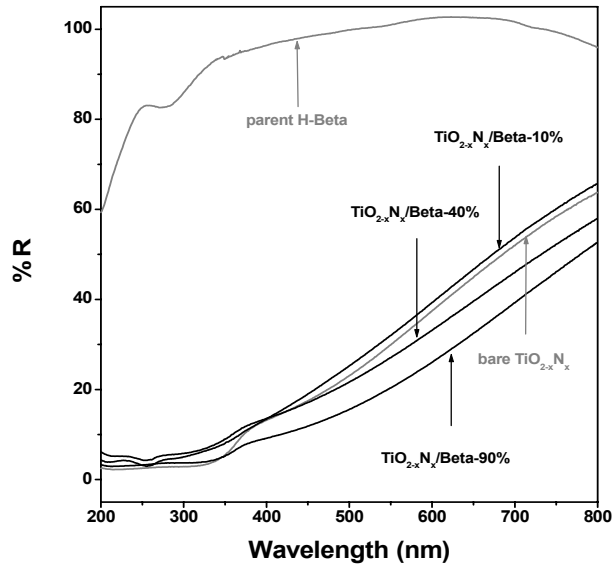

Figure 5.4: UV-vis diffuse reflectance spectra of the naked $TiO_{2-x}N_x$ and the $TiO_{2-x}N_x$/Beta-x% composite samples with different titania loading.

Fig. 5.4 shows the results of diffuse reflectance spectroscopy. For the parent Beta zeolite, only a very weak absorbance in the ultraviolet region could be observed. As for the $TiO_{2-x}N_x$/Beta-x% composite samples, the absorbance behaviour is much different. Strong absorbance was observed and the optical response clearly extended into the visible region, which was similar to the bare N-doped TiO_2 sample. This was resulted from the narrowed band gap after nitrogen incorporation, which also confirmed that the nitrogen incorporation also existed in the titania matrix after coating on the Beta support. Furthermore, with TiO_2 loading increasing, further extension occurred. Two absorbance edges located at 370-380 nm and 460-520 nm appearred respectively. The appearance of the second absorption edge indicates that a new energy band was formed. The band gap energies are summarized in Table 5.1.

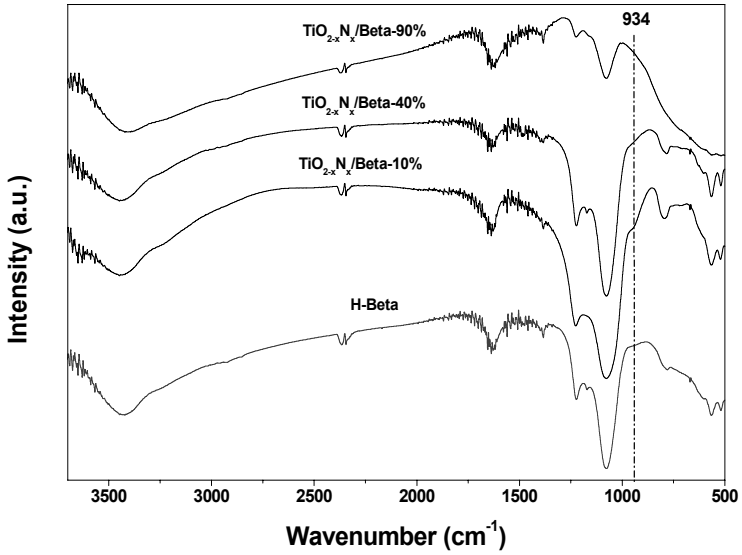

Figure 5.5: FTIR spectra of the materials: $TiO_{2-x}N_x$/Beta-90%, $TiO_{2-x}N_x$/Beta-40%, $TiO_{2-x}N_x$/Beta-10%, H-Beta samples.

Fig. 5.5 shows the FTIR spectra of the $TiO_{2-x}N_x$/Beta-90%, $TiO_{2-x}N_x$/Beta-40%, $TiO_{2-x}N_x$/Beta-10%, and H-Beta samples. The broad peak centred at 3427 cm^{-1} was assigned to the O-H stretching region, and the peak at 1631cm^{-1} corresponding to the O-H bending vibration of adsorbed water molecules [41]. The peaks in the region of 1250-950, 790-650 and 500-420 cm^{-1} were attributed to the asymmetrical stretching, symmetrical stretching and to (O-Si-O or O-Al-O) deformation, respectively [18]. Sun *et al.* reported a peak appearing at 934 cm^{-1} after titania was loaded on the SiO_2 support. This was related to the vibration involving a SiO_2 tetrahedron bonded to a titanium atom through Ti-O-Si bonds [40]. The same peak was also observed in our composite samples, especially in the $TiO_{2-x}N_x$/Beta-10% sample. This further proves that titania particles were immobilized on the Beta zeolite by chemical bonds, which was in good accordance with the XPS results.

5.3.2. Photocatalytic activities

5.3.2.1. Effect of H-Beta zeolite support on the composite photocatalytic ability

To investigate the photocatalytic activities of the composite samples, the MB photodegradation under the visible light irradiation was carried out and compared with the bare $TiO_{2-x}N_x$ sample (shown in Fig. 5.6). In the adsorption-desorption

process (from -120 min to 0 min), it can be seen that for the parent H-Beta zeolite, the final methylene blue removal rate by adsorption could only reach 61%. With the increase of the TiO_2 loading, the amount of adsorbed MB by the composite materials were greatly reduced, and yet still higher than that of the bare N-doped TiO_2 sample. At the adsorption-desorption equilibrium point, the MB removal rates were 17%, 44% and 50% over the $TiO_{2-x}N_x$/Beta-90%, $TiO_{2-x}N_x$/Beta-40%, $TiO_{2-x}N_x$/Beta-10% catalysts respectively, while the bare N-doped TiO_2 sample only achieved 8%. The addition of Beta zeolite appeared to enhance the composite adsorption ability, of which the order was also consistent with the BET results. However, the blockage in the pore channels on H-Beta support after TiO_2 addition may deteriorate with the increase of the TiO_2 loading.

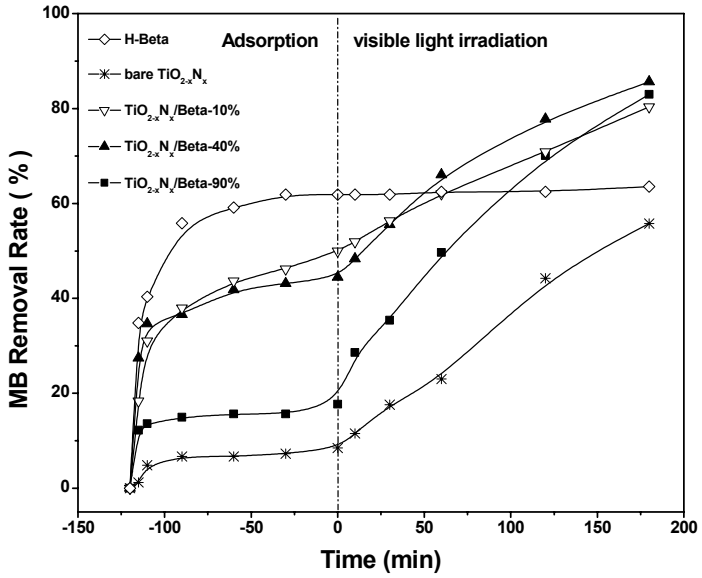

Figure 5.6: Removal efficiency of MB on $TiO_{2-x}N_x$/Beta-x% composite materials under visible light irradiation.

After adsorption-desorption equilibrium, photodegradation of MB by parent H-Beta zeolite was performed under visible light irradiation as a blank experiment. In Fig 5.6, no conversion can be seen by the parent H-Beta zeolite under the visible light irradiation. This means that the H-Beta zeolite was inert for the photodegradation of MB and any direct photocatalysis of MB was negligible. For the composite catalysts, after the photocatalytic reaction commencing, the MB concentration continued to decrease (from 0 min to 180 min). The final MB removal achieved is 85%, 83%, 80%

for the $TiO_{2-x}N_x$/Beta-90%, $TiO_{2-x}N_x$/Beta-40% and $TiO_{2-x}N_x$/Beta-10% catalysts, respectively. For the bare N-doped TiO_2 catalyst, the ultimate MB removal was only about 55%. It is evident that photocatalytic activities were greatly improved after adding the zeolite support compared to the bare N-doped TiO_2.

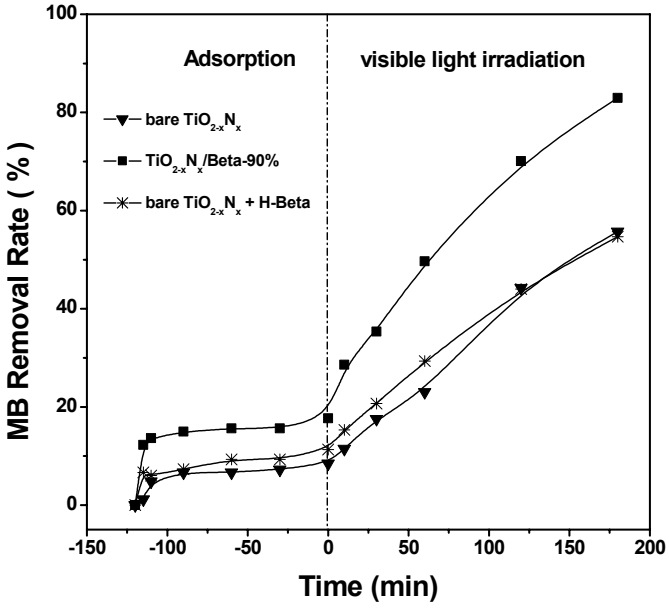

Figure 5.7: Comparison of removal efficiency of MB on the $TiO_{2-x}N_x$/Beta-90%, the $TiO_{2-x}N_x$ and the mixed catalyst of bare $TiO_{2-x}N_x$ (90%) with H-Beta (10%) under visible light irradiation.

In order to demonstrate the synergistic role of the Beta zeolite support for photocatalytic activities in the composite samples more distinctively, the comparison of photocatalytic activity over the $TiO_{2-x}N_x$/Beta-90%, the bare N-doped TiO_2 sample and a mixture of bare N-doped TiO_2 (90%) with H-Beta (10%) was carried out. The results are shown in Fig. 5.7. For the loose mixture of naked N-doped TiO_2 with H-Beta, it was apparent that the MB removal by adsorption was higher than for the N-doped TiO_2 because of the addition of the Beta zeolite. However, the ultimate MB conversion (54.4%) after photocatalytic degradation was almost same lose to that of the bare N-doped TiO_2 (55.8%), and much lower than for the $TiO_{2-x}N_x$/Beta-90% (85.0%). This suggested that due to the successful loading of the titania on the Beta zeolite carrier, a synergistic effect existed that the Beta zeolite, which possessed a high surface area, could easily absorb the MB pollutant and supply a highly

concentrated MB environment for the nearby titania to proceed the photocatalytic reaction.

5.3.2.2. Determining optimal titania loading on the H-Beta zeolite support

One would expect that the titania loading on the H-beta support affect the resulting photocatalytic ability of composites greatly. In Fig. 5.8, it is shown that for the bare $TiO_{2-x}N_x$ sample, the photocatalytic efficiency was the lowest compared with the $TiO_{2-x}N_x$/Beta composite samples. With the addition of H-Beta support, the photocatalytic efficiency was enhanced in the composite samples. For the $TiO_{2-x}N_x$/Beta-10% sample, extraordinarily high efficiency was obtained, which was 3-7 times higher than other samples. However, any higher titania loading than 10% appeared to have adverse effects. For the $TiO_{2-x}N_x$/Beta-90% sample, the photocatalytic efficiency was a little higher than the bare $TiO_{2-x}N_x$ sample. It is speculated that in composite samples some titania particles self-aggregate like the pure titania and the others link with the Beta support, while for the $TiO_{2-x}N_x$/Beta-10% sample, nano-sized titania particles were more well dispersed on the Beta support with strong bonding links. This could make the concentrated MB access the adjacent titania particles near the support more easily.

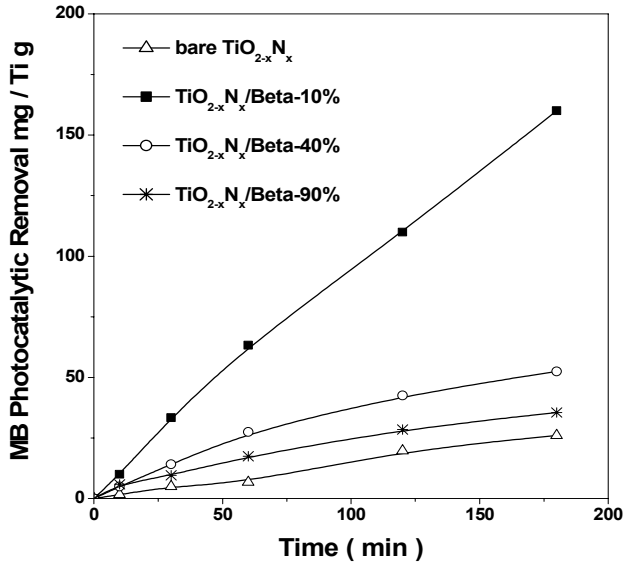

Figure 5.8: Removal efficiency of MB on $TiO_{2-x}N_x$/Beta-x% catalysts under visible light irradiation.

5.3.2.3. Influence of the solution pH values

In real applications, the pH value of wastewater varies depending on the source, which is an important factor influencing the photocatalytic activities [42]. Therefore, herein we investigated the effect of different pH values (pH=2, pH=7 and pH=10) on the performance of composite samples.

Firstly, the adsorption of the bare $TiO_{2-x}N_x$ and H-Beta samples at different pH values were studied as references and the results are shown in Fig. 5.9 (a) and (b). For the bare $TiO_{2-x}N_x$ sample, the adsorption ability was remarkably different at acidic and basic pH. The removal rate by adsorption could attain almost 90% at basic medium (pH=10), while nearly no adsorption was observed at acidic medium (pH=2). At the neutral pH, only a small removal rate (ca. 7%) could be achieved. Reportedly, the pH_{pzc} of titania is about 3.5-6.7, above which its surface became negatively charged. Since the MB is cationic dye, high pH medium would favour the MB adsorption apparently [42]. As for the H-Beta support, the similar trend of adsorption abilities was also found. Together, it is concluded that basic pH favoured the enhancement of the adsorption ability both on the bare N-doped TiO_2 sample and on the H-Beta support, while this effect was more pronounced on the bare $TiO_{2-x}N_x$ sample than on parent H-Beta support. Fig. 9 (c) and (d) shows the results about for MB adsorption of the $TiO_{2-x}N_x$/Beta-90% (A) and $TiO_{2-x}N_x$/Beta- 10% (B) composite samples at different pH values. The MB adsorption behaviour of the $TiO_{2-x}N_x$/Beta-10% sample showed little difference to that of H-Beta. Both of them showed a great improvement of adsorption when the pH reached10. For the $TiO_{2-x}N_x$/Beta-90% sample, the order of absorption between different pH values was similar to the bare $TiO_{2-x}N_x$ sample with slightly better adsorption ability at each pH due to the addition of small amount of H-Beta support.

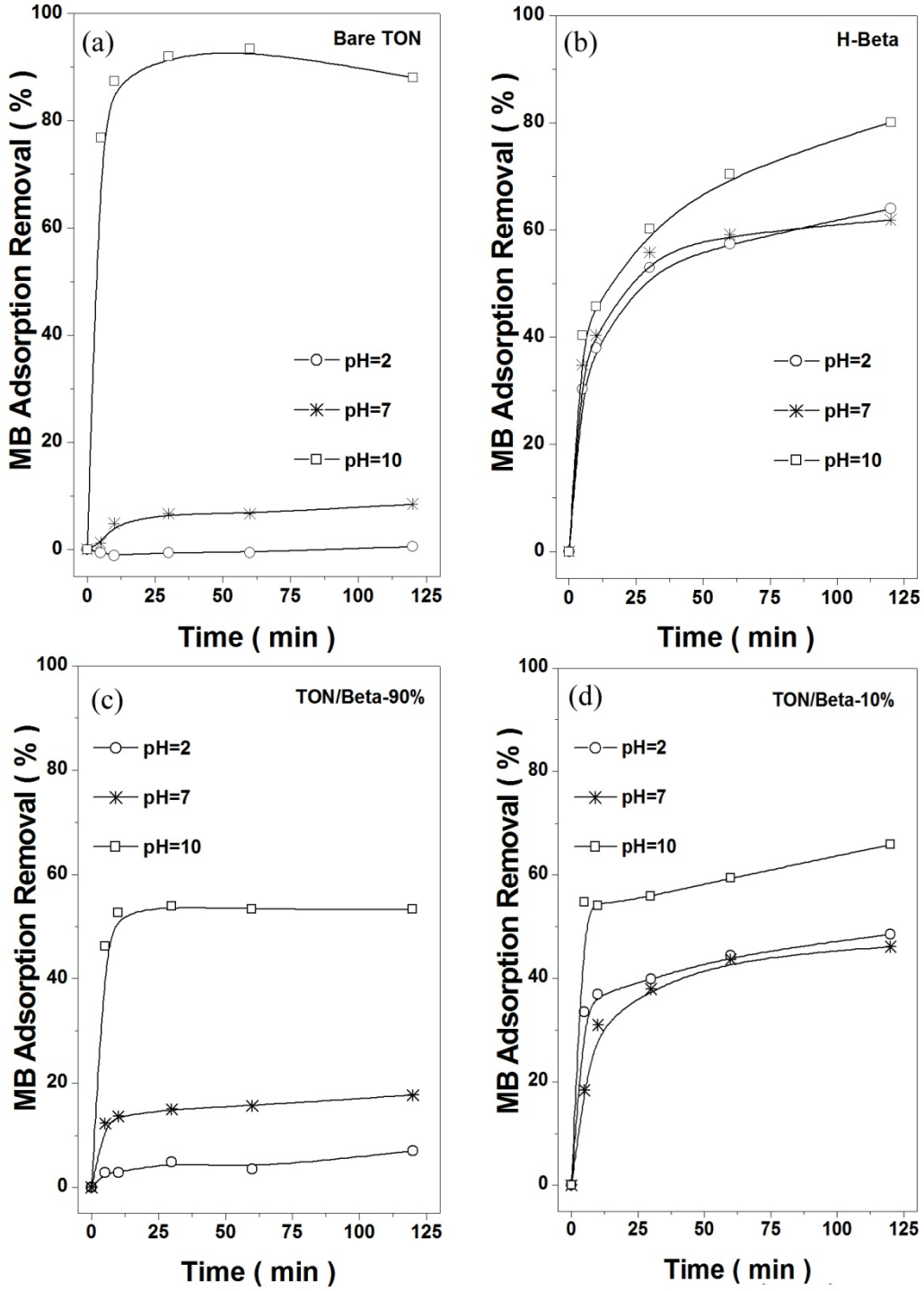

Figure 5.9: Removal rate of MB on bare N-doped TiO_2 (a), H-Beta (b), $TiO_{2-x}N_x$/Beta-90% (c) and $TiO_{2-x}N_x$/Beta-10% (d) during adsorption process.

In Fig. 5.10, further consideration has been given to the photocatalytic efficiency of the $TiO_{2-x}N_x$/Beta-90% and $TiO_{2-x}N_x$/Beta-10% composite samples for the MB degradation under different pH values. From Fig. 10 (A), it can be seen that the photocatalytic efficiency of the $TiO_{2-x}N_x$/Beta-90% sample was influenced by the pH

value greatly. As discussed before, the composite adsorption ability was associated with pH value strongly. Moderate adsorption (pH=7) appear red to be optimal for the continuation of the photocatalytic reaction over the $TiO_{2-x}N_x$/Beta-90% sample. Higher basicity (pH=10) with the overly strong MB adsorption could cover the titania active sites and thus hinder the absorption of light to progress the reaction. On the other hand, high acidity (pH=2) with very weak or no adsorption was not beneficial to the reaction either, because of the low MB concentration adjacent to the active titania. The photocatalytic activity behaviour of the $TiO_{2-x}N_x$/Beta-10% sample was somewhat different, as seen in Fig 10 (B). Although the efficiency order was the same as that of $TiO_{2-x}N_x$/Beta-90% sample (pH=7> pH=10> pH=2), the difference between the curves was narrow with a maximum point only at ca. 10%. Compared with $TiO_{2-x}N_x$/Beta-90% sample, $TiO_{2-x}N_x$/Beta-10% sample exhibited higher photocatalytic efficiency consistently at all three pH values.

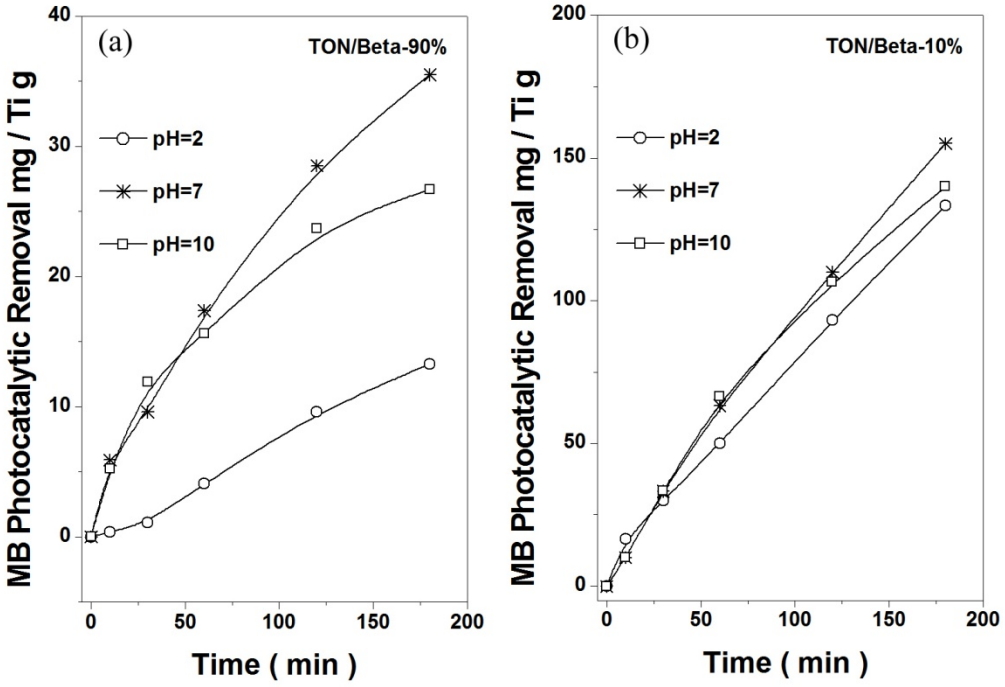

Figure 5.10: Comparison of photocatalytic removal Rate of MB on $TiO_{2-x}N_x$/Beta-90% (a) and $TiO_{2-x}N_x$/Beta-10% (b) samples under visible light irradiation.

5.4. Conclusions

A series of $TiO_{2-x}N_x$/Beta composite samples were prepared using a simple sol-gel method where nitrogen has been incorporated into the titania successfully. It is found that N-doped titania can be evenly dispersed on the Beta zeolite support at a low loading with chemical bonding between titania and the Beta zeolite support. It appeared that the synergistic absorption and photocatalysis of the $TiO_{2-x}N_x$/Beta composite materials could enhance the removal efficiency of methylene blue under visible light irradiation. All of the $TiO_{2-x}N_x$/Beta composite samples showed excellent photocatalytic activities under visible light irradiation, among which the $TiO_{2-x}N_x$/Beta-10% sample achieved the highest rate. This was potentially ascribed to the better dispersion of the $TiO_{2-x}N_x$ on support, which could make the concentrated MB access the adjacent titania particles on the zeolite support more easily. Further investigation also revealed that the $TiO_{2-x}N_x$/Beta-10% sample was consistent to be the most efficient composite material of the photocatalytic degradation of methylene blue in different pH solutions.

References

[1] P. J. Senogles, J. A. Scott, G. Shaw and H. Stratton, Photocatalytic degradation of the cyanotoxin cylindrospermopsin, using titanium dioxide and UV irradiation, Water Res. 35 (2001) 1245-1255

[2] L. Zou and B. Zhu, The synergistic effect of ozonation and photocatalysis on color removal from reused water, J. Photoch. Photobio. A 196 (2008) 24-32

[3] L. Lin, R. Y. Zheng, J. L. Xie, Y. X. Zhu and Y. C. Xie, Synthesis and characterization of phosphor and nitrogen co-doped titania, Appl. Catal. B: Environ. 76 (2007) 196-202

[4] R. J. Tayade, R. G. Kulkarni and R. V. Jasra, Enhanced photocatalytic activity of TiO_2-coated NaY and HY zeolites for the degradation of methylene blue in water, Ind. Eng. Chem. Res. 46 (2007) 369-376

[5] S. X. Liu and X. Y. Chen, Preparation and characterization of a novel activated carbon-supported N-doped visible light response photocatalyst ($TiO_{2-x}N_y$/AC), J Chem. Technol. Biot. 82 (2007) 453-459

[6] Y. M. Xu and C. H. Langford, Photoactivity of titanium dioxide supported on

MCM41, zeolite X, and zeolite Y, J. Phys. Chem. B 101 (1997) 3115-3121

[7] K. F. Lin, P. P. Pescarmona, H. Vandepitte, D. D. Liang, G. Van Tendeloo and P. A. Jacobs, Synthesis and catalytic activity of Ti-MCM-41 nanoparticles with highly active titanium sites, J. Catal. 254 (2008) 64-70

[8] J. Yang, J. Zhang, L.W. Zhu, S. Y. Chen, Y. M. Zhang, Y. Tang, Y. L. Zhu and Y. W. Li, Synthesis of nano titania particles embedded in mesoporous SBA-15: characterization and photocatalytic activity, J. Hazard. Mater. 137 (2006) 952-958

[9] T. P. Ang, C. S. Toh and Y-F Han, Characterization, and activity of visible-light-driven nitrogen-doped TiO_2-SiO_2 mixed oxide photocatalysts, J. Phys. Chem. C 113 (2009) 10560-10567

[10] J. J. Xu, Y. H. Ao, D. G. Fu and C. W. Yuan, A synthesis of fluorine-doped titania-coated activated carbon under low temperature with high photocatalytic activity under visible light, J. Phys. Chem. Solids 69 (2008) 2366-2370

[11] Y. J. Li, X. D. Li, J. W. Li and J. Yin, Photocatalytic degradation of methyl orange in a sparged tube reactor with TiO_2-coated activated carbon composites, Catal. Commun. 6 (2005) 650-655

[12] Y. Tao, C-Y Wu and D. W. Mazyck, Removal of methanol from pulp and paper mills using combined activated carbon adsorption and photocatalytic regeneration, Chemosphere 65 (2006) 35-42

[13] B. Zhu and L. Zou, Removal of color compounds from recycled water using combined activated carbon adsorption and AOP decomposition, J. Adv. Oxid. Technol. 12 (2009) 1-8

[14] M. V. Shankar, S. Anandan, N. Venkatachalam, B. Arabindoo and V. Murugesan, Fine route for an efficient removal of 2,4-dichlorophenoxyacetic acid (2,4-D) by zeolite-supported TiO_2, Chemosphere 63 (2006) 1014-1021

[15] M. Mahalakshmi, S. V. Priya, B. Arabindoo, M. Palanichamy and V. Murugesan, Photocatalytic degradation of aqueous propoxur solution using TiO_2 and H zeolite-supported TiO_2, J. Hazard. Mater. 161 (2009) 336-343

[16] M. Takeuchi, T. Kimura, M. Hidaka, D. Rakhmawaty and M. Anpo, Photocatalytic oxidation of acetaldehyde with oxygen on TiO_2/ZSM-5 photocatalysts: Effect of hydrophobicity of zeolites, J. Catal. 246 (2007) 235-240

[17] A. Bhattacharyya, S. Kawi and M. B. Ray, Photocatalytic degradation of orange II by TiO2 catalysts supported on adsorbents, Catal. Today 98 (2004) 431-439

[18] D. I. Petkowicz, R. Brambilla, C. Radtke, C. D. S. da Silva, Z. N. da Rocha, S. B.C. Pergher and J. H. Z. dos Santos, Photodegradation of methylene blue by in situ generated titania supported on a NaA zeolite, Appl. Catal. A: Gen. 357 (2009) 125-134

[19] M. V. P, Sharma, V. Durgakumari and M. Subrahmanyam, Solar photocatalytic degradation of isoproturon over TiO_2/H-MOR composite systems, J. Hazard. Mater. 160 (2008) 568-575

[20] E. P. Reddy, L. Davydov and P. Smirniotis, TiO_2-loaded zeolites and mesoporous materials in the photocatalytic decomposition of aqueous organic pollutants: the role of the support, Appl. Catal. B: Environ. 42 (2003) 1-11

[21] A. N. Ökte and Ö. Yılmaz, Characteristics of lanthanum loaded TiO_2-ZSM-5 photocatalysts: decolourization and degradation processes of methyl orange, Appl. Catal. A: Gen. 354 (2009) 132-142

[22] A. Corma and H. Garcia, Zeolite-based photocatalysts, Chem. Commun. 9 (2004) 1443-1459

[23] W. Zhang, L. Zou and L. Wang, Photocatalytic TiO_2/adsorbent nanocomposite prepared via wet chemical impregnation for wastewater treatment: a review, Appl. Catal. A: Gen. 71 (2009) 1-9

[24] T. C. Jagadale, S. P. Takale, R. S. Sonawane, H. M. Joshi, S. I. Patil, B. B. Kale and S. B. Ogale, N-Doped TiO_2 nanoparticle based visible light photocatalyst by modified peroxide sol-gel method, J. Phys. Chem. C 112 (2008) 14595-14602

[25] J. F. Zhu, F. Chen, J. L. Zhang, H. J. Chen and M. Anpo, Fe^{3+}-TiO_2 photocatalysts prepared by combining sol-gel method with hydrothermal treatment

and their characterization, J. Photoch. Photobio. A 180 (2006) 196-204

[26] A. Fuerte, M. D. Hernández-Alonso, A. J. Maira, A. Martínez-Arias, M. Fernández-García, J. C. Conesa, J. Soria and G. Munuera, Nanosize Ti-W mixed oxides: effect of doping level in the photocatalytic degradation of toluene using sunlight-type excitation, J. Catal. 212 (2002) 1-9

[27] L. Lin, R. Y. Zheng, J. L. Xie, Y. X. Zhu and Y. C. Xie, Synthesis and characterization of phosphor and nitrogen co-doped titania, Appl. Catal. B: Environ. 76 (2007) 196-202

[28]G. S. Wu, T. Nishikawa, B. Ohtani and A. C. Chen, Synthesis and characterization of carbon-doped TiO_2 nanostructures with enhanced visible light response, Chem. Mater. 19 (2007) 4530-4537

[29] C. Burda, Y. B. Lou, X. B. Chen, A. C. S. Samia, J. Stout and J. L. Gole, Enhanced nitrogen doping in TiO_2 nanoparticles, Nano Lett. 3 (2003) 1049-1051

[30] J. L. Gole, J. D. Stout, C. Burda, Y. B. Lou and X. B. Chen, Highly efficient formation of visible light tunable TiON photocatalysts and their transformation at the nanoscale, J. Phys. Chem. B 108 (2004) 1230-1240

[31] Y-M Lin, Y-H Tseng, J-H Huang, C. C. Chao, C-C Chen and I. Wang, Photocatalytic activity for degradation of nitrogen oxides over visible light responsive titania-based photocatalysts, Environ. Sci. Technol. 40 (2006) 1616-1621

[32] S-K Joung, T. Amemiya, M. Murabayashi and K. Itoh, Relation between photocatalytic activity and preparation conditions for nitrogen-doped visible light-driven TiO_2 photocatalysts, Appl. Catal. A: Gen. 312 (2006) 20-26

[33]Y. Cong, J. L. Zhang, F. Chen and M. Anpo, Synthesis and characterization of nitrogen-doped TiO_2 nanophotocatalyst with high visible light activity, J. Phys. Chem. C 111 (2007) 6976-6982

[34]X. B. Chen, Y. B. Lou, A. A. S. Samia, C. Burda and J. L. Gole, Formation of oxynitride as the photocatalytic enhancing site in nitrogen-doped titania nanocatalytsts: comparison to a commercial nanopowder, Adv. Funct. Mater. 15 (2005)

41-49

[35] M. Alvaro, E. Carbonell, V. Formés and H. García, Enhanced Photocatalytic Activity of Zeolite-Encapsulated TiO_2 Clusters by Complexation with Organic Additives and N-Doping, ChemPhysChem, 7 (2005) 200-205.

[36]Z-Y Wang, F-X Zhang, Y-L Yang, B. Xue, J. Cui and N-J Guan, Facile postsynthesis of visible-light-sensitive titanium dioxide/mesoporous SBA-15, Chem. Mater. 19 (2007) 3286-3293

[37] T. P. Ang, C. S. Toh and Y-F Han, Synthesis, characterization, and activity of visible-light-driven nitrogen-doped TiO_2-SiO_2 mixed oxide photocatalysts, J. Phys. Chem. C 113 (2009) 10560-10567

[38] H. Q. Sun, Y. Bai, H. J. Liu, W. Q. Jin, N. P. Xu, G. J. Chen and B. Q. Xu, Mechanism of nitrogen-concentration dependence on pH value: experimental and theoretical studies on nitrogen-doped TiO_2, J. Phys. Chem. C 112 (2008) 13304-13309

[39] T. Horikawa, M. Katoh and T. Tomida, Preparation and characterization of nitrogen-doped mesoporous titania with high specific surface area, Micropor. Mesopor. Mat 110 (2008) 397-404

[40]D. H. Sun, Y. Huang, B. X. Han and G. Y. Yang, Ti-Si mixed oxides prepared by polymer in situ sol-gel chemistry with the aid of CO_2, Langmuir 22 (2006) 4793-4798

[41] X. F. Song and L. Gao, Synthesis, characterization, and optical properties of well-defined N-doped, hollow silica/titania hybrid microspheres, Langmuir 23 (2007) 11850-11856

[42] A. Mills, M. Sheik, C. ÓRourke and M. McFarlane, Adsorption and photocatalysed destruction of cationic and anionic dyes on mesoporous titania films: Reactions at the air–solid interface, Appl. Catal. B: Environ. 89 (2009) 189-195

CHAPTER 6

A COMPARATIVE STUDY OF CONVENTIONAL AND CHARGE-DRIVEN SELF-ASSEMBLY METHOD TO PREPARE VISIBLE-LIGHT SENSITIVE TITANIA/ACTIVATED CARBON COMPOSITES *

Abstract

In present chapter, an experimental study was devised to explore the possible improvements to the conventional wet chemical impregnation technique of TiO_2/activated carbon composites preparation. The surface characteristics of activated carbon adsorbents were chemically modified with poly (sodium styrene sulfonate), which enabled the charge-driven self-assembly with visible-light sensitive colloidal TiO_2 nanoparticles. Characterization and test results of humic acid removal discovered a significant increase of TiO_2 loading to the activated carbon structure via the charge-driven self-assembly method. Adsorption kinetics studies found that TiO_2/activated carbon composite prepared using the conventional sol-gel method was better described using a two-phase intraparticle diffusion model compared with the one prepared via the charge-driven self-assembly method. Photocatalytic kinetics studies also revealed that TiO_2/activated carbon composites prepared via the charge-driven self-assembly method fitted the pseudo-first-order equation well, which is similar to the unsupported TiO_2 photocatalysts. This suggested the better distribution of TiO_2 coating over the activated carbon surface with poly (sodium styrene sulfonate) modification. As a result, fast photocatalytic regeneration of spent activated carbon adsorbents within composites is achieved.

* This chapter has been adapted from: Chemical Engineering Journal,

6.1. Introduction

In recent decades, nano-size TiO_2 photocatalyst has become a promising candidate for environmental clean-up, i.e. oxidization of a wide range of dissolved organic compounds at ambient or moderate room conditions [1]. Reported advantages include low cost, greatly enhanced surface area, tunable properties which can be modified by size reduction, doping, sensitizer, etc., and good stability i.e. no substantial loss of photocatalytic activity after repeated process cycles for most of dissolved organic pollutants[2]. Besides, due to the intensive research on the photocatalytic activity of TiO_2, the mechanism of its purification on various dissolved organic compounds is well understood as a consequence. It is widely acknowledged that superoxide species and, specifically, hydroxyl radicals, as active reagents for the mineralization of the organic compounds into nontoxic form such as carbon dioxide and water, which is realized through the surface contact of $OH^{\cdot}$ radicals and C-H bonds.

One promising area of TiO_2 based photocatalytic applications is the regeneration of spent porous adsorbents, which is currently one of the most viable industrial solutions to wastewater treatment due to their reasonable efficacy and comparatively low costs. Highlighting its commercial viability is the fact that activated carbon (AC) adsorption has been cited by the US Environmental Protection Agency as one of the best available environmental control technologies[3]. As a result, research works have been made to develop TiO_2/adsorbent composites via wet chemical impregnation for the wastewater treatment [4,5,6], of which many attempted to couple TiO_2 with carbon materials [7,8,9,10]. This would combine advantages of both adsorption and photocatalysis processes: On one hand, adsorbents work as the supporting substrates of nano-size TiO_2 photocatalysts and concentrate the pollutants and intermediates around the surface of TiO_2. On the other hand, the TiO_2 photocatalysts can destruct the pollutants and thus regenerate the adsorbent in situ. In the meanwhile, visible-light activity has also been successfully incorporated on the TiO_2 nanoparticles via wet chemical doping methods (i.e. N, C, S, F, B dopants, etc) [11], although such attempts were rarely found in form of TiO_2/adsorbent composites [6]. In our previous paper, an attempt to enable TiO_2/adsorbent composites with visible light sensitivity via a facile wet chemical N-doping was undertaken and viable photocatalytic ability, especially under visible light, has been demonstrated in terms of methylene blue (MB) removal

[12]. However, developing new, simple and effective approach for controlled impregnation of TiO_2 onto the adsorbent pores with a better coating distribution in a short time with high TiO_2 loading or photocatalytic performance is still a challenging task, especially when considering the various surface characteristics of different adsorbents (i.e. hydrophobicity/hydrophilicity).

More recently, charge-driven self-assembly techniques have been developed to achieve the preparation of functional composites through rational organization of different colloidal particles [13].The ability of assembling functional nanoparticles with fine control over the compositions and properties offers unique advantages for the development of novel composite materials. Using this method, various thin films, core-shells and hollow spheres, and flocculated assemblies of functional metal oxides have been successfully developed [14, 15]. It is well known that AC surface is highly hydrophobic, while TiO_2 colloidal suspensions usually carry positive charge in an acidic medium. The following surface reaction for the colloidal TiO_2 photocatalysts is expected to occur below pH 6.8 (pzc of TiO_2 sol):

$$Ti - OH + H^+ \leftrightarrow TiOH_2^+ \quad (1)$$

During the chemical activation of AC, some chemicals, typically like an acid, strong base, or a salt (phosphoric acid, potassium hydroxide, sodium hydroxide, zinc chloride, respectively), are usually used. This process would introduce surface functional groups (e.g. -COOH and $-SO_3$) as side effects and usually change the AC surface properties to a certain extent. In the same sense, this paper describes a charge-driven self-assembly method utilizing poly (sodium styrene sulfonate) (PSS) as modification agent to AC surface, which is one type of polyelectrolyte with negatively charged functional sulfonate ($-SO_3$) groups and often used for dispersion of particle suspension. This surface modification process leaded to the efficient adsorption of PSS with anionic functional groups ($-SO_3$) on the surface of AC, which was of importance for charge-driven self-assembly of cationic TiO_2 photocatalysts onto its surface. Characterization and photocatalytic evaluation of as-prepared TiO_2/AC composites using humic acid (HA) as a model pollutant were also carried out.

6.2. Experimental

6.2.1 Visible-light sensitive TiO_2/activated carbon composites preparation

All reagents in this work were of analytical grade and used as received. Water used in all preparation was purified by a MilliQ system. Commercially available activated carbon powders PS1300 (Activated Carbon Technologies PTY LTD) were used as adsorbent substrates, which were produced by the vapour activation of coconut shell. For comparison, the TiO_2/AC composites were prepared using two different methods as follows:

Conventional sol-gel method 40ml of titanium (IV) butoxide ($Ti(OC_4H_9)_4$) *(Sigma Aldrich)* were first dissolved in 160ml of ethanol (C_2H_5OH) by 30 min stirring at room temperature to obtain solution A. In addition, 400 ml of deionised water was mixed with nitric acid (HNO_3) by 10 min stirring at room temperature to obtain solution B. Solution B was then added drop-wise into solution A under vigorous stirring, and this was then followed by the hydrolysis of $Ti(OC_4H_9)_4$ under stirring conditions at room temperature until a transparent sol was formed. Visible-light sensitization was achieved by dropwise addition of a certain amount of triethylamine *(Sigma Aldrich)* to the formed TiO_2 sol under continuous stirring (24 h). Finally, formed visible-light sensitive TiO_2 colloidal suspension was mixed with AC particles under the constant stirring.

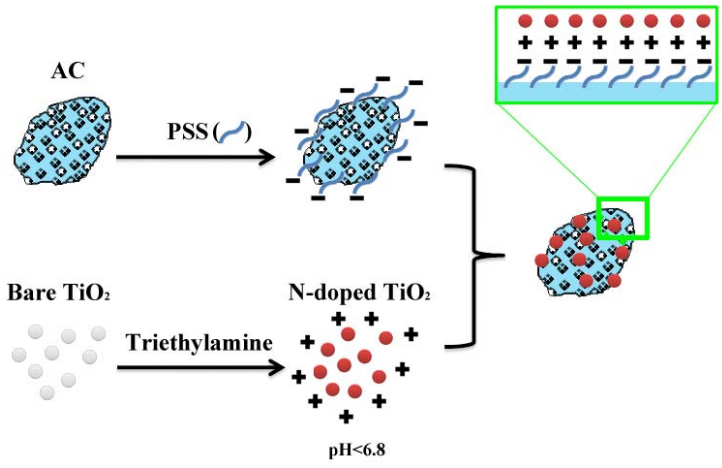

Figure 6.1: A schematic charge-driven self-assembly process of TiO_2/AC composites

Self-assembly method To self-assemble the TiO_2 onto the surface of the AC, the AC powder was first chemically modified by treating the AC with a diluted PSS solution

(Sigma Aldrich). Surface modification was first carried out by dispersing 0.25 g of AC in 50 ml of water containing 0.5 wt% of PSS with an hour sonication and 3 h stirring. The modified product was filtered and washed with deionised water. The charge-driven self-assembly of TiO_2-AC composites was then accomplished in two steps. In the first step, the surface modified AC powders were dispersed in aqueous solution with appropriate pH adjustment to ensure that the surface of AC was highly negatively charged. In the second step, the colloidal suspension of N-doped TiO_2 (via the same preparation described in Method 1) adjusted with positively surface charge was added to the AC suspension subsequently. The electrostatic interaction between the oppositely charged TiO_2 nanoparticles and AC could lead to spontaneous charge-driven self-assembly of the nanosized TiO_2 onto the surface of micro-sized AC, as illustrated in Fig. 6.1.

In all cases the resulting TiO_2 sol/AC adsorbent mixtures prepared by two methods were filtered and dried by evaporation at 100°C in 2-3 h subsequently, followed by 350°C calcinations for 2 h. Nitrogen protection gas was used in all cases to avoid potential carbon loss and temperature ramp during the calcinations was set at 5°C /min. For clarification, the TiO_2/AC composites prepared via the conventional sol-gel method are denoted as C_{SG} and those via the self-assembly method are denoted as C_{SA} in this work.

6.2.2 Characterisation of the experimental materials

The structural properties including the BET surface area, total pore volume and pore size distribution (according to the BJH model) were obtained based on the N_2 adsorption–desorption isotherms, determined at 77K via a Belsorp apparatus, Japan. Before each measurement, samples were degassed using nitrogen at 200°C for 15 h. Morphological properties of composites were examined by a transmission electron microscopy (TEM, Philips CM200) and scanning electron microscopy (SEM, Philips XL 30) as well as energy-dispersive x-ray spectroscopy (EDX). Surface chemical characteristics were investigated by transmission Fourier transform infrared spectroscopy (FTIR) analysis at 4,000–500cm^{-1} wavenumber, which was conducted on a Shimadzu FTIR-8400s instrument using potassium bromide (KBr) pellets for sample preparation. In each preparation, 1–2mg of sample was ground with 100mg of KBr. Thermogravimetric analysis (TGA) was employed via a Universal V3.3B TA

instrument to characterize the TiO_2 loading of as-synthesized TiO_2/AC composites. The TGA analyses were then performed by heating the samples from room temperature to 800°C in an oxygen atmosphere at a heating rate of 10°C/min. The crystalline structure of TiO_2/AC composites was investigated by powder X-ray diffraction (XRD) technique on an X-ray diffractometer (Mini Material Analyser, Diffraction Technology) using Cu Kα radiation (λ=0.154056 nm) and operating in the angle range of 20-80 degree. The scan speed was $0.5°min^{-1}$. The chemical composition of TiO_2/AC composites was studied using X-ray photoelectron spectroscopy (XPS) analysis on a SPECS SAGE spectrometer with a Phoibos 150 hemi-spherical analyzer. In addition, the calibration of XPS to adventitious C 1s has also been performed.

6.2.3 Experimental set-up for dissolved organic compound removal

To evaluate the overall performance of as-prepared TiO_2/AC composites, the removal of HA (molecular weight>2000Da, Sigma Aldrich) was carried out in a 200ml cylindrical glass vessel under a visible light source, which was supplied by a Newport Oriel series Q solar simulator with a 100W Xe lamp. A dichroic mirror (NewSpec 66219) was mounted on the lamp to eliminate infrared and UV irradiation. The total collimated irradiance between 420 and 630nm was approximately 570mW on the surface of sample by a Newport optical power meter 1918-C. For further assessment of as-prepared *TiO_2/AC composites* adsorption ability and that assisted by visible-light photocatalysis separately, HA removal tests were carried out in two modes with and without light. In a typical test, 30 mg TiO_2/AC composites were added into 100 ml of 11.2 mg/L HA solution (a typical concentration observed in natural waters), respectively. For all cases, 2.5ml suspension was retrieved with a filter syringe at a defined time interval and then centrifuged. The concentration of HA was analysed using a Varian Cary 100 UV-Vis spectrophotometer at 254nm, of which the decrease in absorption could indicate the degradation of aromatic structures in HA molecules [16].

In addition, mechanical stability test of TiO_2/AC composites was also devised, where the solution containing C_{SA} composite and HA residuals were taken from the reactor after 4 hr visible-light irradiation, added with 1M NaOH to adjust their pH to 11, and stirred for overnight to desorb HAs from composites. The solution was then filtered

(Millipore 0.45μm) and washed before reusing to remove the HA solution of the same concentration.

6.3. Results and discussion

6.3.1 Characterisation of as-prepared TiO_2/AC composites

Fourier transform infrared spectroscopy (FTIR). The FTIR spectrum of AC samples with and without PSS surface modification is shown in Fig. 6.2. Compared with the bare AC, surface modified AC features several characteristic absorption peaks of PSS although relatively small. For example, the characteristic absorption peaks at 1041 and 1190 cm−1 correspond to S=O symmetrical and asymmetrical stretching vibration, respectively; The small absorption peak at 1415 cm−1 and 2900 cm−1 are attributed to the aromatic ring from polystyrene and C-H stretching vibrations, respectively[17]. These together show the presence of adsorbed PSS over the AC surface.

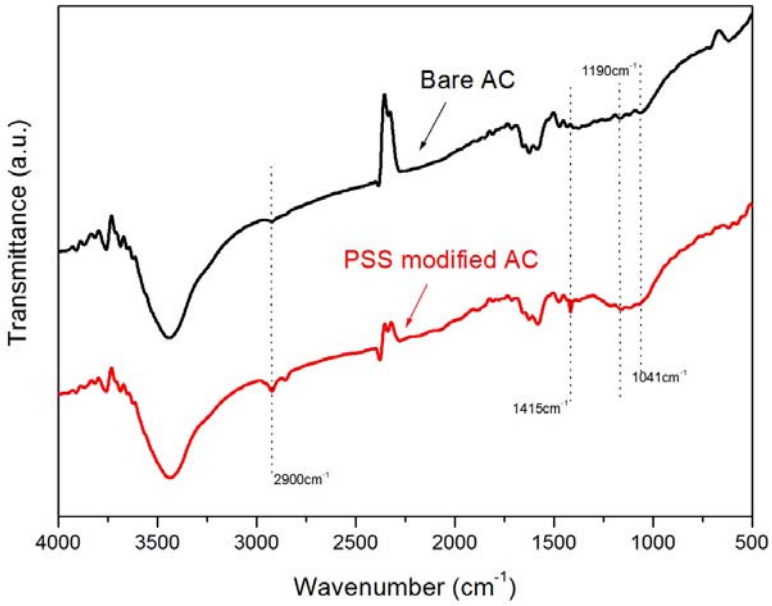

Figure 6.2: FTIR spectra of AC before and after the PSS surface modification

Thermogravimetric analysis (TGA). For TGA analysis of C_{SG} and C_{SA} samples, all decomposition temperatures and associated weight percentages of the individual components are summarised in Table 6.1. Clearly the decomposition profiles of two

composites samples are different. Both samples lose approximately 5% to 6% of their original weight within the first 100°C of the heating profile due to low boiling components. C_{SG} then loses very little weight (0.62% of original weight) leading into the carbon decomposition. C_{SA}, however, loses a total of 5.27% of its weight leading into the carbon decomposition. Higher weight loss of C_{SA} during this stage was probably attributed to the absorbed PSS decomposition, of which the temperature was reported around 300°C in the air [18]. However, a separate TGA analysis of PSS conducted under nitrogen flow suggested that it might not undergo any decomposition at 350°C (the C_{SA} calcinations temperature) as the weight loss was almost negligible up to 450°C. In the final stage, C_{SG} shows the carbon decomposition to represent 90.32% of the samples original weight leaving a remaining residue after heating to 800°C of 2.90%. C_{SA}, however, shows the carbon decomposition to represent 24.56% of the samples original weight leaving a remaining residue after heating to 800°C of 64.95%. Given that TiO_2 usually stays stable up to around 800°C and most likely existed as the burn-off residue, it is indicative that surface modification with PSS was effective to increase the TiO_2 loading in the final TiO_2/AC composites. An overlay of total measured TGA plots is presented in Fig. 6.3 for comparison.

Table 6.1: Decomposition temperatures and corresponding weight loss percentages together at different stage with remaining residue amounts after heating to 800°C

Sample	**Decomp 1**		**Decomp 2**		**Decomp 3**		**Decomp 4**		**Residue (%)**
	T (°C)	**Weight loss (%)**	**T (°C)**	**Weight loss (%)**	**T (°C)**	**Weight loss (%)**	**T (°C)**	**Weight loss (%)**	
C_{SG}	35	6.27	75-350	0.62	-	-	573	90.32	2.90
C_{SA}	36	5.21	100-350	2.54	350-490	2.73	618	24.56	64.95

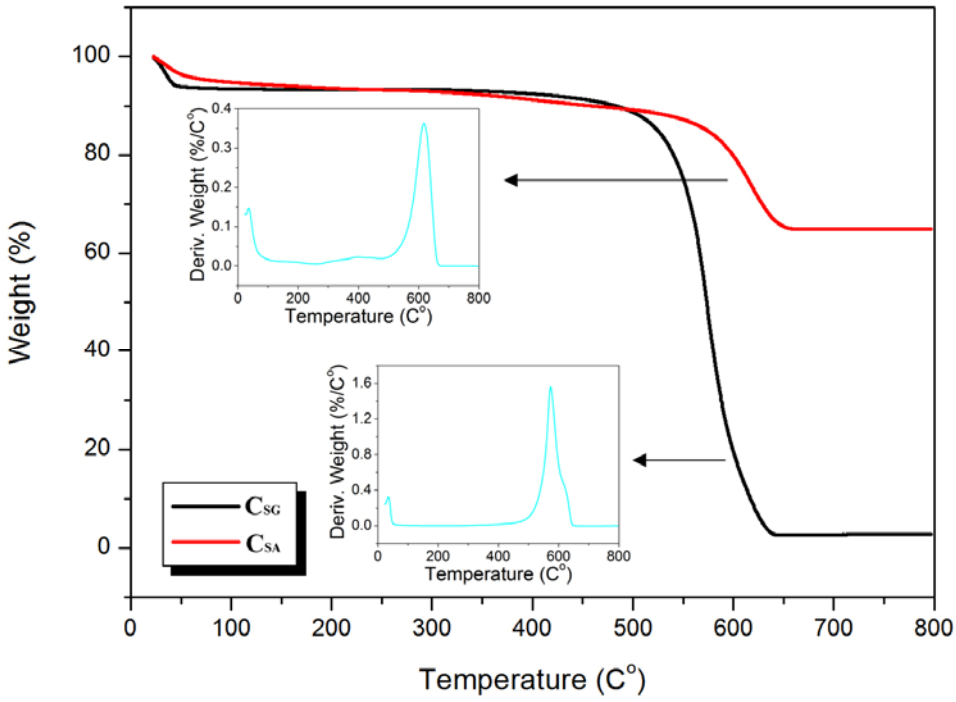

Figure 6.3: Overlay of the measured TGA plots for C_{SG} and C_{SA}, where the insets are corresponding first order derivative weight loss profiles.

X-ray diffraction (XRD). Some structural parameters and features of AC, C_{SA} and bare N-TiO_2 nanoparticles as synthesized under the same condition (N-to-Ti ratio 1 and calcinations 350°C) were obtained from the XRD analysis, which are shown in Fig. 6.4 (a). The broad peak at the 2θ value of 25° typical of carbon materials are observed in the XRD pattern of AC. Anatase phase of the TiO_2 crystal structure could be interpreted from XRD patterns for both C_{SA} and N-TiO_2 nanoparticles, where anatase characteristic peaks are assigned to 2θ values of 25.4°, 37.8°, 48°, 53.9° and 55°, respectively. Based on the XRD results, the crystal size of the TiO_2 microspheres are usually calculated using the Scherrer formula:

$$L=K\lambda/\beta\cos\theta \qquad (2)$$

Where L is the crystalline size in nm, λ (0.154056nm) the wavelength of the X-ray radiation, K the usually taken as 0.89, θ is the diffraction angle, λ is the X-ray wavelength corresponding to the Cu Kα irradiation, and β is the line width at half-maximum height after subtraction of equipment broadening for the peak at 2θ=25.4°. The average crystalline sizes of TiO_2 were estimated to be 5nm for the C_{SA}, which was close to that of the bare N-doped TiO_2 sample.

X-ray photoelectron spectroscopy (XPS). The chemical composition of the C_{SA} powders was interpreted using the XPS survey spectra in Fig. 6.4 (b), where the major sharp photoelectron peaks appear at binding energies of 458 eV(Ti 2p), 531eV (O 1s) and 285eV (C 1s). The atomic ratio of Ti to O of the C_{SA} sample is about 2, in good agreement with the nominal atomic composition of TiO_2. The large carbon peak in C_{SA} powders is most likely attributed to the carbon element from the AC substrate, since the calibration of XPS to adventitious C 1s has been performed. In addition, the C_{SA} sample also contains a small amount of N (binding energies at 401 eV) and S (binding energies at 169 eV) atoms, which probably come from the triethylamine and PSS precursor during the preparation. These elements might result in the visible-light sensitisation of TiO_2 nanoparticles within the composite.

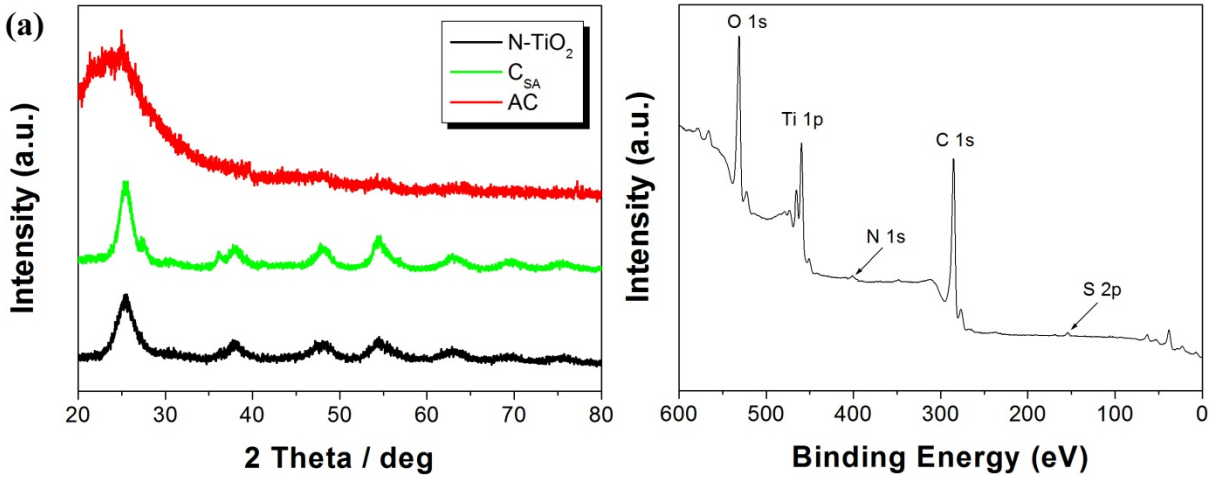

Figure 6.4: XRD pattern (a) of AC, C_{SA} and N-TiO_2 nanoparticles; XPS spectra (b) of C_{SA}

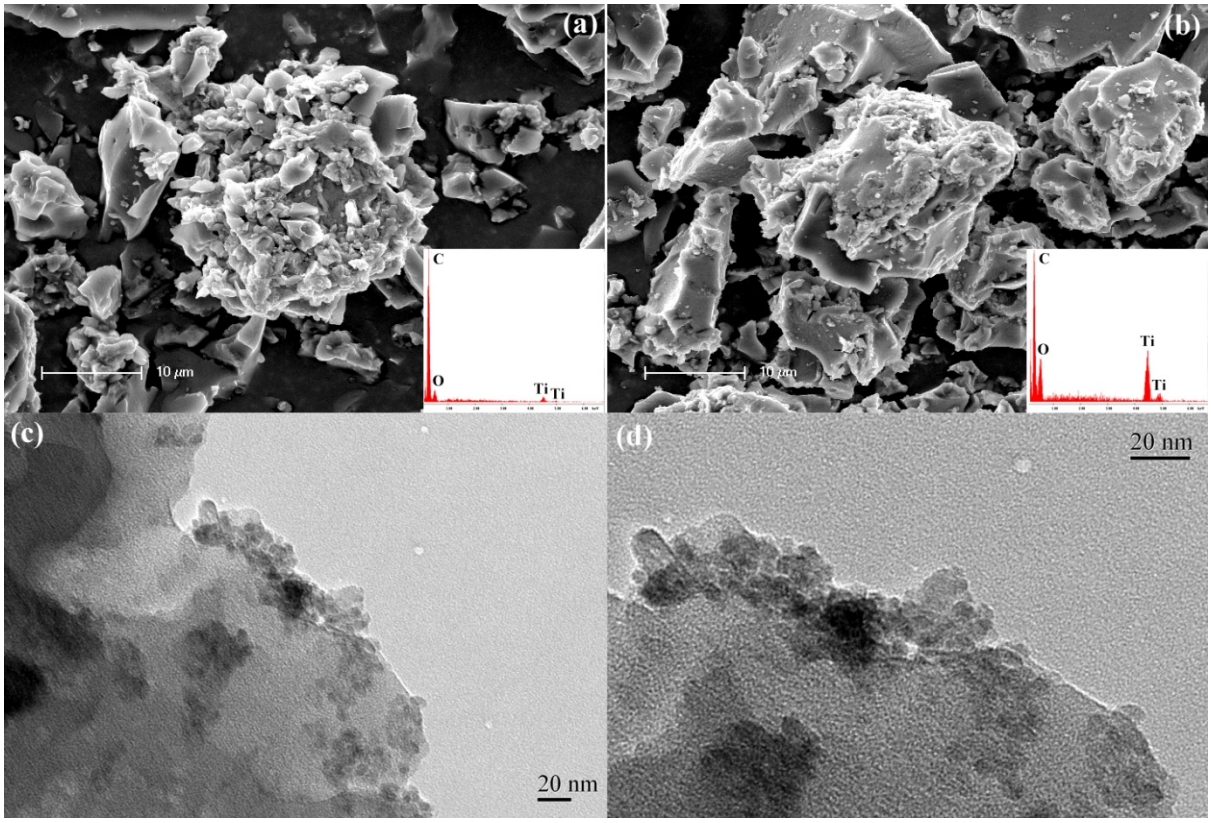

Figure 6.5: Typical SEM images and corresponding EDX results (insets), where (a) is for C_{SG} and (b) is for C_{SA}; Typical TEM image of C_{SA} (c) and that in higher magnification (d)

Scanning electron microscopy (SEM) with energy-dispersive x-ray spectroscopy (EDX) and transmission electron microscopy (TEM). SEM images in Fig. 6.5(a) and (b) represent the morphology of both TiO_2/AC composites, which appeared to be of not much difference. However, the corresponding EDX results in Fig. 6.5 insets suggested otherwise. The EDX spectra in inset of Fig. 6.5(a) belonging to the composites prepared by the self-assembly method features much higher Ti peaks than that of C_{SG} in Fig. 6.5(b). These findings are consistent with aforementioned TGA results, which further confirm the higher TiO_2 loading in C_{SA} samples. TEM images in Fig. 6.5 (c) and (d) shows those TiO_2 nanoparticles were well-anchored across the AC substrate in C_{SA}, whereas some agglomeration is observable. Single TiO_2 particle size is estimated to be around 5nm, which is in good accordance with the XRD calculation.

Nitrogen adsorption-desorption analysis. To clarify the mechanism of adsorption ability and selectivity, nitrogen adsorption-desorption data was obtained and analysed.

Fig.5 represent the nitrogen adsorption-desorption isotherm for AC/TiO_2 composites prepared via two different methods. As seen from Fig. 6.6(a), C_{SG} features type I isotherm, which is usually typical of microporous particles according to the BDDT classification [19]. For C_{SA}, Fig. 5(b) shows that the isotherm shape was somewhat transited to type IV along with the appearance of a slight hysteresis loop (H2 type) at the high pressure. This phenomenon is usually associated with the capillary condensation and suggestive of the presence of some not well-defined mesopores. The pore size distribution pattern of C_{SG} and C_{SA} composites was obtained via the BJH approach, which are depicted as the insets of Fig. 5(a) and (b), respectively. For both C_{SG} and C_{SA} composites, the pore volume is predominantly in the pore size range <10nm, although the shape of pore size distribution profile is much different. While the majority pore size of TiO_2/AC composite prepared by method 1 (C_{SG}) is drawn increasingly towards 1nm, C_{SA} shows a much narrower distribution of pore size and mostly concentrate around 2nm. Two possible mechanisms might contribute to this phenomenon: 1) Some micropores of the AC support were blocked via the method 1 TiO_2 impregnation; 2) some mesoporous structure was created in the final C_{SA} composite during the self-assembly method TiO_2 impregnation. Some other physical properties of AC, C_{SG} and C_{SA} are also summarized in Table 6.2, where the pore area of mesopores was estimated using the DH method. Due to the higher TiO_2 loading, C_{SA} features much less BET surface area as expected than the C_{SG}, which is also consistent with the order of their total pore volume. Higher mesopore area of C_{SA} is also consistent with its nitrogen adsorption-desorption isotherms and BJH pore volume pattern.

Table 6.2: Some physical properties of AC, C_{SG} and C_{SA} composites

Sample	BET surface area (m^2g^{-1})	Pore area of mesopores (m^2g^{-1})	Total pore volume (cm^3g^{-1})	Mean pore diameter (nm)
AC	989	20	0.51	2
C_{SG}	865	21	0.46	2.12

C_{SA}	328	93	0.24	2.91

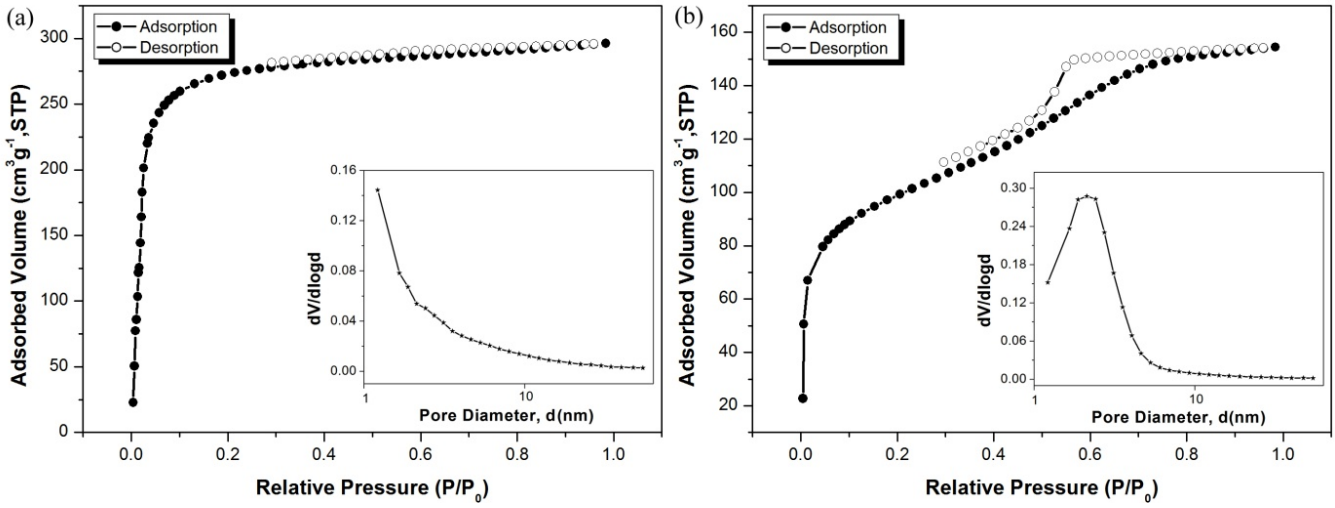

Figure 6.6: Nitrogen adsorption-desorption isotherms at 77k and BJH desorption pore volume (dV/dlogd) plots (inset) for C_{SG} (a) and C_{SA} (b) composites

6.3.2 HA removal using as-prepared TiO_2/AC composites

To evaluate the removal ability of dissolved organic compound by both C_{SG} and C_{SA} composites, HA was used as model pollutant, which widely existed in various underground and brackish water sources. Fig. 6.7 (a) and (b) demonstrates the HA removal rate as a function of time under different light conditions. Without light irradiation, dissolved HA was removed via sole adsorption (upper dash line in black). In neural or alkaline HA solutions, relatively small species are formed, consisting of one or only a few molecules. The diameter of these species has been estimated on the basis of various physicochemical measurements to be 1.2-4nm [20], which make them less favourable for microporous adsorption [21], in this case, C_{SG} composites. With respect to C_{SA} composites, we discussed that the TiO_2 loading process seemed to induce more mesopores formation based on the DH results, which would compensate for the adsorption decrease caused by overall surface area loss. As a result, HA removal rate of C_{SA} composites (~15%) by adsorption was not much lower than those of C_{SG} (~20%).

To better understand the adsorption process of HA by as-prepared TiO_2/AC composites, an intraparticle diffusion model was also employed by plotting the square root of time ($min^{0.5}$) versus the amount of HA adsorbed (mg/g) [22]. As seen in Fig. 6.8, it is clear that adsorption process of C_{SG} follows two phases, where an initial linear portion ended with a smooth curve followed by a second linear portion. Generally, the two phases in the intraparticle diffusion plot suggest that the adsorption process proceeds by both surface adsorption and intraparticle diffusion stages [23]. The initial curved portion of the plot indicates surface or instantaneous adsorption stage, which is usually very fast. The second linear portion is more gradual due to intraparticle or pore diffusion stage, which is usually rate-controlled. Similar results were previously found for many adsorption processes, e.g. acid dye adsorption on activated palm ash [24] or Cd adsorption on activated carbon [25]. In contrast, two-phase linearity was less pronounced for C_{SA} with an improved single-phase linearity coefficient R=0.95. This is probably attributed to its larger pore size, which could somewhat relieve the rate-controlled intraparticle diffusion in the later stage.

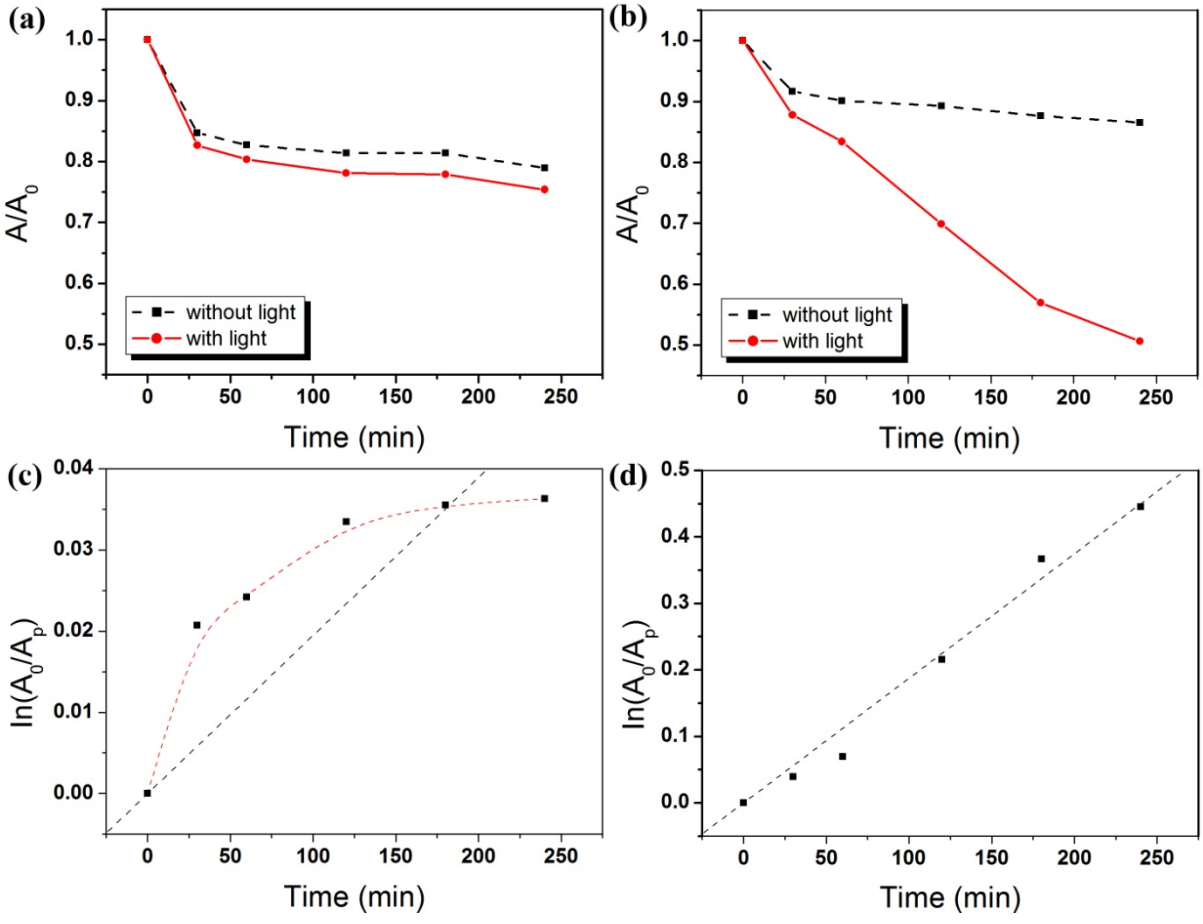

Figure 6.7: HA removal rate with and without visible light irradiation for C_{SG} (a) and C_{SA} (b), where A_0 is the initial light absorption at 254nm and A is that at given time, t; (c) and (d) are pseudo first order representation of the HA removal rate by sole TiO_2 photocatalysis for C_{SG} and C_{SA}, respectively, where A_p is the light absorption at given time, t.

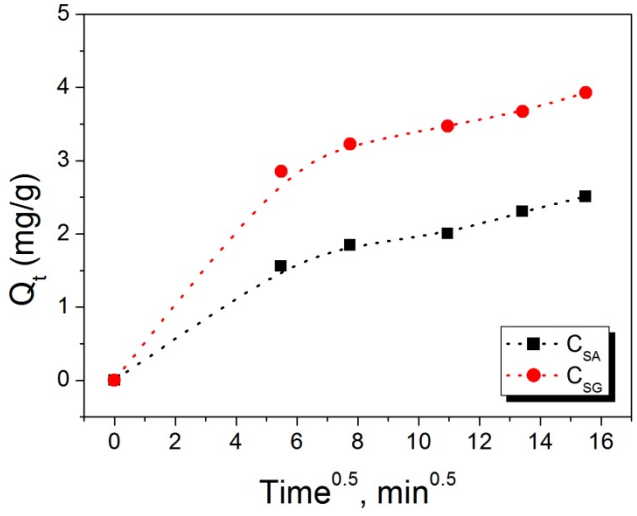

Figure 6.8: Plot of Q_t vs. $t^{0.5}$ for both as-prepared TiO_2/AC composites, where Q_t is the amount of HA adsorbed on TiO_2/AC composites per unit weight (mg/g) at a given time, t.

Upon the visible light irradiation, Fig. 6.7(a) and (b) shows that the HA removal (lower solid lines in red) was increased compared with that under the dark condition for both C_{SG} and C_{SA}. This suggested the successful incorporation of TiO_2 photocatalysts into the AC structure. In addition, the offset between two lines in Fig. 6.7 (a) and (b) can be also viewed as the amount of HA removal by TiO_2 photocatalysis solely. As a result, it is clear that C_{SA} possess much higher photocatalytic ability than C_{SG} within the same given time. This was most likely attributed to the increased TiO_2 loading per weight in C_{SA} composite. Furthermore it is well known that the oxidative decomposition of dissolved organic compound is catalysed by Ti-OH$^{\cdot}$ surface hydroxyl radicals, which are generated in an aqueous environment after photoexcitation of TiO_2 at a certain wavelength [26]. Previously, several experimental results demonstrated that photocatalytic reaction rates of various dissolved organic compounds over illuminated unsupported TiO_2 fitted the Langmuir-

Hinshelwood (L-H) model [27,28], which can be rearranged into a pseudo-first-order equation:

$$\ln\left[\frac{A_0}{A_p}\right] = kt \quad (3)$$

where k is the pseudo-first-order rate constant, A_0 is taken as the initial light absorption of HA and A_p is that at the illumination time *t*. Accordingly, the same pseudo-first-order equation was also employed to characterize the photocatalytic kinetics of both C_{SG} and C_{SA} composites, which were plotted in Fig. 6.7 (c) and (d), respectively. Poor linear fit (coefficient R=0.85) suggested that the photocatalytic kinetics of C_{SG} composites were somewhat different from that of using unsupported TiO_2 photocatalysts alone. Interestingly, the photocatalyitc kinetics of C_{SG} rather resembles a two-phase linearity (red dot line), which is similar to its adsorption kinetics represented by the intraparticle diffusion model in Fig. 6.8. In contrast, significantly improved linear coefficient of C_{SA} composite (coefficient R=0.99) revealed its similarity to the photocatalytic kinetics of unsupported TiO_2 photocatalysts. Mechanistically, this indicated that the supply of adsorbed HA molecules from the AC support to adjacent TiO_2 particles was similar to the collision or diffusion of aqueous HA onto TiO_2 nanoparticles. Previously, it was found that PSS molecules are preferentially adsorbed near the outer surface of adsorbents and therefore do not penetrate the adsorbent particles completely [29]. It is speculated that these anionic adsorbed PSS molecules would then guide positively charged colloidal TiO_2 particles to coat onto the outer surface of adsorbent as well rather than lodge deeper inside the pores. Plus, PSS is also well-known to be a good dispersant of nanoparticles suspension. These together could result in a better distribution of TiO_2 coating and relieved the otherwise lengthy intraparticle diffusion of adsorbed HA species on the AC support to adjacent TiO_2 photoactive sites (see Fig. 6.9), especially when considering some of these species are too large to migrate inside the pore.

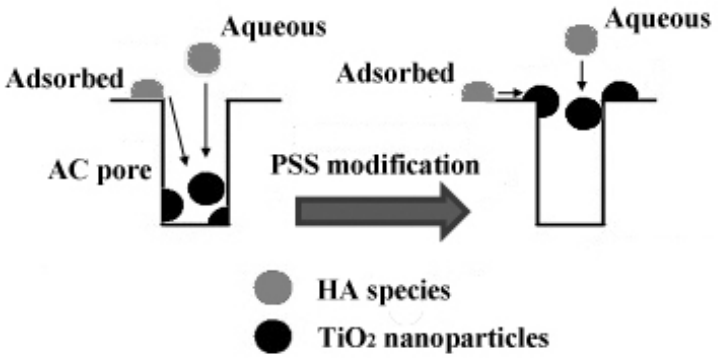

Figure 6.9: Possible mechanism of HA species migration to the TiO_2 photoactive sites

A series of mechanical stability test has also been carried out to investigate coupling strength of TiO_2/AC composite. After 5 removal-regeneration cycles, Fig. 6.10 shows that the removal rate of HA species within 4 hr have a slight decrease but almost negligible, especially considering the likely samples loss during the filtering and transferring. This indicates the strong coupling between TiO_2 photocatalyts and their AC substrate, which would make them more suitable for the practical use.

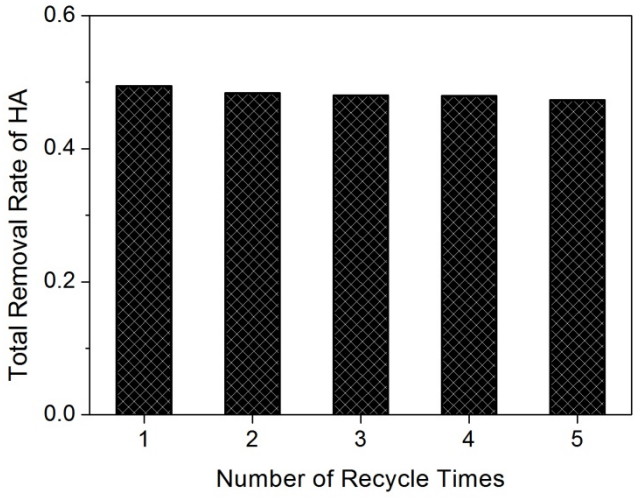

Figure 6.10: Total removal rate of HA species (defined as $1-A/A_0$) associated with 5 removal-regeneration cycles. Experimental conditions were [HA] =11.2ppm and [C_{SA}] =30mg.

6.3.3 pH effects on the performance of as-prepared TiO_2/AC composites

It is well known that pH influence the surface protonation/deprotonation of both TiO_2 nanoparticles and HA in solution greatly. Accordingly, pH effects on both adsorption and photocatalysis of C_{SA} have also been investigated using a variation of three pH values (3, 7 and 11), of which the results are shown in Fig. 9. Fig. 6.11(a) shows that HA adsorption on C_{SA} composites was minimal at pH 11 and rapidly increased with decreasing pH values. Previously, the strong pH-dependent adsorption of HA on oxide surfaces has been observed [30]. A simple electrostatic surface charge model can account for the pH-dependent HA adsorption on TiO_2, where the surface of TiO_2 takes positive charges at pH < 6.8 and negative charges at pH > 6.8. HA with many acidic functional groups are deprotonated and negatively charged in alkaline solution. Therefore, the adsorption of HA at basic pH is strongly inhibited due to the negative–negative electrostatic repulsion. On the other hand, most of HA are fully protonated and scarcely soluble at acidic pH, which could lead a significantly increased adsorption of HA on TiO_2. To clarify further, the adsorption of HA on AC at different pH values was also investigated. As Fig. 6.11 (a) shows, protonated HA molecules at high acidity (pH=3) were also favourable for AC adsorption. As a result, the increased acidity appeared to be optimal for the adsorption ability of both TiO_2 and AC substrates. Fig. 6.11 (b) compares the changes of UV absorbance at 254 nm of HA solution at pH 3, 7, and 11 as a function of the visible light irradiation time. The fact that HA photocatalytic removal efficiency also decreased with pH 3 > 7 > 11 clearly shows that the adsorption of HA on TiO_2 is necessary to initiate the effective photocatalysis, as the photocatalysis at high basicity (pH=11) were almost ceased with near-zero adsorption.

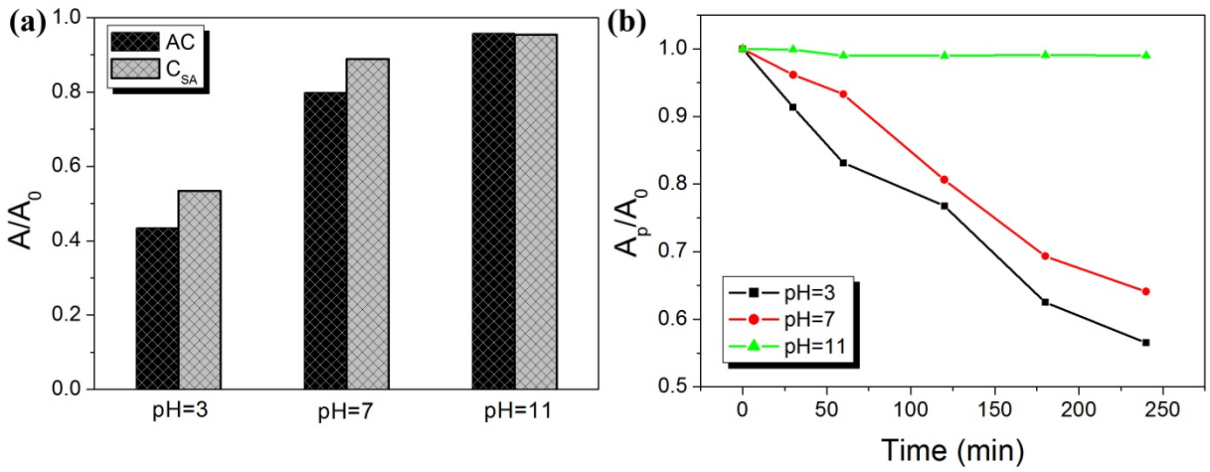

Figure 6.11: Adsorption (a) of AC and C_{SA} and photocatalytic ability (b) of C_{SA} at different pH, where A_0 is the initial light absorption at 254nm and A is that at given time, t. Experimental conditions were [HA] =11.2ppm and [AC or C_{SA}] =30mg.

6.4. Conclusion

A novel charge-driven self-assembly method to synthesize visible-light TiO_2/AC composites was reported. The surface characteristics of AC adsorbent were modified with anionic PSS, while the visible-light sensitive TiO_2 colloidal sols contained well-dispersed N-doped TiO_2 nanoparticles with positive surface charge in acidic medium. As a consequence, loading of TiO_2 was facilitated due to the electrostatic attraction between the anionic PSS and positively charged TiO_2 on the surface. Characterization and HA removal test results confirmed that the TiO_2 loading to the AC structure was significantly increased. Adsorption kinetics study found that TiO_2/activated carbon composite prepared using the charge-driven self-assembly method was less described using a two-phase intraparticle diffusion model compared with the one prepared via the conventional sol-gel method. Photocatalytic kinetics study also revealed that TiO_2/AC composites prepared via the PSS modification method fitted the pseudo-first-order equation well, which is similar to the unsupported TiO_2 photocatalysts. These findings confirmed the better distribution of TiO_2 coating over the AC surface with PSS modification rather deep into their pores. Mechanical stability tests also proved the strong coupling strength between TiO_2 photocatalyts and their AC substrates. Furthermore, both photocatalytic and adsorption ability of HA species for C_{SA} were found to increase significantly with a decreasing order of pH values (3>7>11). This indicated the best working conditions for optimal HA removal. Finally, one can expect that the degree of surface modification on AC plays a key role for the preparation of composites with appropriate loading and distribution of visible-light sensitive TiO_2 nanoparticles, which certainly deserve future investigation.

References

[1] O. Legrini, E. Oliveros, A. M. Braun, Photochemical processes for water treatment, Chem. Rev. 93 (1993) 671-698.

[2] M. Gratzel, Photoelectrochemical cells, Nature 414 (2001) 338-344.

[3] F. Derbyshire, M. Jagtoyen, R. Andrew, A. Rao, I. Martin-Gullon, E. Grulke, Carbon materials in environmental applications. In: L. R. Radovic, editor. Chemistry and physics of carbon, Vol. 27. Marcel Dekker, New York, 2001, pp. 1-66.

[4] B. Zhu, L. Zou, Removal of color compounds from recycled water using combined activated carbon adsorption and AOP decomposition, J. Adv. Oxid. Technol. 12 (2009) 47-54.

[5]B. Zhu, L. Zou, Trapping and decomposing of color compounds from recycled water by TiO_2 coated activated carbon, J. Environ. Manage. 90 (2009) 3217-3225.

[6] W. Zhang, L. Zou, L. Wang, Photocatalytic TiO_2/adsorbent nanocomposite prepared via wet chemical impregnation for wastewater treatment: a review, Appl. Catal. A: Gen. 71 (2009)1-9.

[7] J. Matos, J. Laine, J. –M. Herrmann, Effect of the type of activated carbons on the photocatalytic degradation of aqueous organic pollutants by UV-irradiated titania, J. Catal. 200 (2001) 10-20.

[8] J. Matos, J. Laine, J. –M. Herrmann, D. Uzcategui, J.L. Brito, Influence of activated carbon upon titiania on aqueous photocatalytic consecutive runs of phenol photodegradation, Appl. Catal. B: Environ. 70 (2007) 461-469.

[9] T. Matsunaga, M. Inagaki, Carbon-coated anatase for oxidation of methylene blue and NO, Appl. Catal. B: Environ. 64 (2006) 9-12.

[10] M. Inagaki, F. Kojin, B. Tryba, M. Toyoda, Carbon-coated anatase: the role of the carbon layer for photocatalytic performance, Carbon 43 (2005) 1652-1658.

[11] F. Han, V. S. R. Kambala, M. Srinivasan, D. Rajarathnam, R. Naidu, Tailor titanium dioxide photocatalysts for the degradation of organic dyes in wastewater treatment: a review, Appl. Catal. A: Gen. 359 (2009) 25-40.

[12] W. Zhang, L. Zou, L. Wang, Visible-light assisted methylene blue (MB) removal by novel TiO_2/adsorbent nanocomposites, Water Sci. Technol. 61 (2010) 2863-2871.

[13] G. Decher, Fuzzy nanoassemblies: toward layered polymeric multicomposites, Science, 277 (1997) 1232-1237.

[14] L. Wang, T. Sasaki, Y. Ebina, K. Kurashima, M. Watanabe, Fabrication of controllable ultrathin hollow shells by layer-by-layer assembly of exfoliated titania nanosheets on polymer templates, Chem. Mater. 14 (2002) 4827-4832.

[15] L. Wang, F. tang, K. Ozawa, G. Q. Lu, Layer-by-layer assembled thin films of inorganic nanomaterials: fabrication and photo-electrochemical properties, Int. J. Surface Sci. Eng. (2009) 44-63.

[16] X. Z. Li, C. M. Fan, Y. P. Sun, Enhancement of photocatalytic oxidation of humic acid in TiO_2 suspensions by increasing cation strength, Chemosphere 48 (2002) 453-460.

[17] K. S. Kang, Y. Chen, K. J. Han, K. H. Yoo, J. Kim, Conductivity enhancement of conjugated polymer after HCl-methanol treatment, Thin Solid Film 517 (2009) 5909-5912.

[18] M. J. Roberts, G. A. Lindsay, W. N. Herman, K. J. Wynne, Thermally stable nonlinear optical films by alternating polyelectrolyte deposition on hydrophobic substrates, J. Am. Chem. Soc. 120 (1998)11202-11203.

[19] K. S. W. Sing, D. H. Everett, R. A. W. Haul, L. Moscou, R. A. Pierotti, J. Rouquerol, T. Siremieniewska, Reporting physisorption data for gas/solid systems with special reference to the determination of surface area and porosity, Pure Appl. Chem. 57 (1985) 603-621.

[20] E. T. Gjessing, Physical and chemical characteristics of aquatic humus, Ann Arbor Science Publishers, Ann Arbor, MI (1976).

[21] J. Stárek, A. Zukal, J. Rathouský, Comparison of the adsorption of humic acids from aqueous solutions on active carbon and activated charcoal cloths, Carbon 32 (1994) 207-211.

[22] W.J. Weber, Morris, Kinetics of adsorption on carbon from solution, J. Saint Eng. Div. Am. Soc. Civ. Eng. 89 (1963) 31–39.

[23] Q. Sun, L. Yang, The adsorption of basic dyes from aqueous solution on modified peat-resin particle, Water Res. 37 (2003) 1535–1544.

[24]B.H. Hameed, A.A. Ahmad, N. Aziz, Isotherms, kinetics and thermodynamics of acid dye adsorption on activated palm ash, Chem. Eng. J. 133 (2007) 195–203.

[25] K.Ibrahim, U.Mehmet, K.Hamdi, C.Ali, Adsorption of Cd(II) ions from aqueous solutions using activated carbon prepared from olive stone by $ZnCl_2$ activation, Biores. Technol.99(2008)492–501.

[26] F. Schüth, A. Wingen, J. Sauer, Oxide loaded ordered mesoporous oxides for catalytic applications, Micropor. Mesopor. Mater. 44-45 (2001) 465-476.

[27] I. K. Konstantinou, T. A. Albanis, TiO_2-assisted photocatalytic degradation of azo dyes in aqueous solution: kinetic and mechanistic investigations, Appl. Catal. B: Environ. 49 (2004) 1-14.

[28] T. Sauer, G. C. Neto, H. J. Jose, R. F. P. M. Moreira, Kinetics of photocatalytic degradation of reactive dyes in a TiO_2 slurry reactor, J. Photochem. Photobiol. A: Chem. 149 (2002) 147-154.

[29] N. Ando, Y. Matsui, R. Kurotobi, Y. Nakano, T. Matsushita, Comparison of natural organic matter adsorption capacities of super-powdered activated carbon and powdered activated carbon, Water Res. 44 (2010) 4127-4136.

[30] B. Gu, J. Schmitt, Z. Chen, L. Liang, J.F. McCarthy, Adsorption and desorption of natural organic matter on iron oxide: mechanisms and models, Environ. Sci. Technol. 28 (1994) 38-46.

CHAPTER 7

CONCLUSIONS AND SUGGESTIONS FOR THE FUTURE WORKS

7.1 Conclusions

The recent progress on preparation of TiO_2/adsorbent composites via wet chemical impregnation has indicated the potential applications of TiO_2/adsorbent composites to the future wastewater treatment. However, some major limitations in this area still exist, especially that visible-light capacity has yet to be introduced into TiO_2/adsorbent composites. It is envisaged that this could be realized via a single wet chemical procedure without significant increase of the process complexity. And also, properties of as-prepared composites resultants are expected to depend on the experimental conditions sensitively during the synthesis. In view of these points, systematic experimental investigation has been devised and the major findings of this research are summarised in the following:

- Wet chemical preparation of visible-light sensitive TiO_2 photocatalysts

Optimal visible-light activity was obtained at equal N-to-Ti precursor molar ratio and 350˚C calcinations for the wet chemical N-doping method of preparing titania photocatalysts. The pH value of N-doped TiO_2 sol during the preparation was also found to be an effective indicator of N-doping quality without using any post-synthesis analysis. These findings laid the foundation for the subsequent wet chemical coupling with different adsorbents.

- Wet chemical preparation of different visible-light sensitive TiO_2/adsorbent composites

Synergistic interactions of visible-light sensitive TiO_2/adsorbent composites between their adsorption and visible-light photocatalysis were observed for all tested adsorbents including zeolites (F-9, HSZ-690 and HSZ-930), mesoporous silica (MPS-2.7 and 4) and activated carbon. Under the assistance of visible-light irradiation, all

TiO_2/adsorbent composites achieved higher organics removal rates than those by adsorption process alone.

- Effects of different TiO_2 loading on TiO_2/adsorbent composites performance

The highest photocatalytic efficiency was obtained on the 10% N-doped TiO_2-coated beta zeolites composite sample due to the better dispersion of TiO_2 on the support. The synergistic effect between absorption and photocatalysis of the titania/beta zeolites composite materials was also found for all different TiO_2 loadings composites in terms of methylene blue removal efficiency under visible light irradiation. Furthermore, the 10% N-doped TiO_2-coated beta zeolites composite was also consistent to be the most efficient composite material tested for the photocatalytic degradation of methylene blue even in different pH environment. On a final note, the optimal titania loading to a particular adsorbent most likely depend on the nature of adsorbents used and deserve an independent case-by-case investigation.

- Self-assembly of visible-light sensitive TiO_2 and activated carbon composite

Chemically modified activated carbon with poly (sodium styrene sulfonate) was found to contribute to a significant increase of TiO_2 loading to its structure by enabling the charge-driven self-assembly with visible-light sensitive colloidal TiO_2 nanoparticles. Photocatalytic kinetics studies also revealed that TiO_2/activated carbon composites prepared via the charge-driven self-assembly method fit the pseudo-first-order equation well, which is similar to the unsupported TiO_2 photocatalysts. As a result, a better distribution of TiO_2 coating over the activated carbon surface with poly (sodium styrene sulfonate) modification was obtained along with promising fast photocatalytic regeneration of spent activated carbon adsorbents within composites.

These findings could be utilized in the successful development of TiO_2 photocatalysts/adsorbent composites for cost effective solar-driven environmental technology. As a final comment, it is observed that the removal efficiency of a particular organic contaminant varies greatly even using the same composite. Therefore, the assessment of a suitable treatment process needs to be conducted independently beforehand on a case-by-case base.

7.2 Suggestions for the future work

Visible-light sensitive titania/adsorbent composite reveals its potential to be used for cost effective solar-assisted removal of dissolved organic compounds. Several topics related to the above treatment processes remain to be explored. Thus, in this section future research developments are mentioned that can be followed in a near opportunity:

• Combine titania/adsorbent composite treatment with other oxidation processes, such as hydrogen peroxide and ozonation. As different oxidation process might be more efficient than others in removing a particular dissolved organic content present in wastewaters (for example, ozone reportedly would accelerate the phenolic degradation), the application of combined oxidation process could be feasible and economically interesting; it is also noteworthy that a complementary measurement of total organic carbon (TOC) during the photodegradation assessment would certainly be beneficial in future efforts as completed mineralisation of target dissolved organic is very important to wastewater treatment process.

• Test the removal efficiency of dissolved organic compounds composite present in industry-based water sources by titania/adsorbent composite, especially brackish waters, since this technique is set to be one promising complimentary pre-treatment to the ultrafiltration (UF) or nanofiltration (NF) during the desalination process;

• Design and assess a continuous reactor system that is suitable for utilizing visible-light sensitive titania/adsorbents composite to the treatment of wastewaters. While batch mode treatments using titania/adsorbent composites are tested out in most of lab-scale studies (that is, photocatalytic regeneration of the composites has to been done in a separate way), industry processes usually require continuous operations. This would favourably feature the fluidized bed related design with an external light source. To ensure a rather smooth continuous operation between adsorption and regeneration, several design elements could be explored within the fluidized system, such as the flow pulsation, which with the suitable the flow-off period as the time gap could ensure enough process time for the photodegradation or regeneration of adsorbents in-situ. On the other hand, constructing two or more parallel reaction columns with switches along the main line is also an option. The on-and-off of the reaction flow will alternate between each other when the titania/adsorbent composites of one column are saturated. Judiciously applying these design elements to fluidized

bed system could potentially relieve or even bypass the limiting-step issues of photodegradation or regeneration of adsorbents, and thus ensure the continuity of the process.

Finally, an economical analysis and a life cycle assessment of the visible-light sensitive titania/adsorbent composite treatment studied either with industry wastewaters or brackish water could be made. These analyses will assess the economical and environmental impacts of the treatment process over the entire life cycle “from cradle to grave”.

APPENDIX 1 PUBLISHED JOURNAL ARTICLES AND CONERENCE PRESENTATION FROM THIS RESEARCH WORK

I. Journal Publications

- **W. Zhang**, L. Zou, L. Wang, A parametric study of visible-light sensitive TiO_2 photocatalysts synthesis via a facile sol-gel N-doping method, *Journal of Hazardous Materials,* 2011, submitted.

- **W. Zhang**, L. Zou, L. Wang, A novel charge-driven self-assembly method to prepare visible-light sensitive TiO_2/activated carbon nanocomposites for dissolved organic compound removal, *Chemical Engineering Journal*, 2011,

- H. B. Li, **W. Zhang**, L. Zou, L. K. Pan, Z. Sun, Synthesis of TiO_2-graphene composites via visible-light photocatalytic reduction of graphene oxide, *Journal of Materials Research*, 2011, 27, .

- Q. Shen, **W. Zhang**, Z. Hao, L. Zou, A study on the synergistic adsorptive and photocatalytic activities of $TiO_{2-x}N_x$/beta composite catalysts under visible light irradiation, *Chemical Engineering Journal*, 2010, 165, 301-309.

- **W, Zhang**, L. Zou, L. Wang, Visible-light assisted methylene blue (MB) removal by novel TiO_2/adsorbent nanocomposites, *Water Science Technology*, 2010, 61, 2863-2871.

- **W. Zhang**, L. Zou, L. Wang, Photocatalytic TiO_2/adsorbent nanocomposites prepared via wet chemical impregnation for wastewater treatment: a review, *Applied Catalysis A: General*, 2009, 371, 1-9. **(Top 25 Hottest Paper, October 2009 to March 2010)**

II. Conference presentations

- Oral presentation at *2nd International Conference on Nanotechnology: Fundamentals and Applications (**ICNFA**)*, Ottawa, Ontario, Canada, 27th -29th

July, 2011.

- Oral presentation at *The 8th Asia Pacific Conference on Sustainable Energy & Environmental Technologies (**APCSEET 2011**)*, Adelaide, Australia, 10th-13th July, 2011.

- Oral presentation at *XV Meetings of International Humic Substances Society (**IHSS**)*, Tenerife, Canary Islands, Spain, 27th June-2nd July, 2010. (**15th IHSS travel award winner**)

- Poster presentation at *International Conference on Nanoscience and Nanotechnology (**ICONN**)*, Sydney, Australia, 22th-26th February, 2010.